1

2

3   Phanerozoic Paleotemperatures: The Earth's Changing Climate during the Last

4   540 million years

5

6

7   by

8

9

10   Christopher R. Scotese, Department of Earth and Planetary Sciences, Northwestern University, Evanston, IL,

11   60208, cscotese@gmail.com

12   Haijun Song, State Key Laboratory of Biogeology and Environmental Geology, School of Earth Sciences, China

13   University of Geosciences, Wuhan, 430074, China, haijunsong@cug.edu.cn

14   Benjamin J.W. Mills, School of Earth and Environment, University of Leeds, Leeds, LS2 9JT, UK,

15   and Douwe G. van der Meer, CNOOC International, 945 Bunker Hill Road, Houston, Tx 77024, USA

16

17

18   11/25/2020

19   Version 17c

20

21

22   **Abstract**

23   This study provides a comprehensive and quantitative estimate of how global temperatures have

24   changed during the last 540 million years. It combines paleotemperature measurements

25   determined from oxygen isotopes with broader insights obtained from the changing distribution of

26   lithologic indicators of climate, such as coals, evaporites, calcretes, reefs, and bauxite deposits. The

27   waxing and waning of the Earth's great polar icecaps have been mapped using the past distribution

28   of tillites, dropstones, and glendonites. The global temperature model presented here includes

29   estimates of average global temperate (GAT), changing tropical temperatures (ΔT˚ tropical), deep

30   ocean temperatures, and polar temperatures. Though similar, in many respects, to the temperature

31   history deduced directly from the study of oxygen isotopes, our model does not predict the extreme

32   high temperatures for the Early Paleozoic required by isotopic investigations. The history of global

33   changes in temperature during the Phanerozoic has been summarized in a "paleotemperature

34   timescale" that subdivides the many past climatic events into 8 major climate modes; each climate

35   mode is made up of 3-4 pairs of warming and cooling episodes (chronotemps). A detailed narrative

36   describes how these past temperature events have been affected by geological processes such as

37   the eruption of Large Igneous Provinces (LIPS) (warming) and bolide impacts (cooling). The

38   paleotemperature model presented here allows for a deeper understanding of the interconnected

39   geologic, tectonic, paleoclimatic, paleoceanographic, and evolutionary events that have shaped our

40   planet, and we make explicit predictions about the Earth's past temperature that can be tested and

41   evaluated. By quantitatively describing the pattern of paleotemperature change through time, we

42   may be able to gain important insights into the history of the Earth System and the fundamental

43   causes of climate change on geological timescales. These insights can help us better understand the

44   problems and challenges that we face as a result of Future Global Warming.

45

46

47   Keywords: paleoclimate, paleotemperature, Phanerozoic, climate change, climate history, ice age,

48   icehouse, hothouse, Hirnantian Ice Age, Permo-Carboniferous Ice Age, End Triassic Extinction, K/T

49   Extinction, K/T Impact Winter, PETM, Pleistocene Ice Age, Future Global Warming, $\partial^{18}O$, $\partial^{13}C$

50

51   **Part I. Introduction, Methods, and Discussion**

52   **1. Introduction**

53   There have been several recent studies of the Earth's changing temperature during the Phanerozoic,

54   e.g. Grossman (2012a&b); Veizer and Prokoph, (2015); Scotese (2016); Mills et al. (2019); Henkes et

55   al. (2018); Wing and Huber (2019); Verard and Veizer (2019); Song et al. (2019); Grossman and

56   Joachimski, 2020). All of these studies are based on oxygen isotope measurements of $\delta^{18}O$ in

57   carbonate or apatite microfossils. The first extensive compilation of oxygen isotope data assembled

58   by Veizer and Hoefs (1976) and Veizer et al. (1986, 1999, 2000) has been used by other researchers

59   to characterize temperature change at a variety of temporal and geographic scales (Royer et al.,

60   2004; Prokoph et al., 2008; Grossman, 2012 a&b). Recently, two comprehensive, global Phanerozoic

61   compilations of oxygen isotope paleotemperatures have been assembled (Song et al., 2019 and the

62   PALects database, Grossman et al., 2018).

63   Urey (1951) and Emiliani (1955) were the first scientists to appreciate the utility of oxygen isotopes.

64   For every 4.3°C increase in temperature, there is a 0.1% decrease in the amount of ^{18}O (Epstein and

65   Mayeda, 1953) used to produce the calcium carbonate of the foraminifera's shell. By measuring the

66   ratio of ^{18}O to ^{16}O, also referred to as $\delta^{18}O$, it is possible to estimate the temperature at which the

67   calcium carbonate was produced. Savin et al. (1975), Savin (1977), Miller et al. (1987), Zachos et al.,

68   (2001, 2008) and Cramer et al. (2009) used the changing ratios of ^{18}O /^{16}O in benthic foraminifera to

69   describe the changing temperature of the world's oceans and the growth of the polar icecaps. For an

70   excellent summary of the science of oxygen isotopes see Grossman (2012a).

71   The oxygen isotope record is strongly biased towards tropical regions and measurements of

72   temperature derived from localities above 40˚ N or S are sparse; therefore, paleotemperature curves

73   that exclusively use $\delta^{18}O$ data (Song et al., 2019; Verard and Veizer, 2019; Veizer and Prokoph, 2015;

74   Grossman, 2012a&b; Royer et al. 2004) are measurements of tropical temperature, not global

75   temperature. Only the Phanerozoic paleotemperature curves of Scotese (2016), Mills et al., (2019,

76   2020), Wing and Huber (2019), and Valdes et al. (2018) (Figure 1), either adjust the isotopic

77   temperatures to compensate for the difference between tropical and global temperatures or use

78   non-isotopic temperature information (e.g., HadCM3 paleoclimate model simulations, Valdes et al.,
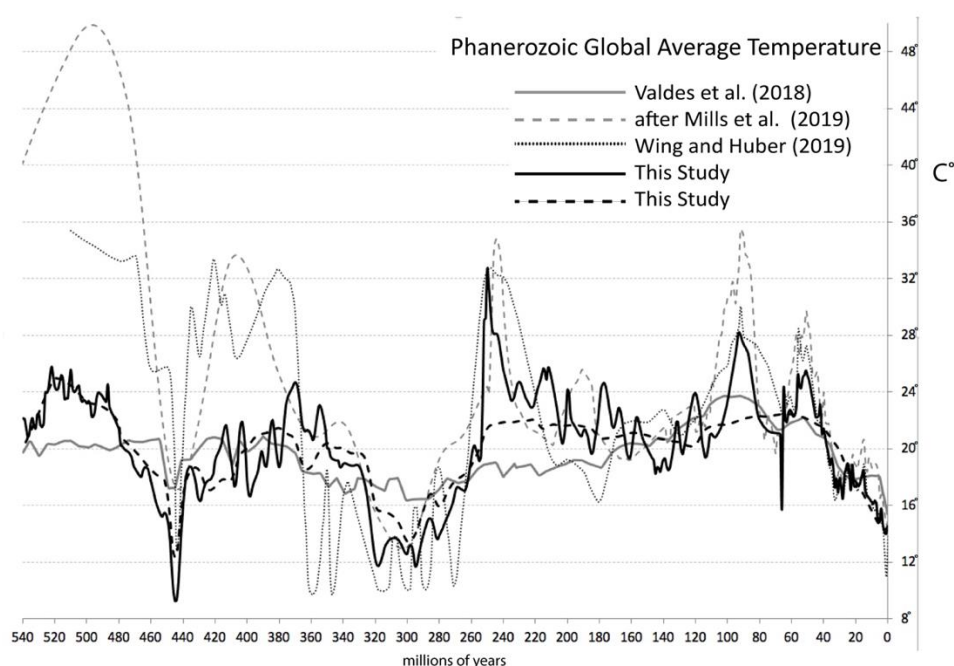
79   2020).

Figure 1. Estimates of Phanerozoic Global Average Temperature (GAT). Sources: Wing and Huber (2019), Valdes et al. (2018), Mills et al. (2019), and This study.

80

81   These curves are in good agreement and show the classic "double hump" Phanerozoic temperature

82   history shown in Figure 2 (Fischer, 1981, 1982, 1984; Frakes, et al., 1992, fig. 11.1; Scotese et al.,

83   1999; Summerhayes, 2015). Temperatures are high during the Early Paleozoic. Cooler temperatures

84   prevail during the Late Paleozoic, followed by warmer Mesozoic and early Cenozoic temperatures,

85 finally returning to cooler temperatures in the Late Cenozoic. This pattern is linked to the "Wegener

86 Supercontinent" cycle (Nance et al., 2014; Van der Meer et al., 2014; 2017), namely: the breakup of

87 the supercontinent, Pannotia, during the latest Precambrian (Powell et al., 1993; Powell, 1995;

88 Scotese, 2009; Nance and Murphy, 2018), the formation of Pangea during the late Paleozoic (~300

89 Ma), its subsequent breakup (~200 Ma), and the assembly of the modern continental configuration.
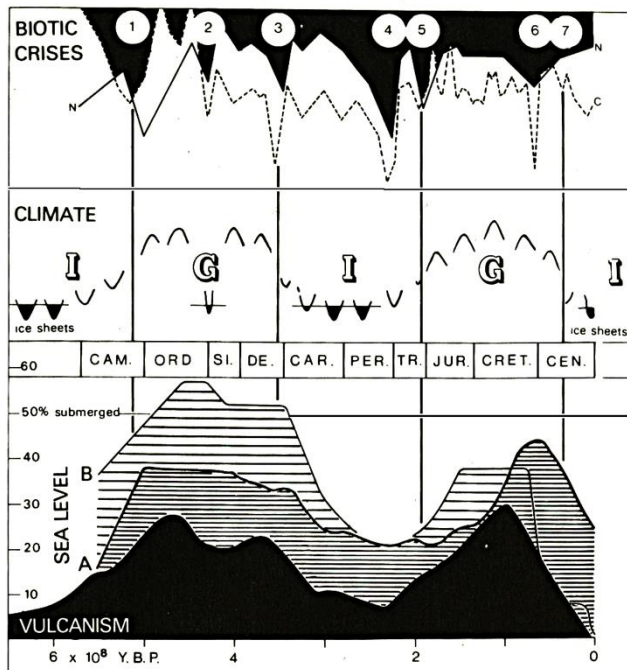
Figure 2. "Double Hump" pattern of Phanerozoic Climate
(Fischer, 1981; 1982), I = Icehouse, G = Greenhouse .

90

91 Specific features that the curves in Figure 1 share in common are:

92 1) A broad sinusoidal pattern with peaks near 20 Ma, 50 Ma, 90 Ma, 245 Ma, 370 Ma, 420 Ma, and

93 500 Ma, with the highest peaks occurring at, 90 Ma, and 245 Ma.

94 2) Broad troughs link the 370 Ma and 245 Ma peaks and the 245 Ma and 90 Ma peaks.

95 3) The three youngest peaks (i.e. 90 Ma, 50 Ma, and 20 Ma) decrease, stepwise, in height.

96 4) The coherence of the curves breaks down during the middle and early Paleozoic. Some curves

97 rapidly trend toward higher isotopic temperatures.

98   5) The temperatures between 330 Ma and 290 Ma (Permo-Carboniferous Ice Age), are ~14˚C on

99   average, but fluctuate 6˚C with a period of ~10 million years.

100 6) A sharp "dip" occurs at in all curves at 445 Ma (Hirnantian Ice Age).

101 The pre-Carboniferous portions of these temperature curves can be divided into two groups: the

102 "hothouse" middle and early Paleozoic versions (Valdes et al., 2018; this study), and the "extreme

103 hothouse" middle and early Paleozoic versions (Mills et al., 2019; Wing and Huber, 2019).

104 It should be emphasized that the paleotemperature curve that we will present here is a "model" of

105 Phanerozoic temperature change. No one line of evidence, such as, lithologic indicators of climate,

106 oxygen isotopic measurements, or CO_2 proxy information (Foster et al., 2017) is sufficient to

107 estimate past temperatures. We combine multiple, independent lines of evidence to produce a

108 synthetic, multi-disciplinary model that describes how global temperature may have varied during

109 the last 540 million years. The temperature predictions made by this model can be used to form

110 hypotheses that can be tested by the acquisition of new $\delta^{18}O$ temperature data, by other

111 independent measurements of paleotemperature (e.g.,Tex 86 or clumped isotope data), as well as

112 the expected effects of temperature on the evolution of life and the environment.

113

114 **2. Methods**

115 **2.1 Derivation of the Phanerozoic Global Average Temperature Curve**

116 Our Phanerozoic Global Average Temperature Curve has been produced by combining: 1) estimates

117 of the changing pole-to-Equator temperature gradient obtained from lithologic indicators of climate

118 (i.e. paleo-Köppen belts), and 2) estimates of tropical changes in temperature obtained from oxygen

119 isotopes. The temperatures obtained from oxygen isotope measurements have been summarized

120 and sometimes temperatures have been modified to better agree with the geological and

121 paleontological record.

122   We only schematically illustrate the extremely rapid (<1 million years), high amplitude temperature

123   fluctuations that occurred during the coldest intervals. These dramatic temperature fluctuations are

124   triggered by variations in insolation due to changes in the three Milankovitch parameters (obliquity,

125   precession, and eccentricity). The effect of on short term climate are discussed in more detail in

126   Kump et al. (1999c), Ruddiman (2001), and Hay (2016).

127

128   **2.2 Estimates of Pole-to-Equator Temperature gradients derived by mapping Köppen Climate**

129   **Belts**

130   Long-term global temperature (>50 million years) is controlled by multiple tectonic and

131   environmental processes that drive the Earth's climate from icehouse to hothouse conditions and

132   vice-versa. The dominant factors are the level of greenhouse gases (principally CO_2), which are

133   regulated by volcanic outgassing and the draw down of CO_2 due to weathering (van der Meer et al.

134   2014, Torsvik et al., 2020) the geographic configuration of the continents and ocean basins

135   (paleogeography and paleoceanography), and the reflectivity of the Earth's surface (albedo). Many

136   of these factors are interconnected by a complex network of positive and negative feedback loops

137   that can accelerate or slowdown changes in long-term global temperature (Hay, 2016; Ruddiman,

138   2001).

139   In this paper we use the geologic record, specifically the paleogeographic distribution of lithologic

140   indicators of climate to map how the Earth's Pole-to-Equator temperature gradient has changed

141   through time.   The expansion, contraction, and shifting position of the Earth's climatic belts

142   provides important insights into the changes in the Earth's long-term climate history.

143   Using modern temperature and rainfall records, we can map five very distinct climatic regions called

144   "Köppen Climate Belts" (Figure 3). The Köppen Climate Belts are defined by seasonal variations in

145   temperature and precipitation (Köppen, 1918). These variations give rise to regional climates and

146   create the mosaic of diverse environments that cover the Earth. These environments include: (A)

147   tropical rainforests near the Equator, (B) desert belts at subtropical latitudes that transition into (C)

148   warm temperate grasslands and forests. In the modern world, as we move poleward, warm-

149   temperate regions are replaced by (D) seasonally warm/cold temperate regions and (E) finally frigid

150   polar regions. These climatic zones extend over the oceans where they are primarily zonal. Each of

151   these climatic zones is characterized by a distinctive, flora, fauna, land-cover, and geology.
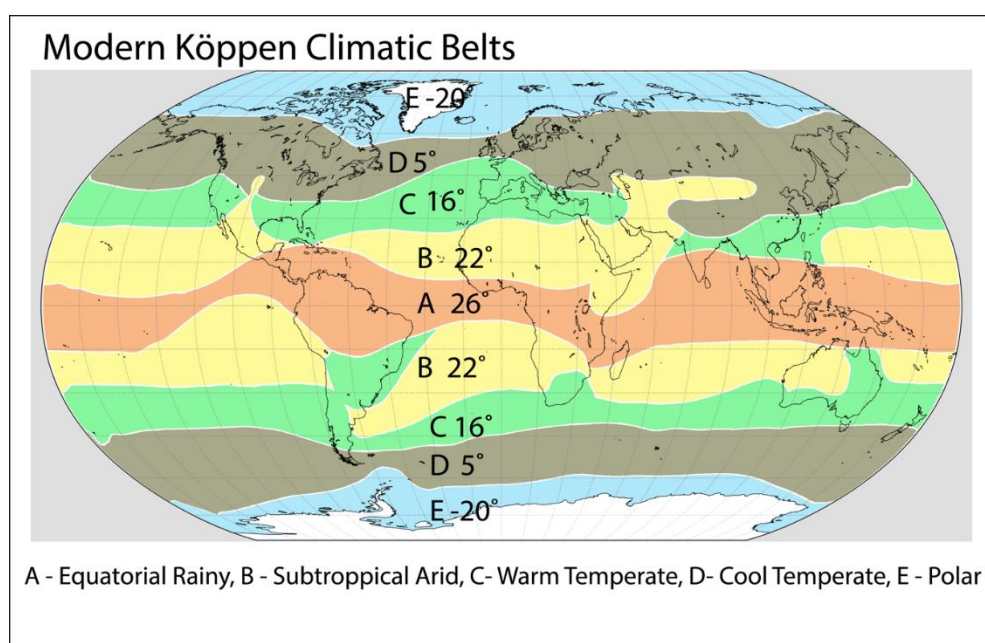
Figure 3. Modern Köppen belts and the average temperature of each belt.

152

153   Using lithologic indicators of climate such as coals, evaporites, and glacial deposits, it is possible to

154   map "paleo"– Köppen Climate Belts for ancient time periods (Ziegler et al., 2003; Boucot et al., 2013;

155   Figures 4 and 5). Over the past 20 years, a global database of over 15,000 lithologic indicators of

156   climate was assembled (Boucot et al., 2013). For a thorough discussion of both lithologic and

157   biological indicators of climate, see Parrish, 1998; Boucot et al., 2013; and Cao et al., 2019. Other

158   important lithologic indicators of climate are: soil minerals such as bauxite, an aluminum ore which

159   forms in warm, wet climates; calcrete, or caliche, which forms in semi-arid regions; and kaolinite

160   which forms in regions with climates that are sometimes wet and sometimes dry (warm temperate

161   climate belt). Dropstones, like tillites, are important indicators of frozen lakes or sea ice. A

162   glendonite it is a pseudomorph of ikaite, a low temperature, hydrated polymorph of $CaCO_3$ that

163   forms at temperatures <4˚ C. Recent experimental data suggests that it may also form at higher

164   temperatures under special conditions (Tollefsen et, 2020). The legend inset on Figures 4 and 5

165   summarizes the association of the various lithologic indicators of climate with warm/cool and
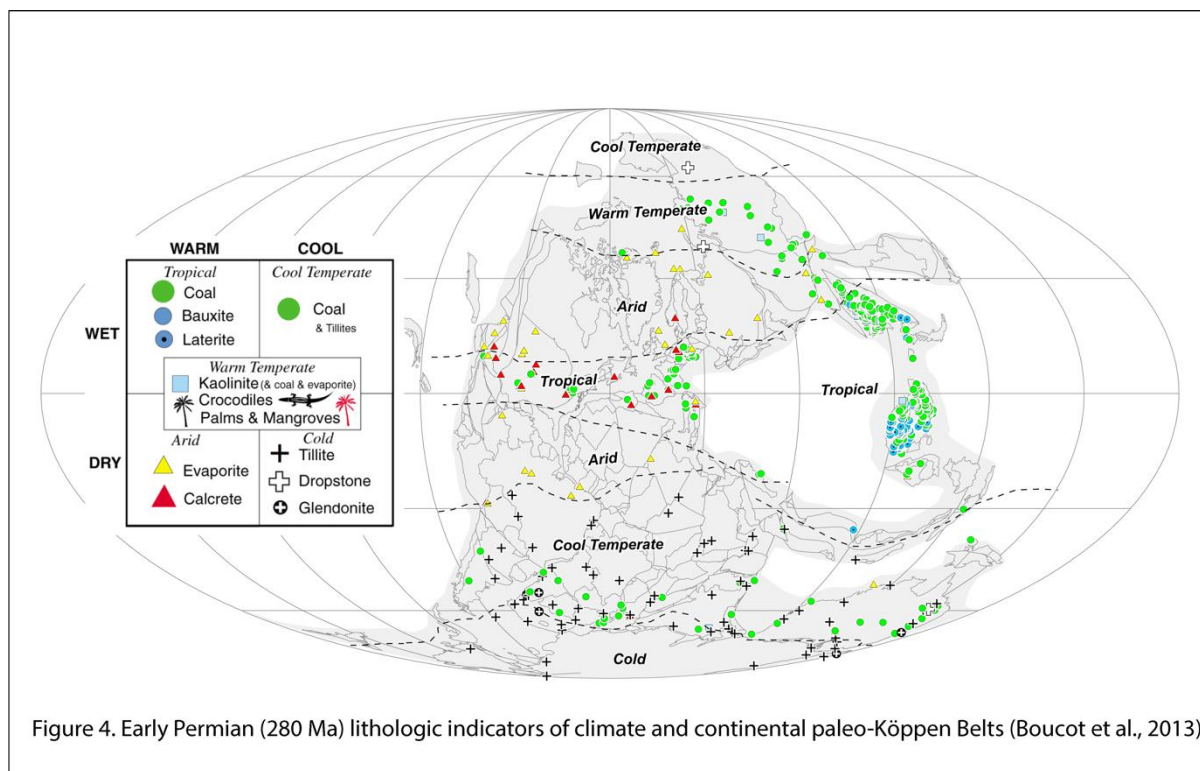
166   wet/dry environmental conditions.

Figure 4. Early Permian (280 Ma) lithologic indicators of climate and continental paleo-Köppen Belts (Boucot et al., 2013).

167

Figure 5. Mid-Cretaceous (100 Ma) lithologic indicators of climate and continental paleo-Köppen Belts (Boucot et al., 2013).
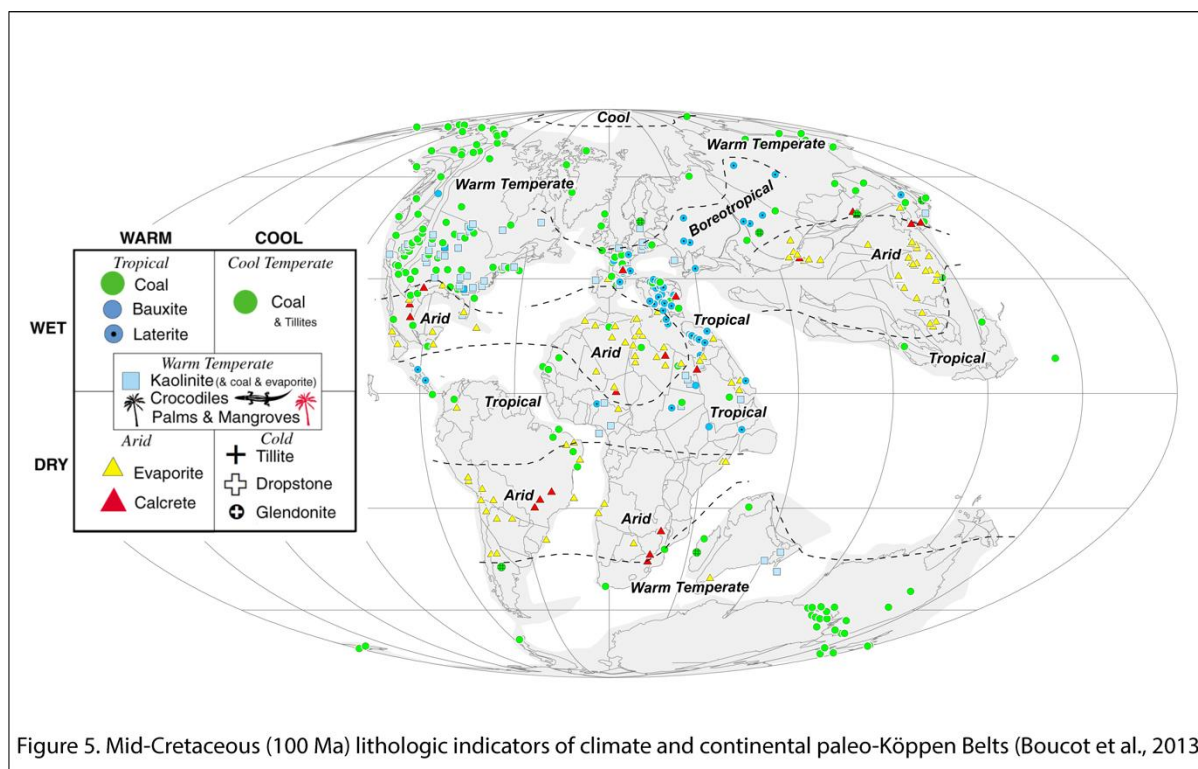
168

169 Bauxites, as a general rule, reflect tropical-subtropical humid, monsoonal conditions. Their modern

170 occurrence is almost entirely restricted to the Equatorial Wet Belt. The occurrence of bauxite

171 deposits in northern Europe and Siberia during the late Jurassic, Cretaceous, Paleocene, and Eocene

172 times (Boucot et al., 2013), is one of the strongest geological indications of warm and wet conditions

173 at high latitudes.

174 When we plot these lithologic indicators of climate on a set of paleogeographic maps we find that

175 there have been times (e.g., Early Permian, Figure 4) when the Earth's climate was much like the

176 present-day "icehouse" world. An icehouse world is simply defined as a time when the Earth is

177 covered by permanent ice at either pole. For permanent ice to accumulate in the polar regions (>67˚

178 N & S) the temperatures must remain below freezing during the summer months. In other words,

179 the global average temperature (GAT) must be less than around 18˚C and the average annual

180 temperature of the polar region must be below -5 ˚C. Though the tropics remain relatively warm

181 (26˚C) in an icehouse world, the polar regions are frigid (-5˚C to - 50˚C).

182   There are also have been times when there was no ice above the polar circle – even during the

183   winter (e.g., Late Cretaceous, Figure 4). During these "hothouse" times, the average temperature of

184   the Earth was generally above 20˚C (68˚F) and the polar regions were relatively warm (5˚C to 15˚C)

185   and no ice could accumulate. It is a well-established fact that no polar ice existed during the

186   Paleocene-Eocene Thermal Maximum (55.6 Ma; McInerney and Wing, 2011) or the Cenomanian-

187   Turonian Thermal Maximum (93 Ma; Ziegler et al., 1985).

188   The long-term temperature curve (Figure 6) was calculated by mapping past extent of the five major

189   Köppen belts using lithologic indicators of climate (tillites, dropstones, glendonites, high latitude

190   mangroves, palms, and crocodiles; temperate coal, evaporites, calcretes, tropical coals, bauxites,

191   and laterites (Boucot et al., 2013)). These paleoclimatic reconstructions, spaced at intervals of 5

192   million years, were used to characterize changes in global temperature along a spectrum of climatic

193   states ranging from Severe Icehouse (GAT = 10˚ - 14˚C) to Extreme Hothouse (GAT = 22˚ - 26˚C;

194   Figure 5). The complete set of more than 100 paleo-Köppen maps illustrating the distribution of

195   lithologic indicators of climate are provided in the Supplemental Materials (Part 3).

Figure 6. Long-Term Phanerozoic temperature trend calculated by estimating the changing area of paleo-Köppen belts
(see Supplementary Materials for data and details of calculations).

196
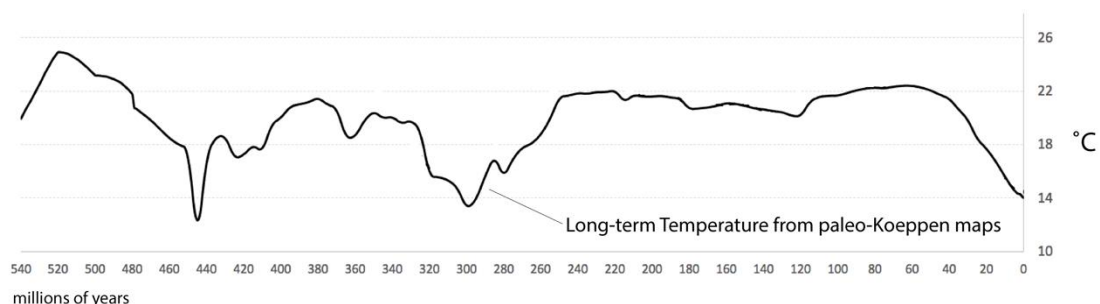
197   The average temperatures of the modern Köppen belts was calculated using the global temperature

198   model of Legates and Wilmott (1990). The Equatorial Rainy Belt has a Mean Annual Temperature

199   (MAT) of 26˚C; the Subtropical Arid Belt's MAT is 22˚C; the Warm Temperate Belt's MAT is 16˚; the

200   Cool Temperate Belt's MAT is 5 ˚C; and the North & South Cold Polar Belts' MAT average -20˚C. The

201   Global Average Temperature (GAT) was then estimated by summing the areas of the 5 major Köppen

202 climatic belts on each of the paleoclimatic reconstruction and then multiplying that area by the MAT

203 of that Köppen belt.   For example, for the modern world (Figure 3): the Equatorial Rainy Belt (A)

204 covers 23% of the Earth's surface, the Arid Belt (B) covers 28%, the Warm Temperate Belt (C) covers

205 20%, the Cool Temperate Belt (D) covers 20%, and the Polar Belt (E) covers 9%. The present-day

206 global average temperature (GAT) = .23*(26˚C) + .28*(22˚C) +.20*(16˚C)+.20*(5˚C) + .09 *(-20˚C),

207 which simplifies to (5.98˚C + 6.16 + 3.2 + 1.0 – 1.8) ˚C = 14.5˚C.

208 On the mid-Cretaceous paleoclimatic reconstruction (Figure 5): the Equatorial Rainy Belt covers 25%

209 of the Earth's surface, the Subtropical Arid belt covers 29%, the Warm Temperate Belt covers 44%,

210 the Cool Temperate Belt covers 2%, and the Cold Polar Belt covers 0%. The GAT = .25*(26˚C)

211 + .29*(22˚C) + .44*(16˚C) + .02*(5˚C) + 0.0, which gives 20˚C. The Boreotropical belt, which is strictly

212 a climatic feature of hothouse worlds is assigned the same average temperature as the Arid Belt.

213 In a similar fashion, the global average temperature for the Early Permian (280 Ma, Figure 4) was

214 calculated as follows: GAT = .20*(26˚C)+.29*(22˚C)+.16*(16˚C)+.30*(5˚C)+.05*(-20˚C), which equals

215 14.6˚C . The global average temperature during the early Permian icehouse was similar to the

216 present-day icehouse.

217 Global temperatures were calculated in this manner for 100 Phanerozoic reconstructions of paleo-

218 Köppen belts (one map ~ 5 million years). For an in-depth discussion of the data and methodology

219 used see the Supplementary Materials. The resulting long-term global temperature curve is shown in

220 Figure 6.

221 The estimates of global temperature obtained in this manner, do not provide a precise or detailed

222 measurement of how the Earth's temperature has changed though time. The width of the Köppen

223 belts are only approximate and are poorly known for older time periods, especially the Early

224 Paleozoic. Though we assume a zonal pattern for the oceans, there are certainly major distortions

225 caused by ocean currents and upwelling (Figure 3). Most importantly, the temperatures assigned to

226   each of the Köppen belts are based on modern icehouse values and may not reflect temperatures in

227   past hothouse worlds.

228   Despite these limitations, the Köppen approach does provide one important bit of information. This

229   procedure tells how the Pole-to-Equator temperature gradient has changed through time. The

230   relative widths of the equatorial wet and the subtropical arid belt do not change significantly

231   through time because they are controlled by Hadley Cell Circulation. The changing in Pole-to-Equator

232   temperature gradient is due nearly exclusively due to the changing width of the Warm Temperate,

233   Cool Temperate and Polar Belts.

234   In icehouse worlds, like the present-day, Pole-to-Equator temperature gradient is very steep. The

235   temperature falls .75˚ - 1˚ C per degree of latitude as we move towards the Pole (e.g., if we start at

236   30˚C at the Equator, we end up with temperatures of -40C˚ to -60˚C at the pole). During hothouse

237   worlds (e.g., Cenomanian-Turonian Thermal Maximum, 93 Ma), the pole-to-Equator temperature

238   gradient was much shallower, approximately .20˚ - .33˚ C per degree of latitude. That means that if

239   we start out at 30˚C at the Equator, the temperature at the Pole would still be well above freezing

240   (0˚ to 12˚C).

241   Figure 7 illustrates the possible range of ancient Pole-to-Equator gradients. The plus signs lie along

242   the modern Pole-to-Equator gradient and describe how temperatures change as a function of

243   latitude. In the present-day world, the temperature near the Equator is 26˚C. The temperature

244   remains nearly constant in the subtropics (0˚ - 15˚ latitude), and then begins to decrease rapidly.

245   Freezing temperatures are reached at 60˚ latitude; falling to -35˚ C at the Poles.
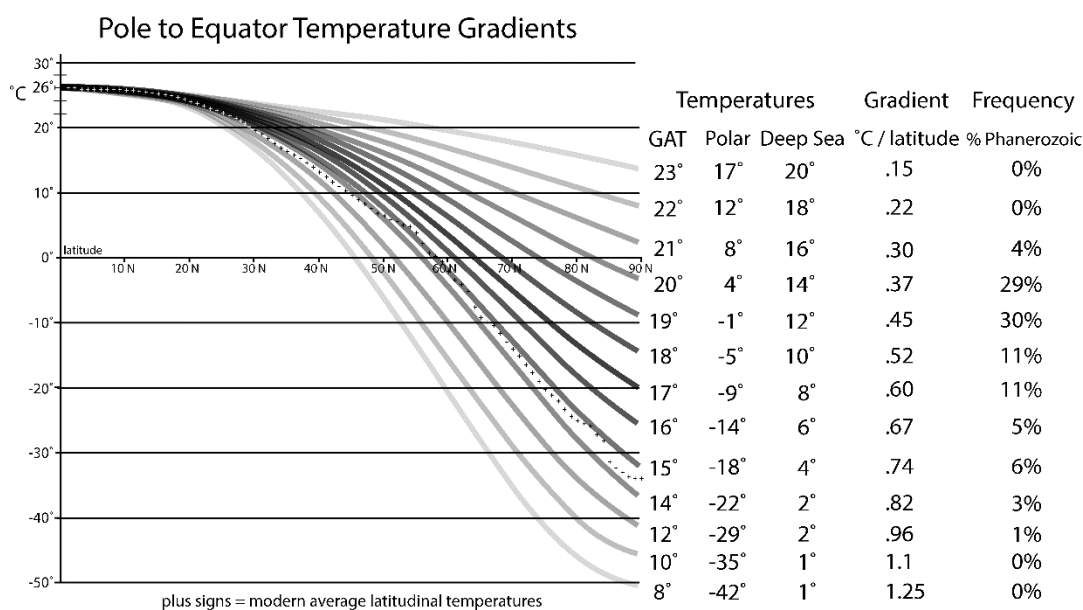
Figure 7. The polar temperature and the Pole to Equator temperature gradient for different Global Average Temperatures (GAT). Polar Temperature = average temperature above 67° latitude (N&S), Deep Sea = the average temperature at the bottom of the oceans (after Valdes et al., 2020). Pole to Equator Gradient = the average change in temperature for every one degree of latitude measured between 30° and 60° latitude. The Pole to Equator temperature gradient is shallow near the Equator and steepens rapidly near the Pole. The plus signs are the combined average temperatures for the present-day northern and southern hemispheres. Frequency % Phanerozoic = the percent of the time during the Phanerozoic characterized by this specific Pole-to-Equator temperature gradient. All of these calculations are based on an average tropical temperature of 26°C (15° N – 15° S).

246

247 The first column labelled "GAT" is the global average temperature obtained by the Köppen

248 technique. The adjacent curve is the Pole-to-Equator temperature gradient associated with that

249 GAT. The modern world (GAT = 14.5°C) falls between the 14°C and 15°C curves. The other columns

250 describe how the polar temperature, the temperature of the deep ocean and the latitudinal gradient

251 (between 30° - 60° latitude), change with each "GAT" curve. These topics will be discussed later. The

252 final column labelled, "Frequency % Phanerozoic", records the frequency of these various GATs

253 during the Phanerozoic. Past hothouse worlds with global temperatures ranging between 19° - 20°C

254 have been the most frequent (~60%). Icehouse worlds with global temperatures similar to the

255 modern world (>15°C) are relatively rare (~10%). It should be noted that some very shallow Pole-to-

256 Equator gradients (GAT > 21°C), though theoretically possible, have probably not been achieved.

257 Conversely, Pole-to-Equator gradients associated with GATs below 10° C, have only been seen in the

258 Snowball Earth worlds of the late Precambrian (Hoffman and Schrag, 1998; 2000; 2002 ; 2009).

259   Though these estimates of Global Average Temperature are based on a methodology rooted in the

260   modern icehouse world, it is possible to make adjustments to these GATs so that they also reflect

261   temperature changes in past hothouse worlds. As can be seen in Figure 7, all of the Pole-to-Equator

262   temperature gradient curves are set to 26°C at the Equator. This equatorial temperature is certainly

263   lower than the equatorial temperatures during hothouse times. In the next section we describe how

264   we used oxygen isotopic data to estimate the change in tropical temperatures through time.

265

266   **2.3 Global Temperature Change (~10 - 20 million years) derived from Oxygen Isotopic Data**

267   In addition to the gradual change in global temperature recorded by the changing pole-to-Equator

268   gradient, we know that the Earth's temperature has varied significantly over periods of 10 – 20

269   million years. The evidence for these temperature changes comes from the measurements of the

270   ratio of ^{18}O /^{16}O (also referred to as $\delta^{18}O$) in the shells and bones secreted by marine organisms

271   (Figure 8).
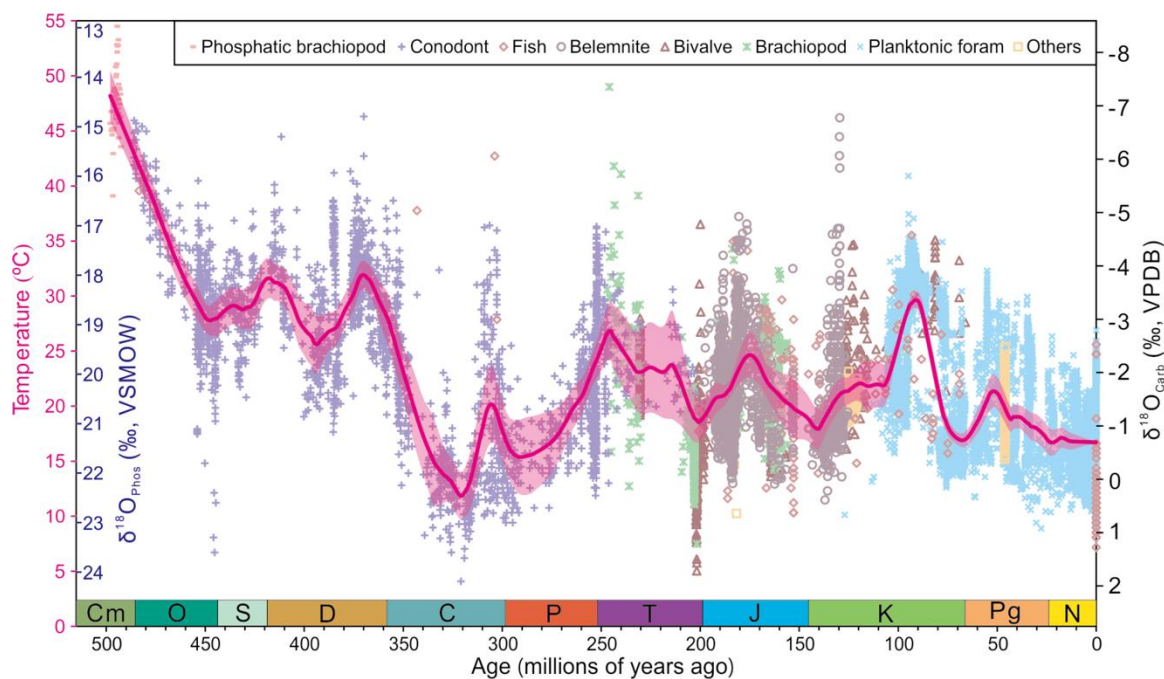
Figure 8. Raw and mean values of oxygen isotopes from phosphatic and carbonate fossils for reconstructing sea surface temperatures over the past 500 million years (modified after Song et al., 2019). The scale of δ18OPhos is used for phosphatic fossils, i.e., phosphatic brachiopod, conodont, and fish. The scale of δ18OCarb is used for carbonate fossils, i.e., belemnite, bivalve, brachiopod, planktonic foraminifer, and others. Magenta curve represents the mean values of sea surface temperatures per million years. Shaded area represents 95% confidence intervals.

272

273   The solid black line in Figure 9A illustrates the isotopic temperature of seawater for the last 500

274   million years based on a compilation of >22,000 oxygen isotope measurements (Song et al., 2019).

275   Isotopic values were converted to temperature using the equation of Lécuyer (2013) for phosphate

276   fossils and by using the equation of Hays and Grossman (1991) for carbonate fossils. Because the

277   samples upon which this curve is based come entirely from tropical and subtropical latitudes (< 40˚

278   N&S), this curve is essentially an estimate of tropical temperatures through time.

279   Each dot in Figure 9A represents the average of all isotopic estimates of temperature that fall within

280   a one million year interval. Error estimates of the average temperature calculation are given in Song

281   et al. (2019). The best-fit curve in Figure 9A was obtained using the Savitsky-Golay smoothing

282   technique which fits successive sub-sets of adjacent data points with a low-degree polynomial by the

283   method of linear least squares (Savitsky and Glay, 1964). We found the Savitsky-Golay method did a

284   better job honoring the data points than either the high-order polynomial or LOESS techniques

285   traditionally employed.

286
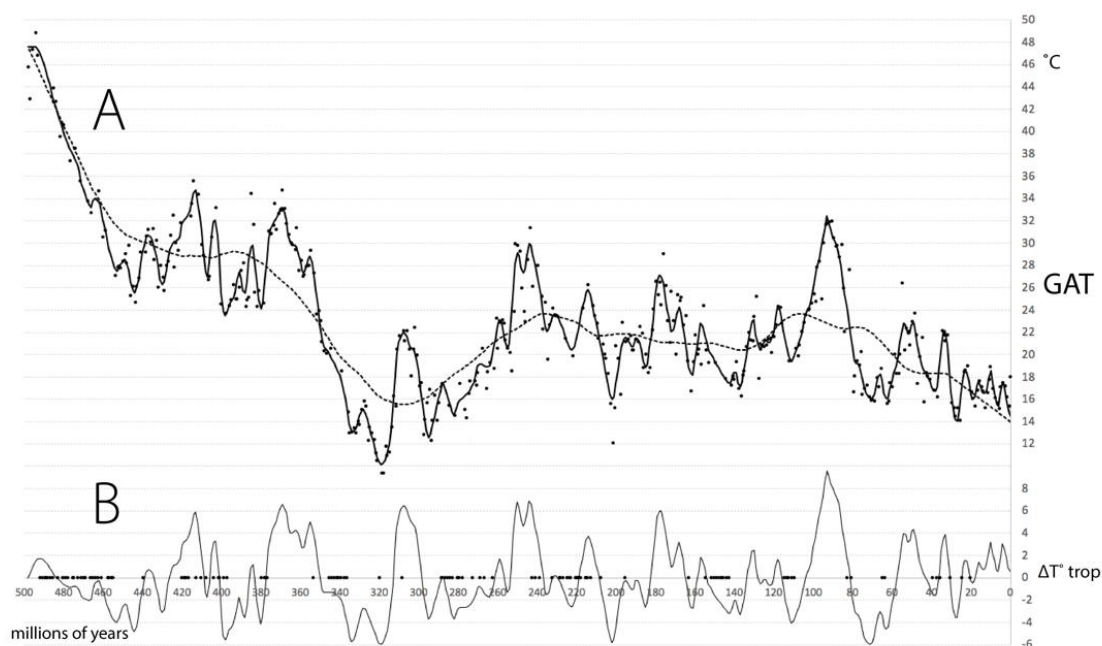
Figure 9. Phanerozoic Isotopic Temperature (Song et al., 2019). A. = Each dot represents the average of all temperatures that fall within a given one million year interval. The best-fit curve was obtained using the Savitsky-Golay smoothing technique (window 11-15, degree 4). B. Change in Tropical Temperature (ΔT˚trop). The black dots along the x-axis are the times when no data are available.

287

288   Though the isotopic temperature curve is relatively flat for much of the Mesozoic and Cenozoic, the

289   curve has a steep, linear negative slope during the early Paleozoic. The isotopic estimates of

290   temperature for these times appear to be much higher (up to +24˚C difference at 500Ma) than the

291   temperatures obtained from lithologic indicators of climate.

292   It should be noted that the isotopic temperatures illustrated in this curve do not take into account

293   regional variations in the isotopic composition of seawater, or proposed Phanerozoic changes in the

294   ^{18}O ^{16}O ratio of seawater. Some researchers believe that there is a long-term trend in the average

295   isotopic composition of seawater (Veizer, 2000; Prokoph et al., 2008; Verard and Veizer, 2019).

296   Others vehemently disagree (Grossman, 2012 a&b). This debate has been going on for more than 30

297   years. It seems incredible that the average temperature of the tropical oceans could have been as

298   high as 50˚C (122˚ F) during the early Paleozoic and late Precambrian. This implies that diurnal or

299   seasonal temperatures were much higher. Even in extreme cases, modern organisms cannot survive

300   when seawater temperatures reach 40˚C (104˚F) (Fraenkel, 1960). Verard and Veizer (2019) propose

301   that a systematic decrease in plate tectonic activity during the last 540 million years may have

302   systematically increased the ratio of ^{18}O to ^{16}O in seawater; however, they admit that the details of

303   the correlation are poor and that tectonic activity prior to the formation of Pangea is not well-

304   known. It may be possible that the $\delta^{18}O$ composition of seawater has not remained constant, nor has

305   it gradually changed in a quasi-linear fashion. Rather the $\delta^{18}O$ could have varied non-monotonically

306   through time.

307   Upon reflection, what may be important is not the "absolute" temperature provided by the isotopic

308   data, but rather the "relative" change in temperature at shorter timescales. For our purposes, the

309   most useful information that can be gleaned from the isotopic temperature record is the change in

310   the tropical temperatures through time (i.e., the $\Delta T°_{trop}$), Figure 9B. In order to calculate the $\Delta T°_{trop,}$

311   we first estimated the long-term isotopic temperature signal by averaging the isotopic data using a

312   60 million year running-average. We chose 60 million years because it best approximated the long-

313   term temperature signal from the Köppen analysis. The 60 million year running average was then

314   subtracted from the best-fit isotopic tropical temperature estimates (Figure 9A, black line) to obtain

315   the $\Delta T°_{trop}$ value (Figure 9B).

316

317   **2.4 Modifying the Isotopic Estimates of Changing Tropical Temperatures Using Geological and**

318   **Paleontological Constraints**

319   The isotopic temperature of seawater can be affected by multiple environmental conditions:

320   hypersalinity or hyposalinity, the presence of continental ice caps, or the water depth at which

321   sampled organisms originally resided (Grossman2012a,b). In this section we review the isotopic

322   estimate of tropical temperature described in the previous section and make modifications based on

323   geological and paleontological constraints.

324 Figure 10 illustrates the changing temperature of the Tropics (ΔT° trop) based on isotopic

325 measurements (dotted line). Superimposed on the dotted line are colored lines that represent

326 seven time intervals when the "raw" isotopic estimates of tropical temperature that do not agree

327 with geological or paleontological information and therefore, must be adjusted or modified. These

328 seven intervals are: the Cambrian, 540 – 485 Ma; the latest Ordovician, 445 -443 Ma; parts of the

329 Permo-Carboniferous, 340 – 275 Ma; the Triassic, 252 – 200 Ma; the Early Cretaceous, 125 Ma – 95

330 Ma; the latest Cretaceous, 80 – 65 Ma; and the Cenozoic (65 – 0 Ma).
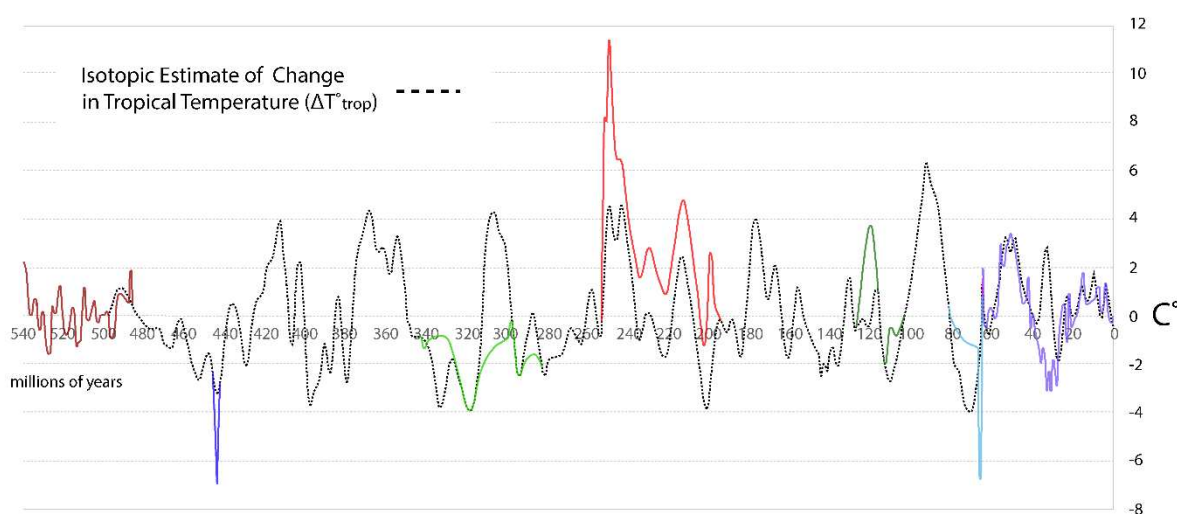
Figure 10. Modifications to the Phanerozoic Isotopic Temperature Curve. The dashed line is the isotopic temperature curve (see Figure 8). The colored lines represent modifications and adjustments made to that curve based on geological and paleontological constraints.

331

332 The procedure that we used to determine whether in isotopic measurements require modification

333 was initially developed at a workshop convened by Scott Wing and Brian Huber at the Smithsonian

334 National Museum of Natural History (April, 2017 & 2018). At those meetings a multidisciplinary

335 group of more than 20 earth scientists convened at the Museum to refine a Phanerozoic

336 paleotemperature curve that eventually became part of an exhibit on Global Warming in the

337 Museum's Earth History Hall (Wing and Huber, 2019). During that meeting participants were invited,

338 based on their geological and paleontological knowledge and expertise, to make additions and

339 revisions to the proposed Phanerozoic temperature curve which was posted as a wall-sized display.

340 The results of that collaborative effort are illustrated in Figure 1 (Wing and Huber, 2019). The

341 criteria used to modify or adjust the isotopic estimate of temperature included the addition of

342   ephemeral events which have not been sampled in the isotopic record (e.g., KT Impact Winter,

343   Permo-Triassic Thermal Maximum), the elimination of spurious thermal maxima during times of

344   icehouse conditions (e.g., late Pennsylvanian thermal maximum), and the elimination of cooling

345   events that would require large, permanent ice caps during times of hothouse conditions (e.g., latest

346   Cretaceous cooling). This same basic procedure was used by the authors to modify and adjust the

347   raw isotopic estimates of temperature so that they better agreed with geological and

348   paleontological constraints. In the following section, we describe the changes that have been made

349   to the raw isotopic estimates and the reasons for these changes.

350   **2.4.1 Cambrian, 540 485 Ma.**

351   There is sparse isotopic data older than 500 million years (Bergmann et al., 2018b; Hearing et al.,

352   2018; Henkes et al., 2018). The data that is available indicates that tropical temperatures were in

353   excess of 40˚C; as noted previously, this is problematic (Fraenkel, 1960). For a more detailed

354   discussion of global temperatures during the Cambrian, see section 5.2.

355   The dark red curve in Figure 10 is a speculative estimate of temperature changes based on the

356   carbon isotope record. They coincide with 10 proposed Cambrian $\partial^{13}C$ isotopic excursions (Zhu et

357   al., 2006). The covariance of $\partial^{13}C$ and $\partial^{18}O$ trends has long been noted (Wenzel and Joachimski,

358   1996; Jenkyns et al., 2002). Approximately 80% of the positive $\partial^{13}C$ excursions are correlated with

359   warmer temperatures (hyperthermals). The correlation is generally attributed to the causal

360   relationship between higher ocean temperatures, the formation of deep water anoxia, and the

361   subsequent preservation of organic carbon.

362   **2.4.2 Latest Ordovician (Hirnatian, 445-443 Ma)**

363   The isotopic estimates of tropical temperatures during the Hirnantian Ice Age (see section 5.3), show

364   a notable dip of 3˚ C. We have exaggerated the dip in temperature to help explain the growth of the

365   massive, Hirnantian south polar ice cap that extended well into the Ordovician tropics (~35˚ S).

2.4.3 Permo-Carboniferous Icehouse

Evaporitic anomalies are known to affect the isotopic measurements made in the great subtropical

epeiric seas of the Paleozoic (Mii et al., 1999). Because evaporation preferentially removed the

lighter isotope of oxygen (^{16}O), the observed isotopic temperature measurements obtained from

organisms living in these evaporitic seas are erroneously too cool. Conversely, freshwater is rich in

^{16}O, so isotopic estimates of temperature made in areas that receive a large influx of freshwater are

erroneously too warm.
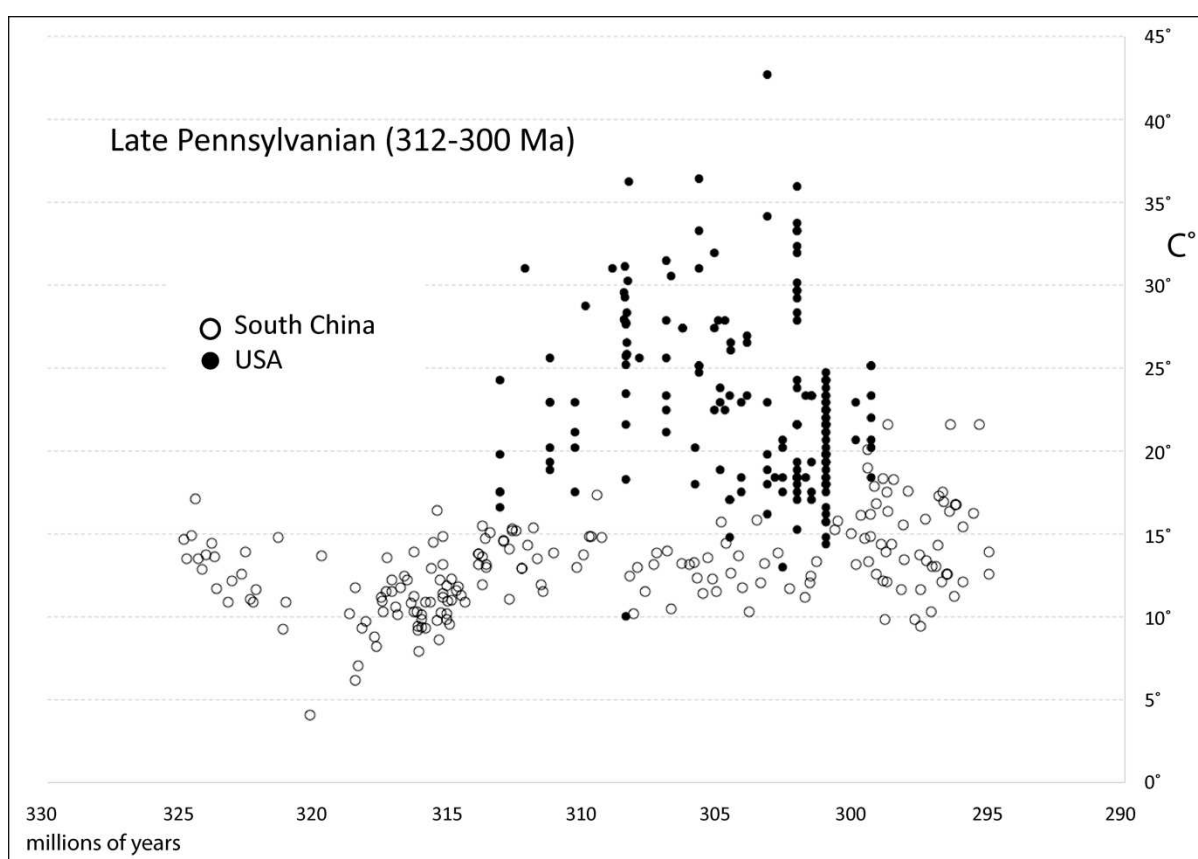
Figure 11. Comparison of isotopic temperature data from the late Pennsylvanian of South China (open dots) and the USA (black dots) (Song et al., 2019).

As Figure 10 shows, a broad temperature peak (dotted line) sits in the middle of the Permo-

Carboniferous Ice Age. A closer examination of the isotopic temperature record reveals that the

isotopic data for the late Pennsylvanian come primarily from South China and the USA (Figure 11).

The isotopic temperatures for China (Chen et al., 2013; 2016) and the USA (Luz et al., 1984;

378   Joachimski et al., 2006; Elrick and Scott, 2010; Rosenau et al., 2014) are very different. The average

379   temperature for the USA data is ~ 25°C, whereas the average temperature for South China is ~13°C.

380   This difference in temperature cannot be explained in terms of latitudinal position. 310 million years

381   ago, both of these regions straddled the paleo-Equator (Scotese, 2014). The difference in isotopic

382   temperatures is more likely due to environmental differences. In the USA, the influx of fresh water

383   rich in ^{16}O from the rising Central Pangean mountain ranges may have altered the ^{18}O / ^{16}O ratio,

384   making the seawater "lighter", giving a false, warmer isotopic temperature. We invoke a similar

385   explanation to explain the much smaller thermal anomaly in the early Permian (~285 Ma).

386   As described above, evaporitic anomalies may cause isotopic temperatures to appear "too cool".

387   We can speculate that this phenomenon may explain the cooler than expected temperatures during

388   the early Carboniferous (~335 Ma).

389   We have applied an ad hoc correction of 4-5°C to the mid-Pennsylvanian isotopic measurements to

390   bring them into line with the geological observations. This adjustment keeps temperatures below

391   the global temperature required to form permanent polar ice caps (see section 3.2). A more modest

392   adjustment of 2-3°C was applied to the earliest Permian (295 – 285 Ma) because extensive south

393   polar glacial deposits indicate the Permo-Carboniferous glacial maximum occurred during the latest

394   Carboniferous – earliest Permian (see section 5.5). Conversely, the isotopic temperatures for the

395   Visean appear to be much too cold suggesting that the Visean represented the depths of the Permo-

396   Carboniferous Ice Age. This is not the case, the Visean was one of the warmest intervals of the

397   Carboniferous (Mii et al., 1999). Consequently, isotopic temperatures have been increased a modest

398   2-3 °C.

399   **2.4.1 Triassic and early Jurassic (252 – 200 Ma)**

400   Three adjustments to the average isotopic temperature were made for the Triassic. The Permo-

401   Triassic Extinction was the greatest mass extinction of the Phanerozoic (see section 5.6). The kill

402   mechanism was massive, global warming (see section 3.1.2). It is likely that average global

403   temperatures reached 40˚C (Sun et al., 2012). The sharp spike in temperatures at the Permo-Triassic

404   have been adjusted accordingly.

405   Global temperatures peaked during the earliest Triassic, fell sharply during the early Triassic (Sun et

406   al., 2012), and extreme hothouse conditions did not ameliorate until the mid-Triassic (Ladinian; see

407   section 5.6). The averaged isotopic temperatures for the late Triassic and early Jurassic are far too

408   low and erroneously suggest possible icehouse conditions. This anomaly is probably due to the fact

409   that some of the isotopic measurements come from belemnites and clams that once inhabited

410   deeper, cooler waters (Dera et al., 2011; Wierzbowski and Joachimski, 2007).   To remedy this

411   mismatch between isotopic and geologic evidence, global temperatures were increased by 2-3 ˚C.

412   Finally, the end of the Triassic was marked by a major extinction event that was most likely triggered

413   by the eruption of the Central Atlantic Magmatic Province (see sections 3.2 and 5.6). There is no

414   oxygen isotope record of this relatively brief event (1-2 million years; Ernst, 2014). To explain the

415   extinction event and other paleontological evidence of global warming, we have added a narrow

416   thermal spike at 200-201 Ma.

417   **2.4.5 Early Cretaceous (130 – 105 Ma) and latest Cretaceous (80 – 65 Ma).**

418   The Late Jurassic – earliest Cretaceous is generally considered to be a relatively cool period with

419   evidence of intermittent polar ice. Towards the end of this interval (~120 Ma), massive volcanic

420   eruptions took place in the Central Pacific (Greater Ontong Java Plateau), along the southern margin

421   of Africa, and forming the Kerguelen Plateau (see section 3.2 for details). The oldest Cretaceous

422   oceanic anoxic event, OAE1a, the Selli/Goguel Thermal Maximum is coincident with these LIP events.

423   Because this oceanic anoxic event is thought to have been triggered by significant global warming,

424   we have added a thermal peak at ~120 Ma. This early Aptian warming was followed by a "cold snap"

425   in the late Aptian – early Albian (see section 5.8). The little "bump" that precedes the Cenomanian-

426   Turonian Thermal Maximum represents the Paquier/Urbino Thermal Maximum (OAE1b) (see Table

427   6).

428   **2.4.6 Cenozoic (65 – 0 Ma)**

429   The classic record of deep ocean temperatures based on benthic foraminifera assembled by James

430   Zachos (Figure 12, Zachos et al., 2001, 2008; Westerhold et al., 2020) provides a framework for

431   describing the temperature fluctuations during the Paleocene-Eocene Hothouse and the Late

432   Cenozoic Icehouse (Koeberl and Montanari, 2009).
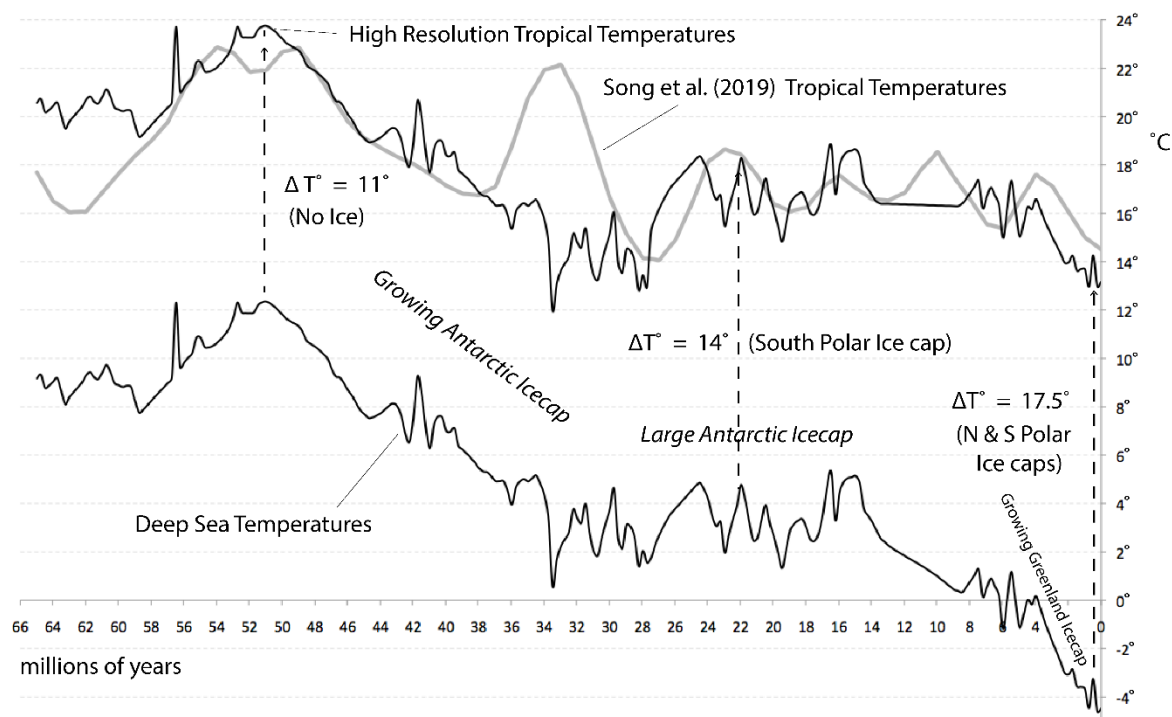
433   Figure 12. Comparison of Cenozoic deep ocean isotopic temperatures and tropical temperatures A. gray line =
low resolution Tropical Temperatures (this study), and the black line = high resolution Δ Tropical Temperatures
for the Cenozoic. B. isotopic temperatures from deep ocean, benthic foraminifera (Zachos et al., 2001, 2008;
Westerhold et al., 2020).

434   The temporal resolution of the Phanerozoic isotopic temperature record from the tropics (Figure 9A)

435   is one control point per million years. While this resolution is adequate for older geological periods,

436   it does not permit a detailed description of Cenozoic temperature changes. We can improve the

437   Cenozoic portion of the temperature curve if isotopic information from deep ocean, benthic

438   foraminifera are used (Zachos et al., 2001, 2008; Westerhold, 2020). The isotopic record from

439   benthic foraminifera provides a nearly continuous record of deep sea temperature changes from

440   beginning of the Cenozoic to the present-day and has a temporal resolution of ~ 100,000 years.

441 As illustrated in Figure 12, we have converted the Cenozoic deep ocean temperatures to a high

442 resolution estimate of global average temperatures by superimposing the high-resolution deep

443 ocean temperature curve on our low-resolution estimate of tropical temperatures. This was done by

444 adding ~11˚C to the pre-ice, Paleogene- early Oligocene portion of the deep ocean temperature

445 curve (65 Ma – 28 Ma), as well as adding ~14˚C to the early and mid-Miocene portion of the deep

446 ocean temperature curve (28 – 14 Ma). The late Miocene to Recent portions of the temperature

447 curve (14 – 0 Ma) were transposed using linear approximation.

448 The overall shape and amplitudes of the superimposed curves are in remarkable agreement (Figure

449 12). The only significant mismatch is the late Eocene – early Oligocene (33 – 38 Ma) portion of the

450 curve. The Oligocene portions of the transposed deep ocean temperature are 6˚ - 8˚ C cooler than

451 isotopic tropical temperatures, which is certainly anomalous. We have chosen to use the updated

452 high resolution Cenozoic tropical temperatures when building our model of Cenozoic global average

453 temperatures.

454 It should be noted that the methods that Hansen et al. (2013) have used to estimate global average

455 temperatures from deep sea temperatures were not used. Though the results he obtained for the

456 Neogene are identical to our estimates, his methodology overestimates global temperatures when

457 applied to hothouse climates.

458 **2.4.7 Summary of Modifications to the Isotopic Temperature Curve**

459 In summary, ~30% of the Phanerozoic isotopic paleotemperature curve was modified using

460 geological and paleontological criteria. In most cases, 2-3˚C were added to or subtracted from the

461 isotopic temperatures.   Three notable exceptions are the Hirnantian Ice Age (-4˚C), the Permo-

462 Triassic Extinction Event (+7 ˚C), and the KT Impact Winter (-6˚C). Two new thermal maxima were

463 added (200Ma, CAMP; 124 Ma, OAE1a), three problematic apparent thermal maxima were removed

464 (315-295 Ma; 285-275Ma, and 40-30 Ma), and two anomalous apparent cool episodes were either

465 reduced (80-65Ma) or eliminated (340-330 Ma).

466   In addition, a high-resolution isotopic curve was used to represent Cenozoic temperatures (see

467   section 5.9) and Cambrian carbon isotope excursions were used as a proxy for temperature (see

468   section 5.2).

469

470   **2.5 Combining the Estimates of the Changes in the Pole-to-Equator temperature gradient with the**

471   **Revised Δ T°$_{trop}$ curve derived from Oxygen Isotope Data**
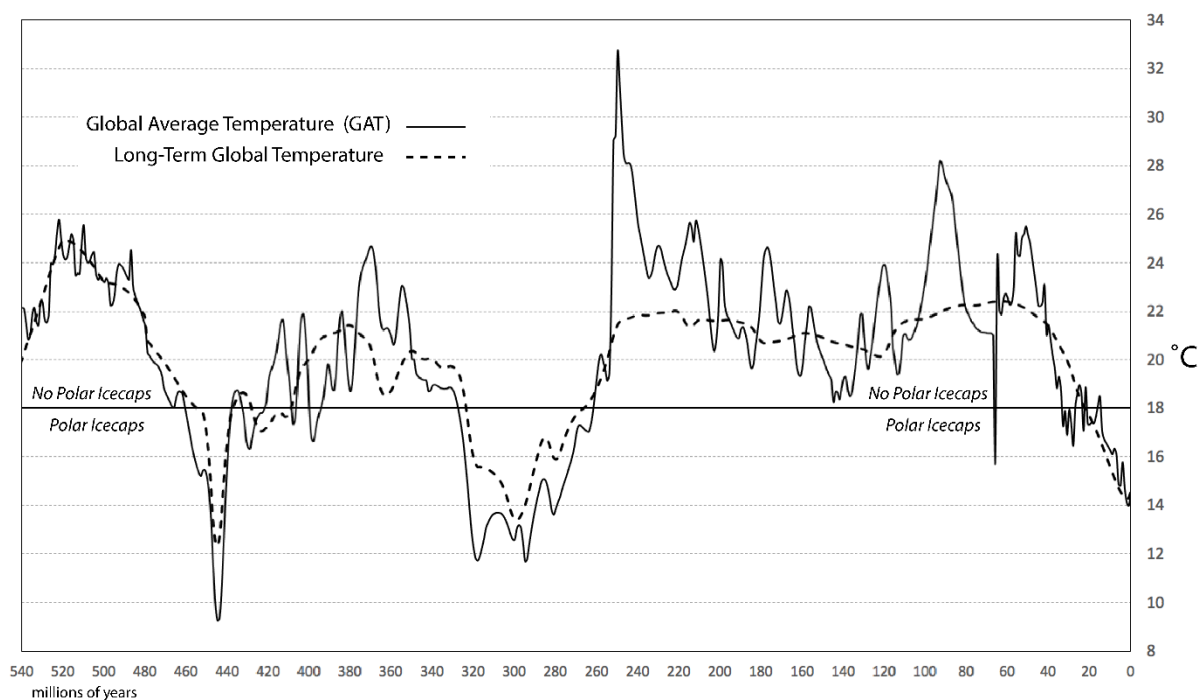
Figure 13. Phanerozoic Global Average Temperature (GAT), blackline = Global Average Temperature, dashed line = Long-term temperature change derived from changes in the pole-to-Equator temperature gradient calculated from the changing area of Köppen Climatic Belt (see Figure 6). When the Global Average Temperature is below 18°C large polar icecaps can form. When the Global Average Temperature is above 18°C large polar icecaps are unlikely to form.

472

473   In the final step of our methodology, we combine the estimates of Global Average Temperature

474   obtained from the changes in the Pole-to-Equator temperature gradient (Figure 6) with the revised

475   changing temperature of the Tropics (ΔT° trop) (Figure 10). The combined geological and isotopic

476   temperature curve (Figure 13) is similar in many respects to the curve derived solely from isotopic

477   data (Figure 9A), but also differs in several important ways.

478   1. The Paleogene portion of the isotopic temperature curve is ~ 1.5˚C cooler than the geologic

479   temperature curve.

480   2. The isotopic temperature curve, overall, tends to indicate slightly warmer temperatures (e.g peak

481   of the Cenomanian-Turonian thermal high).

482   3. The late Carboniferous through Triassic, and the late Jurassic - early Cretaceous portions of the

483   isotopic temperature curve are 1.5˚ - 2˚C warmer than the geologic temperature curve.

484   4. The mid-Ordovician through Devonian portion of the isotopic temperature curve is significantly

485   warmer than the geologic temperature curve (> 6˚ - 8˚C).

486   5. The Cambrian and early Ordovician temperatures indicated by the isotopic temperature curve are

487   nearly double the geologically-inferred (~ 50˚C versus ~ 25˚C, respectively).

488

489   **3. Discussion**

490   A central thesis of this paper is that changes in the Earth's temperature during the Phanerozoic have

491   been caused by factors that act on different time scales. This is not a new idea but rather goes back

492   to the archetypical insights of Alfred Fischer (Fischer, 1981, 1982, 1984), who recognized climatic

493   oscillations and cycles in the biosphere. We recognize three major timescales of temperature

494   change. Long-term changes in temperature (>50 million years) are due to global changes in the rates

495   of volcanic CO_2 degassing associated with seafloor spreading and subduction, as well as long-term

496   changes in the weathering of continents. Long-term changes in temperature (>50 million years) are

497   modeled by mapping the extent of ancient climatic belts (Köppen belts) which vary in response to

498   changes in the Pole-to-Equator temperature gradient. Medium-term changes in temperature (10 –

499   20 million years) can be deduced from changes in the isotopic temperature of the tropical seas.

500   How well does our Phanerozoic temperature model (Figure 13) match the geological record? In the

501   next section we compare the composite Phanerozoic temperature curve with a variety of geological

502   phenomena including: LIP eruptions, bolide impacts, the formation of permanent ice caps, and

503   changes in tropical, deep ocen, and polar temperatures during the Phanerozoic. We also discuss top

504   priorities for future research.

505   **3.1 Short-Term Global Temperature Excursions (< 1 to several million years) due to LIP Eruptions**

506   **and Bolide Impacts**

507   We know that very rapid excursions in temperature can be caused by a variety of tectonic and

508   geological phenomena. For example, global temperatures can rise rapidly due to the release of vast

509   amounts of CO_2 into the atmosphere by eruptions from Large Igneous Provinces (LIP) (Clapham and

510   Renee, 2019). In Figure 14, the black rectangles represent the timing and relative magnitude of 21

511   major LIP eruptions (Ernst, 2014; Ernst and Youbi, 2017). Conversely, temperatures can fall rapidly,

512   creating short-lived icehouse worlds, due to major bolide impact events (e.g., K/T boundary Impact

513   Winter or possibly the Hirnantian Ice Age). Very large impact events (crater size > 150 km) may also

514   trigger large igneous eruptions that create a period of global warming that follows impact-related

515   cooling (e.g., Chicxulub impact event). In Figure 14, the circles illustrate the timing and crater size of

516   the largest, well-established impact events (Spray, 2020).

517

518   **3.2 Large Igneous Provinces (LIPs)**

519   The slow and steady release of CO_2 from the volcanism that accompanies subduction and seafloor

520   spreading is one of the major factors that determine the Earth's thermal equilibrium. This thermal

521   equilibrium changes slowly because the plates move slowly and the continents erode slowly. In

522   contrast, LIPs erupt rapidly, release tremendous amounts of CO_2 and consequently warm the Earth

523   rapidly. The amount of global warming depends on the volume of CO_2 released and the amount of

524   CO_2 in the atmosphere (i.e., climate sensitivity; Royer, 2016). A major LIP eruption during a period of

525   icehouse climate will have a much greater effect than the same LIP eruption during a period of

526   hothouse climate. The warming effects of LIPs will continue as long as voluminous eruptions

527   continue, often for several million years. Beginning soon after eruption, the weathering of subaerial

528   basalts may remove CO_2 from the atmosphere reducing global temperatures to near pre-eruption

529   levels. The rate at which this occurs depends, in part, on the climatic setting of the LIP (Walker et al.,

530   1981; Berner et al. 1983; Marshall et al. 1988; Raymo et al. 1988; Worsley & Kidder 1991; Bluth &

531   Kump 1991; Otto-Bliesner 1995; Gibbs et al. 1999; Berner 2004; Nardin et al. 2011; Goddéris et al.

532   2012, 2014)

533
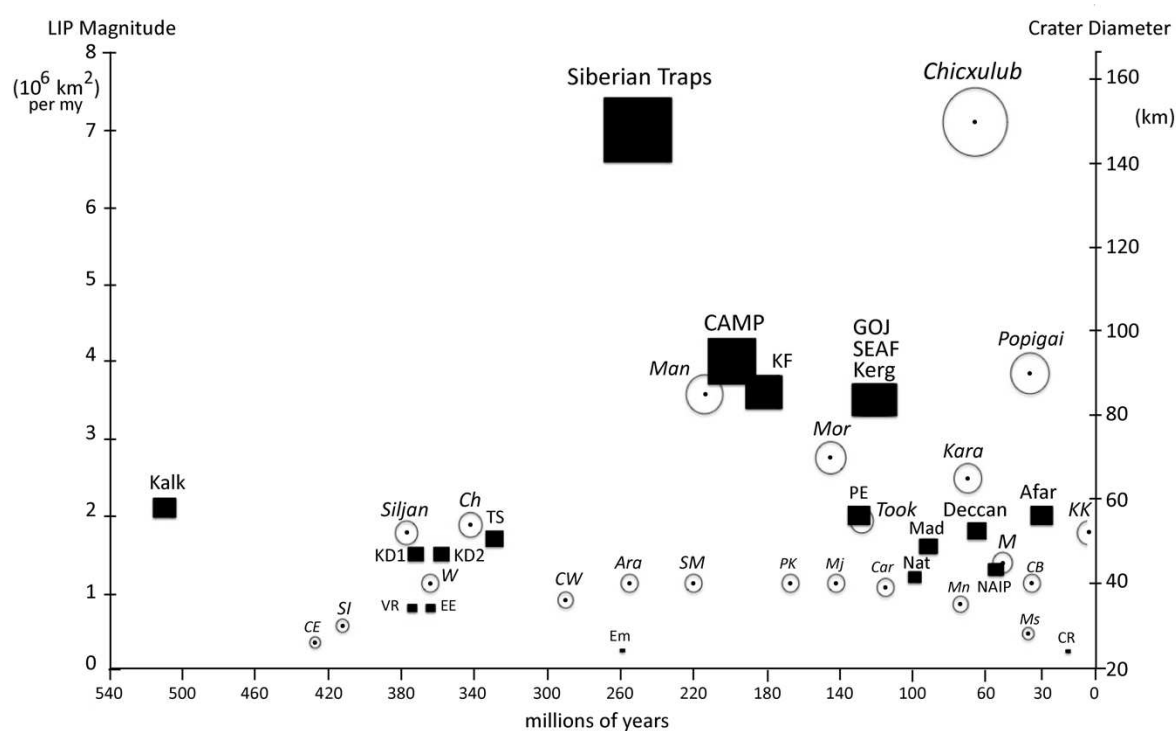
Figure 14. Timing and magnitude of Large Igneous Provinces (rectangles) eruptions and bolide impacts (circles). The size of the rectangles indicates the relative eruptive intensity (106 km2/my) (left-hand scale). See Table 1 and 2 for abbreviations. Sources: Ernst (2014), Spray (2020).

534

535
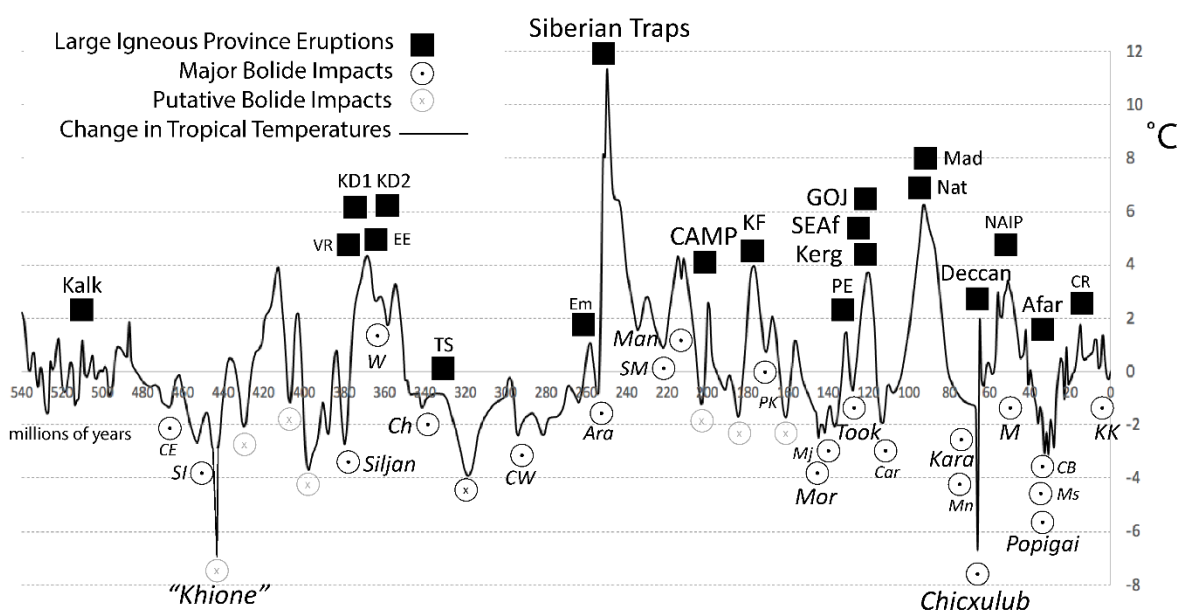
Figure 15. Comparison of the timing of LIPS (black squares, Table 1), large bolide impacts (circles with dots, Table 2), and putative large impact events (light gray circles with x's) with the changes in Tropical Temperature (ΔT°trop). The size of the lettering is roughly proportional to the size of the LIP or bolide imapact. See Table 1 and 2 for abbreviations. Sources: Ernst (2014), Spray (2020).

536

537

538   Table 1 lists 21 of the largest Phanerozoic Large Igneous Provinces (Ernst, 2014; Ernst and Youbi,

539   2017). They are also plotted as black squares in Figure 15. It is clear from a cursory look at Figure 15

540   that there is a strong correlation between warm periods and the eruption of LIPs. 19 of the 21 major

541   LIPS fall within periods of global warming. Most notable are the correlation between: 1) the West

542   Siberian Traps and the Permo-Triassic Thermal Maximum (252 Ma); 2) the correlation between the

543   Barremian-early Aptian Warm Period (125 – 116 Ma) and the synchronous eruptions that formed

544   the Greater Ontong Java plateau (Taylor, 2006), the Southeast African oceanic plateaus, and the

545   Kerguelen Plateau; 3) the Viluy rift and the mid-late Devonian Hangenberg Thermal Maximum (375 –

546   355 Ma); 4) the Karoo-Ferrar LIP and the Toarcian Thermal Maximum (180 Ma) and; 5) the late

547   Paleocene early Eocene Warm Period (58 – 55 Ma) and the eruption of the North Atlantic Igneous

548   Province (NAIP). The one major exception was the East Africa eruptions (Afar LIP) which took place

549   during the period of intense of late Eocene -early Oligocene cooling. Reluctantly, we have excluded

550   the Caribbean LIP (Sullivan et al., 2020) from consideration because the origin of the underlying

551 lithosphere is certainly older (Jurassic?) than the purported age of the LIP (90 Ma), and the age of

552 the surfacing volcanics is not well-constrained.

553 As has been noted by numerous authors, (Kidder and Worsley, 2010; Wignall, 2001, 2015; Rampino

554 and Self, 2015; Bond and Grasby, 2017; Ernst and Youbi, 2017; Clapham and Renne, 2019; Rampino

555 et al., 2019; McKenzie and Jiang, 2019; Schobben et al., 2019; Suarez et al., 2019), the global

556 warming caused by the eruption of large LIPS has often resulted in mass extinctions. LIP eruptions

557 correlate with extinction events during the middle Cambrian (Kalkarindji, 510 Ma); at the Frasnian-

558 Famennian boundary (Kellwasser extinction, 373-372 Ma); during the latest Devonian (Hangenberg

559 extinction, 359-358 Ma); at the Triassic-Jurassic boundary (CAMP, 201 – 200 Ma); the Toarcian

560 extinction (Karroo – Ferrar LIP, 183 – 181 Ma); the Eocene-Oligocene boundary extinction (Afar- E.

561 African Rift, 31 – 29 Ma); not to mention the two greatest extinction events of all time, the Permo-

562 Triassic Mass Extinction (West Siberian Traps, 252 Ma – 251 Ma) and the K/T Extinction (Deccan

563 Traps, 66 Ma – 65 Ma).

564 Though the geochemistry of LIP lavas indicate that most LIPS are derived from deep mantle sources,

565 there remains the possibility that a few of the largest LIPS (e.g., West Siberian Traps, CAMP, and the

566 Greater Ontong Java Plateau ; Ernst, 2014; Ernst and Youbi, 2017) may have been produced by

567 extremely large impact events (crater size > 200 km). Any craters produced by these gigantic impact

568 events would probably have been obscured by the subsequent voluminous volcanic eruptions.

569

570 **3.3 Bolide Impacts**

571 Table 2 lists 29 bolide impact events that generated craters greater than 25 km in diameter (Spray,

572 2020). Figure 14 illustrates the relative size of these craters and the timing of the impact events.

573 The amount of energy generated by an impact event is described by the equation (Hughes, 2003;

574 Rampino, 2020):

575     $E = 9.1 \times 10^{24} D^a$, where E = is the kinetic energy of the bolide impact in ergs, and D = the diameter

576   of the resulting crater.

577   Proposed values for the exponent, a, range from 2.59 (Hughes, 2003) to 3.89 (Melosh, 1989). In

578   either case, it is clear that the energy associated with an impact event correlates with the cube of

579   the impact crater diameter.

580   The amount of aerosols, SO_4, and particulate matter injected into the atmosphere is primarily a

581   function of the energy associated with the impact event. Whether a bolide lands on continental

582   crust or oceanic crust may also affect the character of the impact event. In either case, the cooling

583   effect of impact events drops off rapidly as the size of the bolide decreases. It has been suggested

584   that after the impact of the bolide that formed the Chicxulub crater (150 km), the global mean

585   temperature would have dropped 7˚ - 12˚ C (Vellekoop et al., 2014). By comparison, the impact

586   event that formed the Manicouagan crater in Quebec, which is approximately half the size of the

587   Chicxulub crater, would have generated only 2.5 ˚C of cooling. Impact events that produce craters

588   that are less than 25 km in diameter cause negligible amounts of global cooling (< 1˚C).

589   As illustrated in Figure 15, there are remarkable number of Phanerozoic bolide impacts (circles) that

590   coincidentally occurred during periods of major global cooling (18 of 22). The most notable are the

591   Puchezh-Katunki impact (167 Ma, Middle Jurassic Cool Interval), the Morokweng, Mjolnir and

592   Tookoonooka impacts (145 - 128 Ma, Tithonian- early Barremian Cool Interval), and the Carswell

593   impact (115 Ma, Aptian – Albian Cold Snap). Though the timing of these impact events and the

594   periods of cooling appears to be entirely coincidental, we cannot rule out the possibility that these

595   intense, short-lived cooling events may have triggered ice-albedo feedbacks (Park and Royer, 2011)

596   that accelerated cooling processes already underway.

597   A quick scan of Figure 15 reveals that there are several relatively brief periods of rapid global cooling

598   (-2˚C to -12˚C) that may have been triggered by a bolide impact, but no crater has been associated

599   with these cooling events. This, of course, is not surprising due to the incompleteness of the

600   geological record. The craters that formed during these impact events may have been eroded,

601   tectonically destroyed, or buried beneath a thick pile of sediments. There are no positively identified

602   impact craters in the oceanic basins (Gersonde et al. 1997). Impact events older than 180 million

603   years would have taken place on oceanic crust that has been subducted. Given the proportion of the

604   area of continental crust versus the area of oceanic crust, we would expect that, during the last 540,

605   million years the deep oceans of the Earth were hit by > 20 bolides that could have generated impact

606   craters >50 km in diameter. One or two of these oceanic impacts could have been as large, or larger,

607   than the Chicxulub crater (>150 km).

608   It is possible that as yet unknown bolide impacts may have caused some of the cooling events shown

609   in Figure 15. The most notable putative impact is the "Khione" impact event which could have

610   triggered the latest Ordovician ice age (444 Ma) and mass extinction (Brenchley et al., 1994; Kump et

611   al., 1999a; Sheehan, 2001; Finnegan et al., 2011). The "Khione" (key-OH-nay) impact event is named

612   after the daughter of the Greek god, Boreas, god of winter. Khione is the goddess of snow. The

613   Hirnantian icehouse is especially interesting because it was very short-lived, yet very intense. Ice

614   sheets extended from the South Pole to a paleolatitude of nearly 35˚S (Boucot et al., 2013). The

615   Hirnantian Ice Age is anomalous because it occurred during a time of relatively high global

616   temperatures (GAT = 20˚ - 22˚ C).

617   Other putative oceanic impact events may have caused the rapid drops in global temperature that

618   are observed during the early Devonian (Pragian, 407 Ma), latest Triassic (Rhaetian, 203 Ma), early

619   Jurassic (Pliensbachian, 184 Ma), and mid-Oligocene (28 Ma). These speculative impacts are

620   indicated by the gray circles with x's in Figure 15.

621   As noted earlier, Figure 15 compares the chronology of LIP eruptions (squares) and bolide impacts

622   (circles) with the changes in global temperature. In Tables 1 and 2 we have estimated the

623   magnitude of the warming and cooling effects of these LIP eruptions and bolide impacts,

624   respectively (Black and Gibson, 2019; Vellekoop et al., 2014; Kamber and Petrus, 2019; Suarez et al.,

625   2019). Large LIP eruptions nearly all have significant warming effects (i.e. several degrees

626   centigrade). The cooling effects of most impacts are negligible. Several impacts were large enough

627   that they should have had a noticeable effect on global temperatures (Sudbury, Popigai, Acraman,

628   and Manicouagan). The Chicxulub impact (K/T boundary) and the putative Khione-type impacts

629   undoubtedly had profound effects on global climate, extinction, and the evolution of life.

630   **3.4 Icehouse Worlds**

631   During the past 720 million years, the Earth's climate has transitioned from a frigid icehouse to a

632   steaming hothouse seven times. Three of these icehouse periods took place during the late

633   Precambrian (the Sturtian icehouse, 720 – 660 Ma; the Marinoan icehouse, 635 Ma; and the

634   Gaskiers icehouse, 585 Ma (Ogg et al., 2016). During icehouse intervals, large permanent icecaps

635   occupied either the northern or southern polar regions, or both. These times of icehouse conditions

636   are recorded by glacial debris and tillites on land, dropstones in adjacent deep sea sediments that

637   were released by melting icebergs, and glendonites in shallow marine environments where the

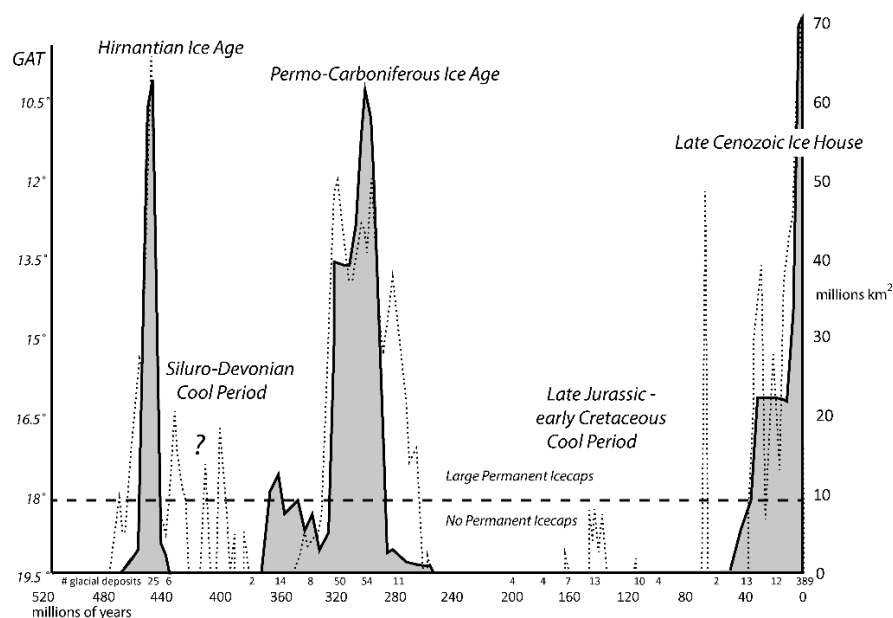638   temperature of the bottom waters is within a few degrees of freezing (Boucot et al., 2013).

Figure 16. Phanerozoic Ice Ages. gray = global area of snow and ice cover (106 km2), dotted line = snow and ice predicted by Global Average Temperatures (GAT < 18°C, Figure 12), numbers = number of glacial deposits (tillites, dropstones, and glendonites, Boucot et al., 2013). Note inverted temperature scale (left side).

639

640   Figure 16 plots the geological record of tillites, dropstones, and glendonites, as well as the area of

641   permanent ice cover during the Phanerozoic (gray shading). Figure 16 also plots the global average

642   surface temperature (GAT) during these icehouse intervals (dotted line). As expected, there is a good

643   correspondence between the times when there is geological evidence for icehouse conditions and

644   the times when the GAT is below 18˚C (dashed line). Permanent polar ice caps can only form if the

645   global average temperature is less than 18˚C. At that global temperature, the average annual

646   temperature of the polar region (>67 ˚ N&S) is not warm enough during the summer months to melt

647   the winter snow and ice. Without a complete summer thaw, snow and ice can accumulate and large

648   ice caps can grow rapidly. Conversely, a large, permanent polar ice cap cannot form if the average

649   global temperature is greater than 20˚C (68˚F). At that temperature, the average annual

650   temperature of the polar regions is ~7˚C, too warm for a permanent ice cap to form. A transition

651   zone exists when global temperature ranges between 18˚C and 20˚C. Snow and ice will be present

652   during the winter months and patches of permanent ice may develop close to the Pole or at high

653   elevations (>500 m).

654   The last three major icehouse intervals (Hirnantian Ice Age (450-444 Ma), Late Paleozoic Icehouse

655   (360 – 285 Ma), and the Late Cenozoic Icehouse (45 – 0 Ma) represent 23% of Phanerozoic time.

656   However, the paleotemperature model presented here predicts that there may have been additional

657   time intervals when icecaps may have existed, albeit briefly. If we accept the correlation of

658   temperature and area shown in Figure 16 at face value, then the largest of these icecaps may have

659   been the half the area of East Antarctica (434 – 385 Ma), the smallest icecaps may have been twice

660   the area of Greenland (150 - 111 Ma). Several of these brief icehouse interludes are plausible

661   because they occur during cool (but not frigid) intervals: 1) the Wenlock Cool Interval (434-326 Ma,

662   2) the Pragian Cool Event (411-406 Ma), (3) the Early-Middle Devonian Cool Interval (401-385 Ma),

663   and 4) the Callovian Cool Event (166-164 Ma), Tithonian-Early Barremian Cool Interval (150-128 Ma).

664   There are sparse, high latitude tillites, dropstones, and glendonites supporting the Jurassic-

665   Cretaceous, and Aptian - Albian cool periods (Boucot et al., 2013). Much of the Siluro-Devonian is

666   considered to be a cool period, but there are no known glacial deposits from this time interval

667   (Boucot et al., 2013).
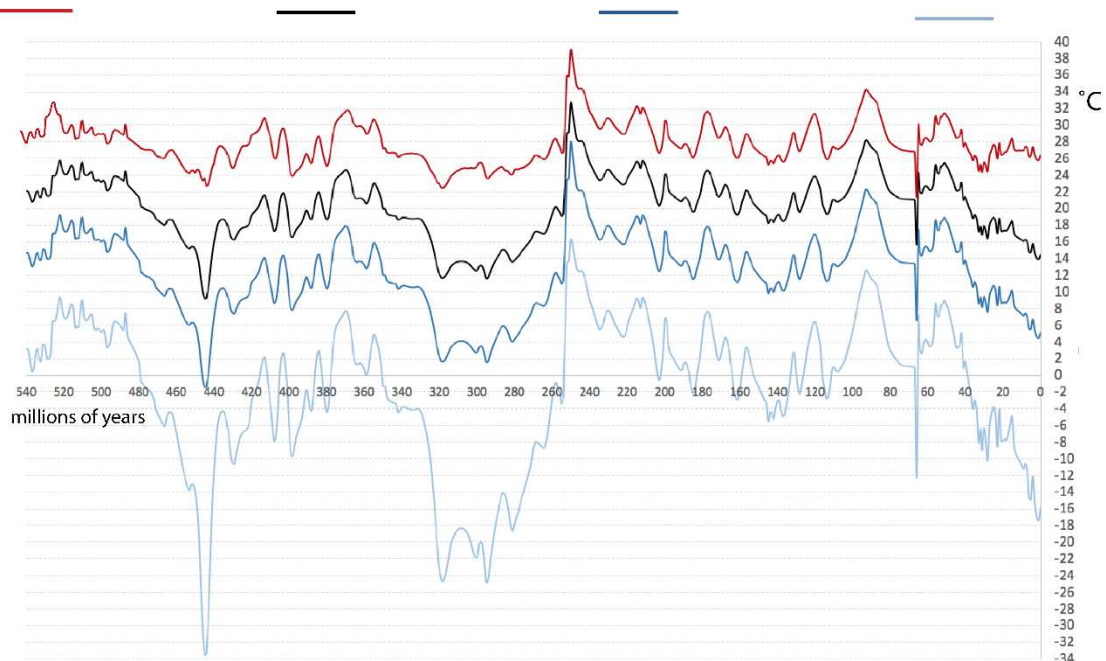
Figure 17. Tropical, Global Average, Deep Ocean, and Polar Temperatures. (a) red line = tropical temperature (15 N - 15 S), (b) black line = global average temperature (GAT), (c) blue line = deep ocean temperatures (after Valdes et al., 2020), (d) light blue line = polar temperature (> 67 N&S).

668

669   **3.5 Tropical Temperatures**

670   Estimating the Phanerozoic history of tropical temperature is straight-forward. Since we know the

671   change in tropical temperature (ΔT°_{trop}, Figure 10), and the present-day average tropical

672   temperature (26°C ; Legates and Wilmott, 1990), then the ancient tropical temperature is simply the

673   sum of the present-day tropical temperature (26°C) and the change in tropical temperature ($\Delta_{trop}T^{\circ}$).

674   Tropical Temperature = 26°C + ΔT°_{trop}

675   For example, the predicted average temperature of the tropical seas during the Paleocene-Eocene

676   Thermal Maximum (55.6 Ma) was 26°C + 5°C = 31°C.

677   The predicted mean temperature of the tropical seas back to 540 Million years is 28˚C. Tropical

678   temperatures, for the most part, are modeled to have fluctuated between 25˚C and 32˚C (Figure 17),

679   with the exception of two periods of extreme warmth (Permo-Triassic (~39˚C) and Cenomanian-

680   Turonian (~34˚C)) and three intervals of extreme cold (Hirnantian(~23˚C), Permo-Carboniferous Ice

681   Age (~23˚C), K/T impact winter (~22˚C))

682

683   **3.6 Deep Ocean Temperatures**

684   During hothouse times, the temperature gradient in the oceans is reduced and the temperature of

685   deep ocean waters can be as high as 20˚C (Valdes et al., 2020). During icehouse times, cold bottom-

686   water is produced adjacent to the polar ice caps and this cold, salty water sinks to the depths of the

687   ocean basins and refrigerates the oceans. In the modern world, the cool North Atlantic and North

688   Pacific bottom waters, and the colder circum-Antarctic bottom-waters form at latitudes of 60˚ N&S

689   (Emiliani, 1954). We assume that this is the approximate latitude where cold deep ocean waters

690   would have originated in the past. We realize that factors, such as the formation of warm, hyper-

691   saline bottom-water in the wide epeiric seas of the middle and early Paleozoic (Chamberlin, 1906;

692   Brass et al., 1982) may also played an important role. Though this estimate of deep ocean

693   temperatures is simplistic and imprecise, it generally agrees with the deep ocean temperatures

694   obtained through climate modeling (Valdes et al., 2020).

695   **3.7 Polar Temperatures**

696   Polar Temperatures were calculated by averaging the temperatures in the polar region above 67˚

697   latitude. The results are shown in Figure 17. For example if the Global Average Temperature (GAT) is

698   14.5˚C (modern value), then the average temperature of the polar region (above 67˚ latitude) is a

699   very cold -20 ˚C. On-the-other-hand, during a hothouse interval like the PETM, the average polar

700   temperature was above 8˚C (Figure 17).

701   It seems rather remarkable that the mean temperature of the polar regions back to 540 Million

702   years is~ 0˚C. This implies that the polar regions have hovered between ice-free and ice-covered

703   conditions. Average Polar temperatures, for the most part, have fluctuated between 12˚C and -12˚C,

704   with the exception of three periods of extreme warmth (Cambrian hothouse (~14˚C), Permo-Triassic

705   extinction (~17˚C), and the Cenomanian-Turonian Thermal Maximum (~13˚C)) and four intervals of

706   extreme cold (Hirnantian Ice Age (~-32 ˚C), Permo-Carboniferous Icehouse (~-24 ˚C), the KT Impact

707   Winter (~-30˚C) and Late Cenozoic Icehouse (~-20 ˚C). Throughout most of the Phanerozoic the

708   average temperature of the southern polar region (-4˚C) has been considerably colder than the

709   average temperature of the northern hemisphere (4 ˚C). Only for a brief interval in the Late Permian

710   was the northern hemisphere colder than the southern hemisphere.

711   **3.8 Top Priorities for Future Research**

712   There are several important issues and areas of research that need further investigation, these

713   include: variations in the isotopic record due to insufficient sampling in time and space and the

714   fundamental changes in the Earth System that have driven temperature change.

715   **3.8.1 Insufficient Sampling in Time and Space**

716   As is the case for any geological investigation, due to the incompleteness of the geological record,

717   there are bound to be gaps in the record of isotopic temperature. The temporal record of isotopic

718   measurements compiled by Song is ~80% complete. That is to say, average isotopic temperatures

719   have only been calculated for 400 of the 500 one million years intervals of the Phanerozoic. The data

720   density can be directly viewed in Figure 9. The black dots along the x-axis in Figure 9B are the times

721   for which there are no isotopic temperature measurements. The missing data is not randomly

722   distributed. There are large data gaps during the: late Eocene (36 - 40 Ma), early Albian (110 - 115

723   Ma), Kimmeridgian -Tithonian (157-143 Ma), Norian (213 – 229 Ma), late Cisuralian (278 - 289 Ma),

724   early Visean (336 - 346 Ma), Emsian (396 – 406 Ma), earliest Devonian (417- 420 Ma), and early and

725   middle Ordovician (455 - 495 Ma). We recommend that these gaps in the data record be priority

726   targets for future research.

727   The sampling of isotopic temperature measurements is also geographically sparse. Most of the

728   sample sites are highly clustered and there are few sample sites from paleolatitudes above 40° N or

729   S. Though the data set can be accurately characterized as "tropical", the possibility remains that for

730   some time periods the isotopic samples may be biased either towards the Equator, or away from the

731   Equator. As we saw in the case of the late Pennsylvanian data, it is also important to identify

732   environmental variables such as salinity or ocean circulation that may affect the isotopic

733   temperature. One of our future research goals is to carefully analyze the isotopic temperature

734   database for these kinds of geographic and environmental biases (Judd et al., 2020).
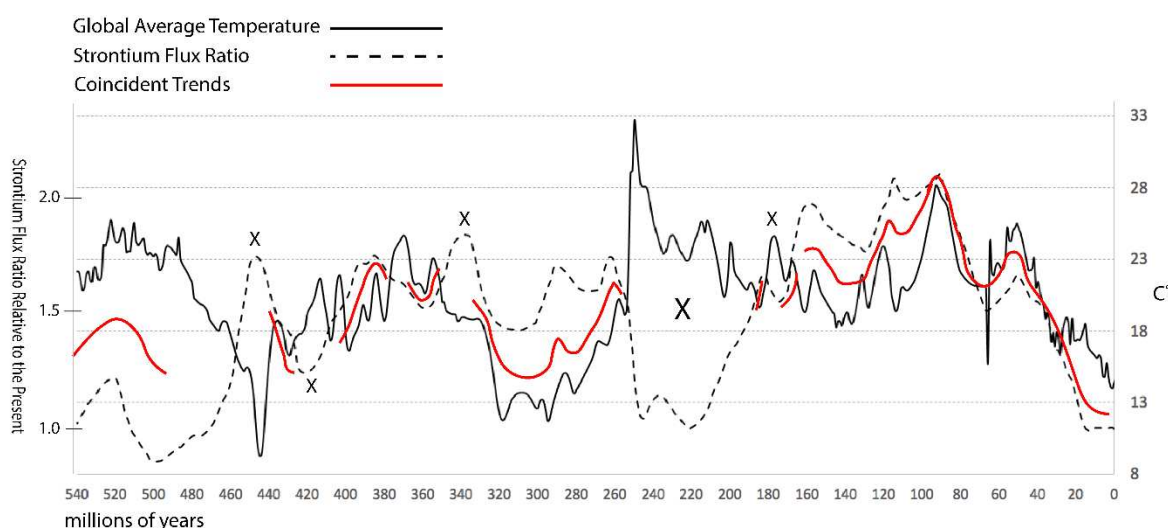
Figure 18. Comparison of Phanerozoic global average temperatures (black line) with strontium flux ratio relative to the present-day flux (dashed line). Red line highlights when the two trends were coincident.

735

736   **3.8.2 Modeling the Fundamental Causes of Global Temperature Change**

737   Correcting the isotopic artifacts and improving the temporal and geographic sampling of isotopic

738   data are important, but they do not address fundamental questions regarding the ultimate causes of

739   changes in the Earth's temperature. Long-term changes in temperature (>50 million years) and

740   medium-term changes in temperature (10-20 million years) are primarily driven by the slow and

741   inexorable changes brought on by plate tectonics and continental weathering (van der Meer et al.

742   2014; Berner, 1994; Brune et al., 2017).

743   To the first order, the amount of CO_2 released into the atmosphere is proportional to the rates of

744   seafloor spreading and subduction (van der Meer et al., 2014). The isotopic composition of the

745   oceans, in particular the ratio of $^{87}Sr/^{86}Sr$, can be used as a proxy for the rate of sea floor

746   spreading (van der Meer et al. 2017). New ^{86}Sr is introduced into the oceans by the weathering of

747   new basaltic oceanic lithosphere which is rich in non-radiogenic, depleted upper mantle-derived

748   ^{86}Sr. On-the-other-hand, continental sources are richer in ^{87}Sr, which is a decay product of ^{87}Rb.

749   Faster periods of seafloor spreading introduce more ^{86}Sr into the oceans. This decreases the ratio of

750   ^{87}Sr to ^{86}Sr of seawater. In Figure 18, the non-radiogenic strontium flux ratio (van der Meer et al.

751   2017) ratio relative to the present (dashed line) is compared to our estimate of Phanerozoic global

752   temperatures (solid line).

753   There appears to be a remarkably good correlation between the global temperature and non-

754   radiogenic strontium flux. For 65% of the Phanerozoic, when the ratio of $^{87}Sr/^{86}Sr$ in the oceans

755   rose or fell (red line), global temperatures also rose or fell. The correlation is especially good for the

756   last 180 million years (breakup of Pangea) and during the Permo-Carboniferous Ice Age (assembly of

757   Pangea, 320 Ma – 255 Ma). For other time intervals, the isotopic and temperature records are in

758   partial agreement (e.g., Cambrian, 540 – 500 Ma; Devonian – early Carboniferous, 400 – 345 Ma).

759   However, there are also significant time intervals when the isotopic and temperature record are

760   completely out-of-synch (marked by X's). Most notable are the Hirnantian Ice Age and the Triassic

761   Hothouse. This suggests that there are other factors besides the volcanic degassing of CO_2 that drive

762   global temperature change. E.g. during the Hirnantian Ice Age, a massive bolide impact and

763   subsequent positive ice-albedo feedbacks might have cooled the Earth despite the fact that plate

764   tectonic activity was high at the time. During the Triassic, on-the-other-hand, the increased degree

765   of aridification due to extreme hothouse temperatures (>40˚C) and mega-monsoonal desertification

766   across the interior of Pangea may have slowed down chemical weathering and allowed CO_2 to build

767   up in the atmosphere which increased global temperatures.

768   We can speculate that other geological processes that occur with rates of change that match the

769   temperature peaks and troughs might also have produced the observed pattern of Phanerozoic

770   temperature change. For example, mountain building and unroofing, periods of ophiolite obduction

771   and subsequent chemical weathering, the opening of oceanic gateways, and some evolutionary

772   events (e.g., the emergence of land plants) all occur on timescales comparable to the rates of change

773   seen in the ΔT°_{trop} curve. A careful and systematic analysis of the evolutionary, paleogeographic,

774   tectonic, paleoceanographic, and environmental changes that may have driven global temperatures

775   will continue to be a fruitful area of research.

776

777   **Part II. Phanerozoic Paleotemperature Timescale**

778   **4. A Phanerozoic Paleotemperature Timescale**

779   The main goal of our research has been to construct a continuous record of temperature change

780   during the last 540 million years (Figures 19-21). In the second half of this paper, we document this

781   record of temperature change with specific paleotemperature events that are analogous to the

782   "golden spikes" (GSSP) of the geological timescale (Gradstein et al., 2012). In some ways, this

783   paleotemperature timescale is similar to the linear magnetic reversal time scale that was assembled

784   at the beginning of the plate tectonic revolution more than 50 years ago. However, instead of

785   normal and reverse magnetic polarity events, the paleotemperature timescale is defined by

786   "warming" and "cooling" temperature intervals called "chronotemps". Our preliminary attempt to

787   identify these warm and cool intervals is illustrated by the cool (black) and warm (white)

788   subdivisions of the global average temperature curve (Figure 19-21).

789   The Phanerozoic paleotemperature timescale can be subdivided into 24 pairs of warm and cool

790   intervals. It should be noted that the resolution of this version of the timescale is 1 million years;

791   rapid temperature excursions shorter than a million years (e.g. PETM, K/T Impact Winter) are not

792   well-resolved. The cool sections of the temperature timescale are labeled c1 – c24. Some of these

793   cooling events are well-known like the Pleistocene Ice Age (c1) or the Hirnantian Ice Age (c22). Other

794   cool intervals are more speculative (c6, Aptian-Albian Cold Snap) and require further investigation.

795   Similarly, the warm intervals are labeled w1 – w24. Some of these warming events are well-known

796   like the Permo-Triassic Thermal Maximum (w13) and the Toarcian Warm Interval (w9). Other warm

797   intervals are more speculative. Also, there is no strict equivalence between two cool intervals or two

798   warm intervals. Two cool intervals may have very different minimum, maximum, and average

799   temperatures (Tables 3 – 7). The same is true for the warm intervals.

800   Each warm and cool time interval is illustrated in Figures 19-21 and supporting references are given

801   in Tables 3-7. These tables provide precise information about the name of each interval, the start

802   time and end time, the Tropical Temperature, the Polar Temperature, and the Global Average

803   Temperature (GAT) of each interval, as well as the timing of major LIP eruptions and bolide impacts.

804   Key citations for each chronotemp are also provided. Each interval may contain several discrete

805   short-term temperature events or excursions. For example during the Paleocene-Eocene hothouse

806   (W5, PEH), there were several thermal maxima, the PETM (W5.9, Paleocene-Eocene Thermal

807   Maximum), EETM (W5.6, Early Eocene Thermal Maximum), and METM (W5.1, Middle Eocene

808   Thermal Maximum). Conversely, a few temperature intervals may be grouped into a larger,

809   geologically meaningful temperature interval; for example, the Late Paleozoic Icehouse (C13-C17)

810   consists of the cool intervals: C13 (Late Permian Cooling), C14 Mid-Permian Cool Interval, C15

811   (Permo-Carboniferous Icehouse), C16 (Early Mississippian Cooling), and C17 (Famennian-Earliest

812   Tournaisian Ice Age), as well as the intervening warm intervals.

813   We have tried to standardize the names and abbreviations used to describe the various

814   chronotemps depending on the length of a temperature event (icehouse, ice age, cool interval, cool

815   event), its magnitude (e.g. thermal maximum, glacial maximum), or if the chronotemp represents a

816   transition between warm or cool time intervals (e.g. warming or cooling). Often discrete

817   temperature intervals are connected by prolonged periods of warming or cooling (e.g Eocene-

818   Oligocene Transition). We have used a gray scale gradient in Figures 19-21 to schematically

819   represent the rate of cooling or warming.

820   We do not use the term "climate" as part of the naming convention to avoid confusion with broader

821   climatic considerations (i.e., precipitation, temperature gradients, equability, etc.), and have avoided

822   the use of other somewhat pejorative terms such as "optimum". Also, whenever possible we have

823   used a specific stage name (e.g., Cenomanian-Turonian Thermal Maximum) rather than a more

824   generic geological description (e.g., Cretaceous Thermal Maximum). We also prefer the term

825   "interval" rather than "period" because of the geological connotation of the latter term. "Events"

826   tend to be temperature phenomena that last only a few million years or less. "Excursions" are

827   events that depart from the norm, i.e, a warm event during a cool interval.

828   Unfortunately, in our attempt to rationalize and standardize the naming conventions, older more

829   established names that have precedence have been mostly discarded (e.g., the Mid-Miocene

830   Climatic Optimum (MMCO) has become the Middle Miocene Thermal Maximum (MMTM).

831   What are the advantages to dividing the timescale into discrete temperature events and giving each

832   of them a number and a name? Some may argue that our state of knowledge is still too primitive

833   and that attempting to build a paleotemperature timescale is premature. We would argue that by

834   constructing a paleotemperature timescale, even if this first version is imperfect, we now have a

835   structure that can be built upon, refined, corrected, and expanded. Also having a paleotemperature

836   timescale is essential if we are to understand the tempo and mode of climate change during Earth

837   history. By characterizing, in a quantitative way, the pattern of paleotemperature change through

838 time, we may be able to gain important insights into the history of the Earth System and the

839 fundamental causes of climate change.

840 **5. Climate Modes of the Phanerozoic**

841 **5.1 Introduction**

842 In this section we will review the evidence used to construct the Phanerozoic Paleotemperature

843 Timescale (Tables 3-7, Figures 19-21). The 24 pairs of warm and cool temperature intervals listed in

844 Tables 3-7 can be grouped into eight distinct "climate modes" (after Frakes, 1989; Frakes et al.,

845 1992; Vaughan, 2007). Four of these climatic groups represent four warm periods in Earth history

846 (Cambro-Ordovician, Siluro-Devonian, Triassic, and mid Cretaceous-Paleogene), three climatic

847 groups represent cold periods in Earth History (Late Ordovician-Silurian, Late Paleozoic, and Late

848 Cenozoic), and one "cool" period made up of mixture of cool and warm intervals (Jurassic – early

849 Cretaceous). These warm and cool modes are similar to the eight warm and cool modes outlined by

850 Frakes et al., (1992). The only major differences are: the Famennian/Tournaisian Ice Age is included

851 in the Late Paleozoic Icehouse, the early Mesozoic warm mode includes only the Triassic, and the

852 Jurassic – Early Cretaceous Cool Period includes the entire Jurassic. The average global temperature

853 during the cool climate modes is 16 ˚C, the average global temperature during the warm climate

854 modes is ~20˚C, and the average temperature during the mixed or mild mode is 17.5˚C which is close

855 to the average temperature of the Phanerozoic (18˚C). It should be noted that the global

856 temperatures during these climatic modes are not entirely warm or entirely cool, but rather

857 alternate between relatively cooler and relatively warmer times.

Figure 19. A Paleozoic Paleotemperature Timescale. white = warm time intervals, black = cool time intervals. Solid black line = Global Average Temperatures (GAT), < 18°C = large permanent, icecaps, > 18°C = no large, permanent icecaps. Light gray jagged lines = a schematic representation of >50 glacial/interglacial cycles during the Permo-Carboniferous. Timescale = International Chronostratigraphic Chart v2020/01. Refer to Table 3 for more information and sources of data for each chronotemp and abbreviations.

858

5.2 Cambro-Ordovician Hothouse (W23 – C24, 458–541 Ma), Table 3, Figure 19

860   The Cambro-Ordovician warm climate mode starts at the base of the Cambrian (541 Ma) and

861   extends through most of the Ordovician (late Darwillian, 458 Ma). Global temperatures were

862   highest during the Cambrian and cooled during the early Ordovician. There is uncertainty regarding

863   the maximum temperatures during the Cambrian because the interpretation of early Paleozoic $\partial^{18}O$

864   values remains controversial.

865   Measurements of the isotopic composition of early Paleozoic seawater are enriched in the lighter

866   isotope of oxygen (^{16}O). This apparent enrichment has given rise to two explanations: 1) the

867   composition of seawater has become systematically enriched in the heavier isotope of oxygen (^{18}O)

868   through time (Kasting et al., 2006; Jaffres et al., 2007) or 2) the composition of seawater has

869   remained constant (Henkes et al., 2018) and therefore the lighter $\partial^{18}O$ values accurately reflect

870   warmer paleo-temperatures during the early Paleozoic and late Precambrian. Recent studies of the

871   $\partial^{18}O$ composition of Precambrian oceans suggest that the composition of seawater has been

872   systematically enriched in the heavier isotope of oxygen (^{18}O) (Galili et al., 2019; Hodel et al., 2018)

873   and therefore, isotopic temperatures for the Early Paleozoic and late Precambrian may be in error.

874   The proponents of the "hot" early Paleozoic temperature model suggest that prior to the Darwillian,

875   tropical sea surface temperatures were 8˚ - 10˚ warmer than modern tropical sea surface

876   temperatures. This interpretation is supported by clumped isotope estimates of tropical

877   paleotemperatures for the late Precambrian (>50˚C; Bergmann et al., 2018a), late Cambrian (32˚C),

878   early Ordovician (36˚C), and middle Ordovician (~40˚C; Bergman et al., 2018b; Henkes et al., 2018).

879   Measurements of $\partial^{18}O$ from pristine, phosphatic euconodont fossils from England give

880   temperatures of 20˚ - 25˚C for near polar latitudes (>70˚S, Hearing et al., 2018). The equivalent

881   temperature at tropical latitudes would have been > 40˚C. According to "hot" model, temperatures

882   would have exceeded 50˚C during the latest Precambrian (Ediacaran; Bergmann et al., 2018a; see

883   Figure 5).

884   The "cool" early Paleozoic temperature model proposes that Cambro-Ordovician tropical

885   temperatures were only modestly elevated (28˚ - 32˚C) in comparison to modern average tropical

886   sea surface temperatures (26˚C) and that cool temperate conditions (4˚ -12˚C) prevailed near the

887   poles (Figure 17). This interpretation is consistent with the occurrence of bauxites (Boucot et al.,

888   2013) and "Bahamian-type" carbonates at low latitudes and the restriction of archaeocyathid reefs

889   to tropical and subtropical latitudes (McKerrow et al., 1992). During the early Paleozoic, temperate

890   and polar latitudes were characterized by clastic facies with strata containing unweathered mica

891   flakes indicative of cooler temperatures (Boucot et al., 2013). The late Cambrian and early

892   Ordovician world was latitudinally subdivided into four distinct trilobite provinces - Bathyurid,

893   Dikelokephalinid, Ptychopygine/Megalaspid, and Calymenacean-Dalmanitacean (Cocks and Fortey,

894   1990; McKerrow et al., 1992) - indicating a moderate pole-to-equator temperature gradient. Landing

895   et al. (2020) also noted that trilobites first appeared in the warm shelf environments of Siberia and

896   Laurentia and later spread to the cooler, higher latitude waters of Baltica and Gondwana. In the

897   "cool" temperature model, global temperatures increased during the middle and late Cambrian as

898   the continental cratons were flooded and the resulting decrease in the planetary albedo warmed the

899   Earth (Landing and Westrop, 2004; Landing, 2012).

900   Temperatures continue to fall during the middle Ordovician (Trotter and Barnes, 2008). Trotter and

901   Barnes (2008) proposed that sustained, cooler tropical temperatures (26˚-30˚C) provided a more

902   hospitable environment for evolutionary innovation and may have been the impetus for the Great

903   Ordovician Biodiversification Event (GOBE; Webby et al., 2004).

904   As noted earlier (section 3.1.2.1), the ~2˚ temperature fluctuations during the Cambrian shown in

905   Figure 19 are speculative. They coincide with 10 proposed Cambrian $\partial^{13}C$ isotopic excursions (Zhu

906   et al., 2006). It should be noted that the global synchroneity of some of these excursions (in

907   particular TOCE and REOCE) has been disputed (Landing, personal communication). The covariance

908   of $\partial^{13}C$ and $\partial^{18}O$ trends has long been noted (Wenzel and Joachimski, 1996; Jenkyns et al., 2002).

909   Approximately 80% of the positive $\partial^{13}C$ excursions are correlated with warmer temperatures

910   (hyperthermals). The correlation is generally attributed to the causal relationship between higher

911   ocean temperatures, the formation of deep water anoxia, and the subsequent preservation of

912   organic carbon.

913   **5.3 Late Ordovician – Silurian Icehouse (C21 – C22, 426-458 Ma), Table 3, Figure 19**

914   The most spectacular, short-term cooling event of the Phanerozoic is the Hirnantian Ice Age (445 –

915   441 Ma; Brenchley, et al., 1994; Sheehan and Coorough, 1990; Sheehan, 2001; Finnegan et al.,

916   2011). Whether the Hirnantian Ice Age (C22) was preceded by a prolonged, stepwise cool-down is

917   still debated. Biostratigraphic (Brenchley et al., 1994) and geochemical data (Finnegan et al., 2011)

918   indicate that the maximum glacial advance was very short-lived (less than one million years; Ling et

919   al., 2019). The repercussions of the Hirnantian Ice age were felt worldwide and left indelible

920   signatures in the geochemical, paleontological (Sheehan and Coorough, 1990; Finnegan et al., 2012),

921   and sedimentary rock record .

922   The widespread occurrence of latest Ordovician tillite deposits (Beuf et al., 1971; Boucot et al., 2013)

923   indicates that ice sheets covered ~50% of Gondwana and extended to latitudes of ~35 S. The

924   enormous extent of snow and ice cover increased the Earth's albedo and triggered ice-albedo

925   feedbacks that rapidly cooled the Earth. The asymmetric latitudinal disposition of the Earth's land

926   masses during the late Ordovician, namely the fact that no large continents occupied the northern

927   hemisphere, probably prevented the Earth from slipping into another "Snowball Earth". Only thin

928   sea-ice accumulated on the freely circulating, open northern oceans. This meant that during the late

929   Ordovician, the northern hemisphere remained relatively warm and prevented a runaway Snowball

930   Earth-like global freeze.

931   Multiple explanations have been proposed for the cause of the Hirnantian Ice Age. Crowley and

932   Baum (1991, 1995) suggested that the growth of the Gondwana ice cap was facilitated by the

933   combination of increased precipitation and cold temperatures along the northern margin of

934   Gondwana. Other authors have invoked increased chemical weathering of young mountains

935   (Taconic ranges) or recently obducted ophiolites that lead to a drawdown in atmospheric CO_2, which

936   promoted globally cooler temperatures (Kump et al., 1995, 1999b,c; Swanson-Hysell and

937   Macdonald, 2017; Landing, 2018). This effect may have been enhanced by the evolution of simple,

938   non-vascular land plants (Lenton et al., 2012).

939   A more spectacular explanation, as discussed in section 3.3, is that the Hirnantian Ice Age was

940   triggered by a bolide impact as large or larger than the Chicxulub impact. There is no geologic record

941   of this massive impact on the continents. Though the impact site may be buried under younger

942   continental strata, it is more likely that the Khione impact targeted the late Ordovician ocean basin

943   and that the impact crater was subsequently subducted. This hypothesis was first proposed in 1986

944   by Kent Colbath who noted the rapid extinction of tropical acritarch genera in the southern

945   Appalachian basin and their subsequent replacement with more cosmopolitan taxa in the earliest

946   Silurian. The extinction of warm, shallow water tropical faunas during the latest Ordovician and

947   their replacement by cool-water benthic taxa or cosmopolitan planktonic taxa has been confirmed

948   by numerous other studies (Sheehan, 2001). The Hirnantian extinction event ranks second in terms

949   of taxonomic severity (~46% marine genera extinct). Only the Permo-Triassic Extinction (58% marine

950   genera extinct; Sepkoski, 1996; Bambach et al., 2004) was more cataclysmic.

951   Though some snow and ice in the polar regions of South America (central Brazil and Bolivia) lingered

952   into the earliest Silurian (Grahn and Caputo, 1992; Grahn and Gutierrez, 2001; Díaz-Martínez and

953   Grahn, 2007), rapid warming during the Llandovery (W22) was followed by a period of slow

954   ecological recovery. The remainder of the early-middle Silurian was characterized by a moderate

955   pole-to-equator temperature gradient which was cool by early Paleozoic standards but warmer than

956   today's world (Moore et al., 1994). Most early and middle Silurian tropical taxa were widely

957   distributed (i.e., cosmopolitan) with the exception of the high latitude, cool-water brachiopods,

958   Clarkeia (southern hemisphere; Boucot, 1990; Benedetto and Sanchez, 1996) and Tuviella (northern

959   hemisphere; Cocks, 1972). Three carbon isotopic excursions occurred during the middle and late

960   Silurian. Two of these excursions (Ireviken and Mulde) bracket the Wenlock and may have been

961   caused by the growth of ephemeral, south polar ice caps (Brand et al., 2006).

962

963   **5.4 Siluro-Devonian Hothouse (W18 – W21, 365-426 Ma) Table 4, Figure 19**

964   The late Silurian through late Devonian hothouse includes four warm intervals (W21 – W18)

965   separated by three relatively cool episodes (C20 – C18). There is no geological evidence for

966   permanent polar icecaps during any of the cool intervals (Boucot et al., 2013). The following

967   summary of the Siluro-Devonian warm mode is based on the isotopic evidence summarized by

968   Joachimski et al. (2009), the biogeographic information synthesized by Stock (2005), the lithologic

969   indicators of climate assembled by Boucot et al. (2013), and a comprehensive synthesis of the

970   Frasnian-Famennian crisis by Racki (2020).

971   The Siluro-Devonian Warm Interval spans the early Ludlow to early Lochkovian time interval

972   (Joachimski et al., 2009; Munnecke et al., 2010; Trotter et al., 2016). It is followed by a pair of brief

973   cooling and warming events during the Pragian (C20) and early Emsian (W20), respectively. The

974   Pragian Cool Event coincides with a widespread fall in sea level (~100m) during the earliest Devonian

975   and the resulting unconformity marks the end of the Tippecanoe Supersequence. This fall in sea

976   level is seen on most continents, but is especially prominent on North America (Schuchert, 1910,

977   1955; Sloss, 1963).

978   After a brief warming event in the early Emsian, temperatures continued to fall during the

979   remainder of the Emsian and into the middle Devonian (Eifelian – middle Givetian; Joachimski et al.,

980   2004, 2009; van Gelderin et al., 2006). The Early-Middle Devonian Cool Interval (C19, GAT = 18.7°C)

981   was followed by a brief, rapid rise in temperature during the late Givetian (W19, Givetian Thermal

982   Maximum, GAT = 21.2°C). Late Givetian warming coincided with the Taghanic onlap (Brett et al.,

983   2009), the start of a global transgressive cycle that would culminate with the highest sea level of the

984   Paleozoic (late Frasnian; Haq et al., 1987; Haq and Schutter, 2009). Global temperatures cooled

985   briefly during the early Frasnian but rose steadily through the remainder of the Frasnian, culminating

986   in the Kellwasser Thermal Maximum (W18.2, 372.5 Ma). A recent synthesis of Frasnian and

987   Famennian isotopic, paleontologic, and tectonic information (Racki, 2020) provides numerous

988   detailed insights into the paleoclimatic events that took place across the Frasnian-Famennian

989   boundary.

990 According to Racki (2020), the Kellwasser Event, also known as the Frasnian-Famennian Extinction

991 Event, can be subdivided into two pairs of rapid warming/cooling events. The first event, the Early

992 Kellwasser Event (373 Ma), may have been triggered by the eruption of the Vilui and Kola LIPS (see

993 Table 1). Shortly thereafter, continued volcanic eruptions (Pripyat-Dneiper-Donets LIP) triggered a

994 second episode of rapid warming and cooling (Late Kellwasser Event; 372 Ma). An alternate

995 hypothesis invoking a bolide impact has also been proposed (McLaren, 1970, 1983). The combined

996 Kellwasser Extinction Event was the fourth most severe extinction event when measured in terms of

997 ecological severity (McGhee et al., 2013). It is associated with highest sea level of the Paleozoic

998 (Johnson, 1988; Johnson et al., 1985; Sandberg et al., 2000) as well as with a dramatic increase in

999 $^{87}Sr/^{86}Sr$ composition of seawater (Zhang et al., 2020).   For a more detailed account of the Frasnian-

1000 Famennian Extinction Event see McGhee(1996, 2005), Racki(2005), and Sandberg(2000, 2002).

1001 The isotopically inferred temperature events outlined above are in good agreement with the

1002 paleoclimatic conditions inferred from paleobiogeography and lithologic indicators of climate.

1003 According to Boucot et al. (2013), the global climatic gradient during the Early Devonian through to

1004 the Eifelian was "moderate", resulting in cool but not freezing temperatures in temperate latitudes.

1005 Like much of the earlier Paleozoic, the high southerly latitudes of Gondwana were characterized by

1006 an exclusively clastic facies with unweathered mica flakes and a distinctive cool-water fauna

1007 (Malvinokaffric province). Conodonts (Girard et al., 2005) and reef-like stromatoporoids (Stock,

1008 2005), which preferred warm waters, were absent from the cooler, temperate shallow seas of

1009 central and southern Gondwana. Global temperatures warmed in the Givetian and Frasnian; and the

1010 Malvinokaffric province was eliminated, replaced by warmer water faunas. Faunas at low latitudes

1011 became less endemic and more cosmopolitan (Stock, 2005). Temperatures continued to warm

1012 throughout the Frasnian and Famennian, until the onset of the Late Famennian Ice Age (discussed in

1013 the next section).

1014

5.5 Late Paleozoic Icehouse (C13 – C17, 253-365 Ma) Table 4, Figure 19

Spanning more than 100 million years, the Late Paleozoic Icehouse was the longest interval of cold climates during the Phanerozoic. Polar ice existed, more or less continuously, at either the South or North Poles with the exception of brief warming events during the Mississippian (Tournaisian and Visean Warm intervals, W17 and W16, respectively), latest Pennsylvanian (Latest Gzhelian Thermal Excursion, C15.3,) and late Permian (Emeishan Thermal Excursion, W14). Global average temperatures ranged from 13˚C during the depths of the Permo-Carboniferous Ice Age to ~22˚C during the Early Tournaisian Warm Interval, the warmest time period during the Carboniferous or Permian.

The Late Paleozoic Icehouse began in the latest Devonian with the formation of a short-lived, medium-sized south polar icecap (Caputo et al., 2008). This ice cap, centered in Brazil, stretched from the proto-Andean mountains, eastward to Rio de Janeiro and Gabon, and northeastward into equatorial west Africa and Niger. The Famennian Ice Age (C17) lasted less than 5 million years and is correlated with the widespread extinction of marine faunas. This late Devonian extinction event ranks fourth in terms of taxonomic severity (50% genera lost; McGhee et al., 2013).

During the early Mississippian (Tournaisian), global climate first warmed (W17), then cooled dramatically (C16; Grossman et al., 2008). Throughout the remainder of the Mississippian, Gondwana moved steadily northward across the South Pole. Ice sheets contracted, then expanded, moving southward into south-central Argentina. The south polar ice cap nearly vanished during the Visean Warm Interval (W16), retreating to the highlands of the proto-Andes of Bolivia and western Argentina, as well as into the remnants of the Pan-African mountain ranges in southeastern Brazil and southwest Africa (Fielding et al., 2008).

These latest Devonian and Mississippian machinations were just a prelude to the impending Permo-Carboniferous Ice Age (313 – 291 Ma.) Beginning in the early Serpukhovian (latest Mississippian, 330 – 326 Ma), the world began to cool once again. However, this time it would remain cool, with Global

1040   Average Temperatures (GAT) less than 18˚C for nearly 80 million years. Starting in the earliest

1041   Pennsylvanian (Bashkirian, 323.2 Ma), a large ice cap began to develop at the South Pole and grew

1042   equatorwards reclaiming the southern reaches of the Amazon basin, crossing south-central Africa,

1043   and extending across Antarctica and most of Australia (Mory et al., 2008). Though often portrayed

1044   as a single, large Ice sheet (Scotese et al., 1999), the South Polar Ice Cap was actually composed of

1045   several growing, glacial nuclei (Fielding et al. 2008, 2010; Montañez and Poulsen, 2013) that

1046   coalesced and expanded equatorwards reaching latitudes of 35˚ south by the mid-Pennsylvanian

1047   (315.2 Ma, Moscovian).

1048   Beginning in the early Moscovian (~313 Ma), the growing South Polar Ice Cap began to rhythmically

1049   wax and wane in synchrony with the changes in the shape of Earth's orbit (Milankovitch cycles;

1050   Milankovitch, 1920; Kump et al., 1999b; Hay, 2016) that regulated the amount of solar energy

1051   received by the Earth. The expansion and contraction of the South Polar Ice Cap caused cyclical

1052   changes in sea level. Paired transgressions and regressions, separated by ~400,000 years, pulsed

1053   across the broad, flat continental cratons generating more than 55 repeating sedimentary packages

1054   called "cyclothems" (Wanless and Weller, 1932). Cyclothems have been mapped across the mid-

1055   continent of North America (Illinois and Mid-Continent Basin; Heckel, 2013) and, to a lesser extent,

1056   the Appalachian basin. Cyclothems have also been identified in similar aged rocks in Donets Basin of

1057   the Ukraine (Montañez et al., 2007; 2016).

1058   The cyclothems are direct evidence of Permo-Carboniferous glacial-interglacial cycles (Wanless and

1059   Shepherd, 1936; Heckel, 1994, 2008; Montañez and Poulsen, 2013) and are identical in nature to

1060   glacial-interglacial sedimentary sequences deposited during the Pleistocene Ice Age (C1.3). The

1061   oldest cyclothems in the mid-continent are middle Pennsylvanian in age (Desmoinesian /early

1062   Moscovian, ~313 Ma; Heckel, 2013). During one particularly warm interglacial episode, the Latest

1063   Gzhelian Thermal Excursion (C15.3), global temperatures may have warmed sufficiently to have

1064   temporarily reduced or eliminated the South Polar Ice Cap (Davydov et al., 2010). However,

1065   whatever the cause, the warmth did not last and glacial-interglacial cycles resumed in earnest. The

1066   youngest cyclothems are early Permian in age (late Sakmarian, 291 Ma). Cyclothems bracket the

1067   coldest phase of the Permo-Carboniferous Ice Age (C15.2, GAT = 13˚C) and disappear shortly after

1068   the Permo-Carboniferous Glacial Maximum (C15.1, 299 – 293, early Asselian – early Sakmarian;

1069   Montañez and Poulsen, 2013).

1070   The deep oceans were "refrigerated" during much of the Carboniferous and early Permian (Valdes at

1071   al., 2020). Cold bottom-waters generated by the seasonal melting of the South Polar Ice Cap filled

1072   the oceans with near-freezing waters from the bottom up. Along some continental margins, this

1073   cold bottom-water was carried to the surface by upwelling. Glendonites formed in shallow marine

1074   sediments where the temperatures were < 4˚C (De Lurio and Frakes, 1999). Glendonites occur in

1075   association with the shallow water carbonates of the Rundle Group of western Canada which was

1076   located near the equator during the Visean (Brandley and Krause, 1994). At south polar latitudes,

1077   numerous glendonites are found in fine-grained clastic sediments deposited along the margins of

1078   Gondwana (Boucot et al., 2013). In addition, the thermal continuity of these cool shelf and deep

1079   shelf environments allowed early Permian marine faunas to migrate freely between cool temperate

1080   southern latitudes, across the tropics, and into cool temperate northern latitudes (Waterhouse and

1081   Shi, 2013; Shi, 2001).

1082   By the middle Artinskian (285 Ma), global temperatures had warmed (W15) signalling the end of the

1083   Permo-Carboniferous Ice Age (Ziegler et al., 1997). Though the large South Polar Ice Cap was gone

1084   for good, intermontane glaciers inhabited the highlands of eastern Australia, the Trans-Antarctic

1085   Ranges of Eastern Antarctica (Frank et al., 2015), and the far northern, mountainous reaches of

1086   Siberia until the end of the Permian.

1087   Though the coldest portion of the Late Paleozoic Icehouse was over, the Permian remained a "cool"

1088   world, with a moderate pole-to-equator temperature gradient (.75˚C per 1 degree of latitude). An

1089   exception was the Emeishan Thermal Excursion (W14), which occurred 260 million years ago during

1090 the late Capitanian. As the name implies, this brief thermal excursion was the result of the eruption

1091 of the Emeishan flood basalts in southwestern China (Ernst, 2014; Rampino and Shen, 2019). The

1092 Emeishan eruption was precursor to the much more massive West Siberian eruptions that would

1093 end the Late Paleozoic Icehouse, terminate the Paleozoic Era, and cause the greatest extinction

1094 event of all time (Erwin, 1993, 1995, 2006).
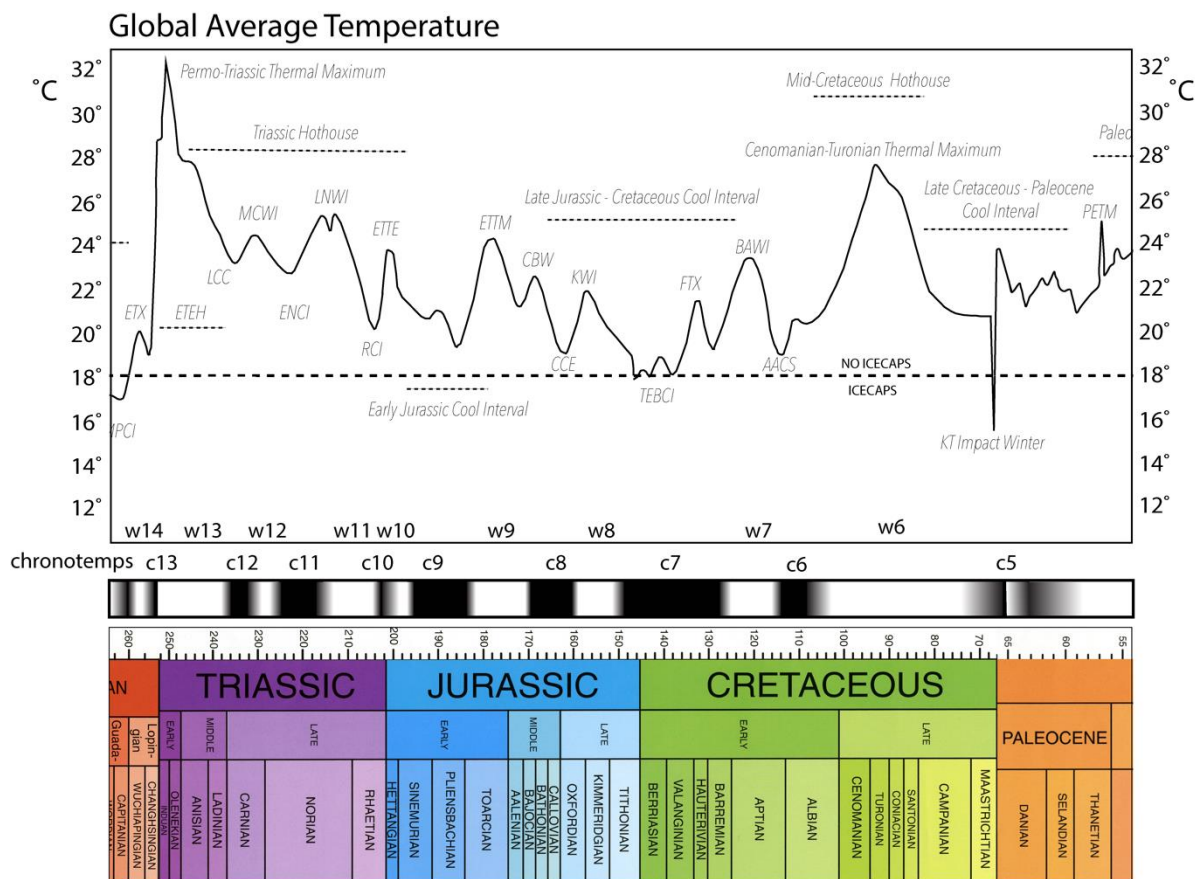
Figure 20. A Mesozoic Paleotemperature Timescale. white = warm time intervals, black = cool time intervals. Solid black line = Global Average Temperatures (GAT), < 18°C = large, permanent icecaps, > 18°C = no large, permanent icecaps. Timescale = International Chronostratigraphic Chart v2020/01. Refer to Table 3 for more information and sources of information for each chronotemp and abbreviations.

1095

1096 **5.6 Triassic Hothouse (W10 – W13, 253 – 199 Ma), Table 5, Figure 20**

1097 At the beginning of the Mesozoic Era, the Earth was an extreme hothouse world with average

1098 tropical temperatures approaching 40˚ C. It now widely accepted that the extreme global warming

1099 the ended the Late Paleozoic Icehouse was caused by the voluminous eruption of the West Siberian

1100 Large Igneous Province (LIP)(Ernst, 2014). During a brief interval (~ 1 million years) at the Permo-

1101   Triassic boundary (252.1 Ma; Kamo et al., 2003), more than 15 million km^3 of basaltic lava flowed

1102   from rifts beneath the West Siberian basin (Reichow et al., 2005, 2009; Saunders et al., 2005) and

1103   the Putorana and Tunguska plateaus. This outpouring buried more than 50% of Siberia (7 million

1104   km^2) under a mantle of basaltic lava 1-4 km deep (maximum 6.5 km). The primoridial, mantle-

1105   derived CO_2 released by these eruptions was supplemented by additional CO_2 derived from the

1106   combustion of thick, buried coal deposits (late Carboniferous – early Permian) that lay along the

1107   subterranean path of the erupting volcanics. The Permo-Triassic Mass Extinction is marked by a ∂^{13}C

1108   spike (Gruszczynski, et al., 1989; Grossman, 1994; Scholle, 1995).

1109   The combined primordial and coal-derived CO_2 (~5000 gigatons) more than doubled atmospheric

1110   levels of CO_2. As a result, tropical temperatures surged from ~25˚C prior to the eruption to nearly

1111   40˚C. This "Super Hothouse" global warming parched life on land and led to the formation of an

1112   anoxic "Strangelove" ocean (Hsu et al., 1985; Kump, 1991; Hotinski et al., 2001; Zhang et al., 2001;

1113   Grice et al., 2005; Heydari et al., 2008).

1114   As the atmosphere warmed rapidly, the greatest effect was felt near the poles. The cold polar air

1115   masses warmed and the cold surface waters at high latitudes, which were the oceanographic engine

1116   that had previously filled the Late Permian oceans with cold oxygenated bottom water, began to

1117   warm and the engine stalled. As the oceans warmed, they became stratified and began to stagnate.

1118   Organic carbon accumulated in the deep ocean, using up any available oxygen. Anoxia set in (Song

1119   et al., 2014). The first ocean to become anoxic from top to bottom was the landlocked PaleoTethys

1120   Ocean (Wignall and Hallam, 1992; Şengör and Atayman, 2009). The NeoTethys soon became anoxic;

1121   the deeper more isolated portions of Panthalassa (between the Panthalassic mid-ocean ridge and

1122   western North America, -were the last to become toxic. The poisonous waters from PaleoTethys,

1123   NeoTethys, and Panthalassa spilled onto the shelves and the Late Permian benthic, neritic, and

1124   planktonic fauna began to die out. The oceans belched great volumes of CH_4 into the atmosphere

1125   and the level of atmospheric oxygen fell. As temperatures rose even higher, the food chain

1126   collapsed and many complex marine ecosystems were wiped out forever.

1127   On land the conditions were just as extreme. The equatorial regions baked. Average summer

1128   temperatures in the subtropical regions of Pangea exceeded 40 degrees C. Near the poles,

1129   temperatures were warm and seasonal changes were nearly eliminated. The movement of warm air

1130   masses and ocean currents into the polar regions made any attempt at winter cooling impossible.

1131   The interior of Pangea, 1000's of kilometers distant from any source of water, was an intolerably

1132   hot, abiotic desert.

1133   A few isolated habitats may have been refugia from the killing heat. Mountains that poked up into

1134   the westerly trade winds still received abundant rainfall during the winter months. The young peaks

1135   of the Cape Mountains in South Africa, where our burrowing mammal-like reptilian ancestors clung

1136   to life, was such a refugia. In the oceans, species that could tolerate the warmer sea surface

1137   temperatures or that could retreat to the cooler, deeper environments on shelf-edge and slope, also

1138   survived. Most importantly, some species that were able to reproduce rapidly and (e.g.

1139   microgastropods) were able to take advantage of the favourable conditions that sporadically

1140   appeared.

1141   The Permo-Triassic Mass Extinction dwarfs all other mass extinction events. During the Permo-

1142   Triassic Mass Extinction, 57% of all marine families went extinct (Sepkoski, 1989), and an estimated

1143   96% of all marine species were extinguished (Raup, 1979), though time percentage has been revised

1144   downwards to 81% by Stanley (2016). At the individual level, this means that 90 - 99% of all living

1145   things were wiped out. The Permo-Triassic Mass Extinction killed more species in low latitudes and

1146   led to a reduced latitudinal diversity gradient in the Early Triassic (Song et al., 2020). Though the

1147   extinction event appears to be geologically "instantaneous" for most taxonomic groups (especially

1148   brachiopods, bryozoans, crinoids, tabulate and rugose corals), arguments have been made that

1149 other taxa were already in decline (e.g. trilobites, graptolites, conodonts). For these "perched"

1150 fauna, the massive warming event was the coup de grace.

1151 Details of the rapid rise and fall of temperatures during the Early Triassic (252-247 Ma) have been

1152 described by Sun et al. (2012). The Early Triassic Extreme Hothouse (W13) was not a single spike, but

1153 rather a series of ups and downs. The Permo-Triassic Thermal Maximum (W13.4, 253-251 Ma) was

1154 followed by a 4˚C fall in temperature (W13.3, Dienerian Cooling, 251-249 Ma), a 6˚C rise in

1155 temperature (W13.2, Latest Smithian Thermal Maximum, 249-248 Ma), and finally a 6˚C fall in

1156 temperature by the end of the Early Triassic (W13.1, Latest Olenekian Cooling, 248-247 Ma).

1157 The severity of the extinction event is revealed by subsequent "gaps" in the fossil record. Plants and

1158 animals were not able to quickly re-establish the complex ecosystems that prevailed before the

1159 extinction event. There are no significant coal deposits (i.e. no complex rainforest ecosystems) until

1160 20 million years after the mass extinction event ("coal gap"; Veevers et al., 1994; Looy et al., 1999).

1161 The Permo-Triassic Mass Extinction Event wiped out diverse tropical and temperate rainforest flora.

1162 It is interesting to note that the forests and scrublands were replenished by a new stock of plants

1163 (pteridosperms and conifers) that evolved from xerophytic ancestors (Zechstein flora) that were

1164 "pre-adapted" to the hot, dry conditions that prevailed in the Early Triassic (Looy et al., 1999;

1165 Hochuli et al., 2010).

1166 In the early Triassic oceans, there were similar reef and chert "gaps". In the shallow marine seas and

1167 on far-flung oceanic atolls, there were no coral reefs (Stanley, 2003). Reef ecosystems did not

1168 become re-established until the Middle Triassic (Ladinian), approximately 14 million years after the

1169 Permo-Triassic mass extinction wiped out tabulate and rugose corals (Flügel, 2002). These new reefs

1170 were built by a new type of coral animal (scleractinians) whose Permian ancestor was a soft-bodied

1171 "anemone-like" anthozoan that did not build limestone reefs. The radiolarian plankton were

1172 similarly wiped out, resulting in the absence of bedded-chert deposits in the deep oceans.

1173   Global temperatures fell during the Middle Triassic, reaching moderate hothouse temperatures

1174   (24˚C) by the end of the Anisian (Trotter et al., 2015). These less extreme temperatures facilitated

1175   the re-establishment of tropical and temperate rainforests, coral reefs, and radiolarian plankton.

1176   The cooling trend continued through the remainder of the Middle Triassic (Ladinian) and into the

1177   early Late Triassic (C12, Ladinian-Carnian Cooling, 242-233 Ma; Trotter et al., 2015). Dense forests of

1178   the tree-like lycopod, Pleuromania, grew near the poles (Ziegler et al., 1994). The pattern of growth

1179   rings in Pleuromania indicates that these plants grew at rates 10 – 100 times faster than modern

1180   trees (Taylor et al., 2000). This suggests that though the climate was highly seasonal, light rather

1181   than temperature was the limiting growth factor.

1182   During the middle Carnian, temperatures warmed (Rigo and Joachimski, 2007; Trotter et al., 2015;

1183   Sun et al., 2016), rainfall increased and the once extensive carbonate platforms along the margins of

1184   southwestern Tethys were flooded by clastic deposits carried onto the continental shelf by hyper-

1185   active river systems (Dal Corso et al., 2018a,b). This dramatic change in climate is known as the

1186   "Carnian Pluvial Event" (W12.1, 233-230 Ma; Ruffell et al., 2015; Ogg, 2015). It has been proposed

1187   that these climatic events were triggered by the formation of the Wrangellian oceanic plateau and

1188   associated volcanic islands (Greene et al., 2008; 2009 a, b, 2010). The CO_2 released by the eruption

1189   of these basalts warmed the atmosphere which in turn intensified the Pangean monsoonal weather

1190   system (Parrish, 1993) and brought more moisture to the interior of the continent. This rainfall fed

1191   new river systems that transported vast amounts of sand, silt, and mud to oceans.

1192   The arrival of huge amounts of sediments shut-down carbonate factories, promoted deep water

1193   anoxia, and increased environment stress. During the Carnian Pluvial Event (CPE), important

1194   ammonite groups became extinct (Balini et al., 2010), conodonts went through a major crisis (Rigo et

1195   al., 2007; Martinez-Perez et al., 2014), and other groups such as bryozoans and crinoids show a

1196   sharp decline (Simms and Ruffell, 1989). On the continents, new floras evolved that were adapted to

1197   wetter conditions (Roghi et al., 2010; Preto et al., 2010; Mueller et al., 2016a,b). After this event,

1198 modern conifers and bennetitaleans evolved (Willis and McElwain, 2002; Kustatscher et al., 2018)

1199 and dinosaurs emerged as the dominant and most diverse terrestrial fauna (Benton, 1993; Bernardi

1200 et al., 2018).

1201 The Mid-Carnian Warm Interval (W12, 234-227 Ma), which included the Carnian Pluvial Interval, was

1202 followed by the Early Norian Cool Interval (C11, 227-217 Ma; Trotter et al., 2015). Global

1203 temperatures spiked again during the late Norian, (W11, 214-209 Ma; Trotter et al., 2015), before

1204 cooling off slightly at the end of the Triassic (C10, Rhaetian Cool Interval, 209-201; Trotter et al.,

1205 2015). The dip in temperatures during the late Norian can be attributed to a brief cooling excursion

1206 triggered by the Manicouagan impact (W11.1 214 Ma; Spray, 2020).

1207 At the end of the Triassic and into the earliest Jurassic (201.3 Ma), flood basalts erupted across a

1208 large portion of North America, South America, Africa, and southern Europe (estimated area ~10

1209 million km^2; Marzoli et al., 1999; McHone and Puffer, 2003; Hames et al., 2003). During a brief

1210 episode of ~600,000 years), the Central Atlantic Magmatic Province (CAMP) released approximately

1211 80,000 gigatons of CO_2 into the atmosphere (Whiteside et al., 2010; Torsvik et al., 2020). This

1212 exhalation of greenhouse gases increased global temperatures 3˚- 6˚ C (McElwain et al., 1999;

1213 Beerling and Berner, 2002; Korte et al., 2009; Dera et al., 2011) giving rise to the brief End Triassic

1214 Thermal Event (W10, 201–199Ma).   This rapid episode of global warming triggered the now familiar

1215 cascade of catastrophic environmental changes: increased terrestrial weathering and erosion

1216 Ahlberg et al. (2003), changes in ocean chemistry (i.e., mercury poisoning; Sanei et al., 2012) oceanic

1217 acidification (Hautmann, 2004, 2008; Clarkson et al., 2015), photic zone euxinia, falling marine

1218 productivity, and possible deep ocean anoxia (Isozaki, 1997).

1219 The End Triassic Extinction (ETE) is ranked third in terms of taxonomic severity, with an estimated

1220 73% extinction of marine genera (McGhee et al., 2013). The once widespread seed fern Dicrodium

1221 disappeared from the fossil record (van de Schootbrugge et al., 2009). There was a 90% species

1222 turnover in the terrestrial megaflora (McElwain and Punysena, 2007). A "fern-spike" suggests

1223   widespread changes in vegetation across Europe and North Atlantic (van de Schootbrugge et al.,

1224   2007; Bonis et al., 2010). A number of non-marine clades of vertebrates went extinct, though marine

1225   reptiles and fish actually flourished (McCune and Schaeffer, 1986; Benton et al., 2013; Friedman and

1226   Sallan, 2012). The End Triassic Extinction was the most severe extinction crisis ever experienced by

1227   scleractinian corals (Flügel , 1994; Flügel and Kiessling, 2002; Kiessling et al., 2002) and was

1228   catastrophic for reef communities. Bivalves and ammonoids, though they were hit hard by the End

1229   Triassic Extinction, had been in decline throughout the latest Triassic (Rhaetian; Hallam, 2002). For

1230   excellent summaries of the events surrounding the End Triassic Extinction, see Preto et al. (2010),

1231   Whiteside and Grice (2016), Bond and Grasby (2017), and Torsvik et al. (2020).

1232

1233   **5.7 Jurassic – Early Cretaceous Cool Interval (C7 – C9, 199-128 Ma), Table 5, Figure 20**

1234   Not all climate modes can be neatly pigeon-holed as either a steaming hothouse world or a frigid

1235   icehouse world. The 71 million year interval from the beginning of the Jurassic (Hettangian, 199 Ma)

1236   through the Early Cretaceous (early Barremian, 128 Ma) is made up of more than 16 distinct warm

1237   and cool events (Table 5). Cooler events make up ~67% of this time interval and justify the

1238   designation "Jurassic – Early Cretaceous Cool Interval", though the appellation, "Jurassic – Early

1239   Cretaceous Mixed Interval" would work as well.

1240   The Jurassic - Early Cretaceous Cool Interval is made up of three cool, but not cold, intervals

1241   separated by two warm intervals. Both of these warmer intervals, the Toarcian Warm Interval (W9)

1242   and the Kimmeridgian Warm Interval were hothouse worlds with average global temperatures of

1243   22˚C. The average global temperature during the Jurassic – Early Cretaceous Cool Interval was a

1244   relatively mild 17.5˚C, which is close to the average temperature for the entire Phanerozoic (18˚C).

1245   The Early Jurassic Cool Interval (C9, 199-183 Ma) and the Middle Jurassic Cool Interval (C8, 174 – 164

1246   MA) are both characterized by moderate pole-to-equator temperature gradients with annual

1247   average polar temperatures several degrees above freezing. Dropstones and glendonites found in

1248   northeastern Siberia (Boucot et al., 2013) are evidence of cold winters in the northern hemisphere

1249   during much of the early and middle Jurassic (late Pliensbachian – early Bathonian). The winter snow

1250   and ice, however, did not persist. The warm summers melted any seasonal snow and ice, preventing

1251   the growth of permanent ice caps in either hemisphere (Sellwood and Valdes, 2006).

1252   Distinctive Jurassic plant groups occupied different latitudinal climatic zones. The greatest diversity

1253   of plants occurred at mid-latitudes (40˚ N&S) where forest were composed a mixture of ferns,

1254   cycads, sphenopsids (like horsetails), pteridosperms (seed ferns), and conifers (Rees et al., 2000).

1255   The equatorial regions, which were sparsely populated, were hot and dry and dominated by

1256   xeromorphic (arid-adapted) forms, small-leafed conifers, and cycads. Large-leafed conifers and

1257   deciduous gingkos grew in the polar regions (Rees et al., 2000).   These plant groups suggest that the

1258   tempemperatures were seasonally cold, but not frigid. Estimates of tropical seawater temperatures

1259   from $\partial^{18}O$ measurements are 4˚ to 6 ˚C cooler than modern tropical temperatures (Dera et al., 2011)

1260   indicating a moderate pole-to-equator temperature gradient.

1261   The Early Jurassic Cool Interval (C9) was followed by the Toarcian Warm Interval (W9), during which

1262   temperatures spiked 4˚- 8˚C (Dera et al., 2011). This warm pulse has been attributed to increased

1263   atmospheric CO_2 arising from the eruption of the Karroo-Ferrar LIP (Pankhurst et al., 1998, 2000;

1264   Elliot et al., 1999; Courtillot and Renne, 2003; Jourdan et al., 2005; Ernst, 2014; Ernst and Youbi,

1265   2017). The global nature of this warming event is recorded by widespread oceanic anoxia (Toarcian

1266   OAE; Jenkyns et al., 2002; Jenkyns, 2010; van de Schootbrugge et al., 2013).

1267   Much has been made of the extremely arid conditions and unbearable heat of equatorial and

1268   subtropical Pangea (30N to 30 S). By modern standards, the climate at low latitudes during the

1269   Toarcian Warm Interval was unbearably hot. Average equatorial sea surface temperatures which

1270   were the warmest of the Jurassic exceeded 30˚ C and temperatures in the interior of Pangea often

1271   exceeded 40˚ C (Crowley, 1994). The intense summer heating of the large land areas north and

1272   south of the Equator strongly deflected the Intertropical Convergence Zone (ITCZ) during the

1273   summer months. This modification of the basic Hadley Cell circulation pattern has been called

1274   "mega-monsoonal" atmospheric circulation (Parrish 1993). Megamonsoons resulted in drier

1275   conditions along the Equator and the formation of a broader Subtropical Arid Belt.

1276   Though the equatorial and subtropical regions of Pangea were arid during the Early Jurassic, most of

1277   the world was covered by lush, habitable forest vegetation (Rees et al., 2000). Abundant Early

1278   Jurassic coal deposits are found in both the warm and cool temperate belts (up to 60 N& S) (Boucot

1279   *et al.*, 2013). Bauxite deposits, indicative of warm and wet conditions, are found in Europe and west

1280   central Asia (Kazakhstan) (30N - 45N).

1281   The early Jurassic Toarcian hothouse (W9) was followed by a relatively cool period during the middle

1282   Jurassic (Jenkyns et al., 2002; Dera et al., 2011). In a rare turnabout, during the early Jurassic, the

1283   South Polar region appears to have been warmer than the North Polar region. Dinosaurs and small

1284   flying reptiles, which would have had difficulty surviving freezing winters, inhabited the central

1285   Antarctica Transantarctic Ranges (Hammer and Hickerson, 1996); whereas dropstones and

1286   glendonites, indicative of freezing winter conditions, have been reported from Arctic Siberia (Boucot

1287   et al., 2013; 70 N – 80 N).

1288   Global temperatures warmed again during the late Oxfordian and Kimmeridgian (W8, Kimmeridgian

1289   Warm Interval, Podlaha et al., 1998; Jenkyns et al., 2002; Dera et al., 2011). The "mega-monsoonal"

1290   atmospheric circulation that characterized the earlier Mesozoic (Parrish, 1993) was still in place, but

1291   showed signs of weakening. As the newly formed intra-Pangean ocean basins (Central Atlantic

1292   Ocean and Western Indian Ocean) widened, they brought new sources of moisture to the interior of

1293   Pangea. The influx of moisture from these young ocean basins dampened the severe, seasonal

1294   swings in temperature and precipitation that had plagued the dessicated core of Pangea since the

1295   Late Permian. For other climate model results for the Late Jurassic see Moore *et al*. (1992), Valdes

1296   and Sellwood (1992), Valdes (1994), Sellwood and Valdes (2006).

1297   The Kimmeridgian Warm Interval (164-150 Ma) was followed by a long interval characterized by

1298   cool, but not frigid, temperatures (Tithonian-early Barremian Cool Interval, C7, 150 – 128 Ma). The

1299   Tithonian-early Barremian Cool Interval was punctuated by isolated warm events (Weissert (136

1300   Ma) and Faraoni (131 Ma) thermal excursions).

1301   Global Climate during the earliest Cretaceous (Berriasian to Barremian) can be characterized as

1302   something "in-between" a hothouse and an icehouse (Frakes *et al*., 1992). The average global

1303   temperature was about 17˚ C. This was five degrees warmer than the Late Cenozoic Icehouse (C1,

1304   12˚ C), but seven to nine degrees cooler than the Mid-Cretaceous – Paleogene Hothouse (W5-W6).

1305   Evidence for more temperate climatic conditions is based on the occurrence of dropstones,

1306   glendonites, and a few tillites (pebbly mudstones, Boucot *et al.*, 2013) in polar latitudes that co-

1307   occur with evidence of temperate forests (coal, plant fossils) and dinosaurs. Dropstones of Early

1308   Cretaceous age (Berriasian/Barremian) are widespread in South Australia, Queensland, New South

1309   Wales, and the Northern Territory of Australia (Boucot *et al*., 2013). Glendonites occur in South

1310   Australia and New South Wales . In the northern hemisphere there are dropstones in Siberia and

1311   Svalbard, and glendonites in northern Siberia, Svalbard and the Arctic Islands (Grasby et al., 2017;

1312   Brassell, 2009; Frakes and Francis, 1988; Frakes and Francis, 1990,1993; Frakes et al., 1995; De Lurio

1313   and Frakes, 1999; Vickers et al., 2019).

1314   The best interpretation for this mixture of cool and warm climatic indicators is that it was cold

1315   enough in the winters for lakes and rivers to freeze over. Snow covered the ground and there were

1316   glaciers at higher elevations. In the summer months it was warm enough to support the growth of

1317   lush vegetation and an influx of dinosaurs migrating in from warmer regions.

1318 It is interesting to note that the Kimmeridgian Anoxic Event is the only potential oceanic anoxic

1319 event for the time interval spanning the middle Jurassic (Aalenian, 174 Ma) to the early Barremian

1320 (128 Ma). It does not appear to be as widespread as the Cretaceous OAE events. The lack of anoxic

1321 basins during the earliest Cretaceous seems quite unusual in light of the fact that there were many

1322 "restricted" marine basins that would have been ideal habitats for anoxia to develop. The lack of

1323 OAEs may have been due to the fact that the bottom waters during the middle and late Jurassic

1324 through to the earliest Cretaceous were relatively well-oxygenated. The occurrence of glendonites

1325 at high latitudes during much of the Early Cretaceous indicates that cool, oxygen-rich bottom waters

1326 were being generated at polar latitudes preventing the bottom waters in lower latitudes from

1327 becoming anoxic.

1328 **5.8 Mid Cretaceous – Paleogene Hothouse (W5 – W7, 39.4-128 Ma), Table 6, Figure 20**

1329 If one imagines where the current phase of anthropogenic global warming is heading, one

1330 immediately thinks of the hothouse worlds of the Late Cretaceous and Eocene (Huber, 1998; Huber

1331 et al., 2000). During the Mid Cretaceous – Paleogene Hothouse global temperatures were indeed

1332 much warmer than the present-day (GAT = 28˚C during the Late Cretaceous versus GAT = 15˚C for

1333 the Modern). It remains to be seen whether we will succeed in warming the Earth to that degree,

1334 but at least we now know what a warmer world would look like.

1335 The Mid Cretaceous – Paleogene Hothouse is one of the best documented paleotemperature

1336 intervals. Table 6 lists some of the key references for this time interval and summarizes their

1337 primary conclusions regarding regional and global temperatures. The best single source for

1338 information about the Cretaceous portion of this hothouse interval is the O'Brien et al. (2017)

1339 summary of sea surface temperatures (SSTs) based on oxygen isotope and TEX_{86} temperature

1340 estimates. The TEX_{86} technique uses the lipid chemistry of the cell membrane of a common group of

1341 pelagic protokaryotes (Thaumarchaeota) to estimate temperatures (Schouten et al., 2002). The

1342 paleotemperatures are derived by measuring the ratio of key lipids (crenarchaeols). It has been

1343   noted that TEX$_{86}$ temperature estimates tend to be ~50% higher than ∂^{18}O temperature estimates

1344   (O'Brien et al., 2017; Figure 8). Approximately 90% of the available TEX$_{86}$ paleotemperature

1345   estimates for the Cretaceous have been obtained from samples that are Aptian or younger in age.

1346   Moreover, there are very few ∂^{18}O temperature estimates for times older than the mid-Albian

1347   (O'Brien et al., 2017). Fortunately, as noted earlier, geological evidence (glendonites, dropstones,

1348   and rare tillites) from the Early Cretaceous helps to fill in these data gaps.

1349   Both oxygen isotope and TEX$_{86}$ measurements identify an early Barremian – middle Aptian warm

1350   interval (W7, 128 – 118 Ma, GAT = 22˚C), which was followed by a cooler period during the late

1351   Aptian-early Albian (C6, 118 – 111 Ma, GAT = 19˚C), which preceded the rapid ramping up to a

1352   thermal maximum during the latest Cenomanian- earliest Turonian (W6.2, 94 – 93 Ma, GAT = 28˚C).

1353   According to O'Brien et al. (2017), temperatures cooled gradually during the remainder of the Late

1354   Cretaceous reaching a minimum of ~21˚C in the late Maastrichtian, just prior to the KT impact

1355   event.

1356   The Mid Cretaceous – Paleogene Hothouse (W6) began in the latest Barremian – earliest Aptian

1357   (~128 Ma) with two thermal events, the Haupblatterton Thermal Event (W7.5; Mutterlose et al.,

1358   2009) and the oldest Cretaceous oceanic anoxic event, OAE1a, the Selli/Goguel Thermal Maximum

1359   (W7.4; Erba et al., 2015; Herrle et al., 2015; O'Brien et al., 2017). Average global temperatures

1360   during the Mid Cretaceous – Paleogene Hothouse was a ~23˚ C. Surface waters in the Cool

1361   Temperate regions (SST = 21-23˚C) were only slightly cooler than the superheated tropical seas (29˚

1362   C; O'Brien et al., 2017). Oceanic bottom waters were also much warmer than the present-day (9˚ -

1363   17˚ C; Valdes et al., 2020).

1364   The Selli/Goguel Thermal Maximum (OAE1a) is the first of nearly a dozen potential thermal spikes

1365   that characterize this time interval (see Table 3). The nature and origin of these OAEs has been

1366   much debated (Schlanger and Jenkins, 1976; Arthur and Sageman, 1994; Meyer and Kump, 2008).

1367   Previous notions that OAEs were simply the result of rapid rises in sea level (Arthur and Sageman,

1368   1994) or due to the stagnation of the ocean basins caused by thermohaline density stratification,

1369   have fallen out of favour. There are two current schools of thought. The first argues that the OAE's

1370   were "unusual", synchronous, global events. According to this argument, "catastrophic" tectonic

1371   events triggered "unusual" atmospheric, biologic, geochemical, and oceanographic conditions that

1372   promoted extensive deepwater anoxia that resulted in the formation of carbon-rich black shales

1373   (Total Organic Carbon often > 30%). Proponents of this school of thought argue that the following

1374   scenario may explain the widespread occurrence of the carbon-rich black shales associated with the

1375   early Aptian Selli/Goguel Thermal Maximum (OAE1a):

1376   • The eruption of the mid Cretaceous superplume (Larson, 1991; Larson and Erba, 1999)

1377   radically changed atmospheric and oceanic chemistry.

1378   • Greenhouse gases from the erupting lavas, (i.e. CO_2), warmed the Earth.

1379   • Increased warmth accelerated chemical weathering on land; consequently, a greater flux of

1380   nutrients was carried to the oceans.

1381   • Land-derived nutrients, together with a higher concentrations of biolimiting metals made

1382   available by increased hydrothermal activity associated with the extensive submarine

1383   eruptions (Duncan and Huard, 1997; Jones and Jenkyns, 2001) promoted greater marine

1384   productivity resulting in more carbon deposition.

1385   • The increased productivity depleted the available supply of oxygen in the water column,

1386   which led to basin-wide anoxic or dysoxic conditions.

1387   • Water-column anoxia, in turn, favoured the preservation of the carbon by inhibiting

1388   bacterial decay and carbon recycling.

1389   • The results were widespread carbon-rich black shales (Demaison and Moore, 1980)

1390   A second school of thought argues that the OAEs do not represent unusual or catastrophic, global

1391   events, but rather represent "business as usual". In other words, a certain constellation of biologic,

1392   geochemical, tectonic, atmospheric, and oceanographic conditions favour the development of local,

1393   basin-wide anoxia. The Cretaceous were unusual only in the sense that this constellation of

1394   favorable conditions was more likely to occur than one might have been expected. In essence the

1395   paleogeography of the Aptian/Albian (and Cenomanian/Turonian) was especially favourable for the

1396   formation of highly productive, anoxic basins that promoted "nutrient trapping" (Meyer and Kump,

1397   2008).

1398   These two schools of thought epitomize the classical conflict between "catastrophic" versus

1399   "uniformitarian" explanations of Earth processes. As in the case of most false dichotomies, each

1400   hypothesis may hold part of the answer. Each hypothesis may explain different aspects of the Earth

1401   System processes that produce oceanic anoxic events. The "catastrophic" hypothesis may be the

1402   best explanation for the rare, but truly global, "mega" OAE events (i.e. Selli/Goguel Thermal

1403   Maximum (OAE1a) and Cenomanian-Turonian Thermal Maximum (OAE2), whereas the

1404   "uniformitarian" hypothesis may be a better explanation for the more frequent, regional, and less

1405   intense OAE events (OAE1b, OAE1c, OAE1d, OAE3).

1406   The Aptian-Albian Cold Snap (C6, 118-111 Ma) separates the Selli/Goguel Thermal Maximum

1407   (OAE1a) from the remaining Late Cretaceous OAE's. For a brief interval in the late Aptian and Early

1408   Albian, the global climate cooled off sufficiently for winter snow and ice to return to the northern

1409   and southern polar regions (Pucéat et al., 2003; Jenkyns et al., 2012; Erba et al., 2015; Herrle et al.,

1410   2015; O'Brien et al., 2017). Glendonites are reported from Ellesmere Island, Axel Heiberg Island,

1411   Svalbard, northern Greenland, and east-central Australia (Eromanga Sea) indicating that cool bottom

1412   waters once again had chilled the deep ocean basins (Frakes and Francis, 1988; Grasby et al., 2017;

1413   VIckers et al., 2019).

1414   The warmest Cretaceous temperatures occurred during the Cenomanian-Turonian Thermal

1415   Maximum (W6.2, 94 – 93 Ma). Second only to the Permo-Triassic Thermal Maximum (W13), the

1416   global average temperature reached 28˚C and the pole-to equator temperature gradient was

1417   flattened with a temperature differential of only ~20°C degrees between the polar region (13°C) and

1418   the tropics (34°C). Not even a hint of ice existed at the poles during the Cenomanian-Turonian

1419   Thermal Maximum (Ziegler et al., 1985). The presence of tropical plants and dinosaurs on Antarctica

1420   (Dettmann, 1989; Cantrill and Poole, 2012) and above the Arctic Circle indicates that temperatures

1421   rarely fell below freezing even during the winter months (Wolfe and Upchurch, 1987; Parrish and

1422   Spicer, 1988). Recent descriptions of angiosperm leaf floras from Antarctica indicate that similar

1423   warm and wet conditions existed near the South Pole during the Late Cretaceous (Hayes *et al.*,

1424   2006). In general, during times of hothouse conditions, the equatorial and subtropical belts expand

1425   slightly poleward; the Polar and Cool Temperate belt are replaced by an expanded Warm Temperate

1426   belt that brings tropical conditions to latitudes above 50° north and south (Paratropical Belt of

1427   Boucot et al., 2013; the megathermal rainforests of Morley, 2011).

1428   Despite the overwhelming geological and paleontological evidence for warm polar regions during

1429   the Mid-Cretaceous Hothouse, early climate simulations tended to "run cold" and had a difficult

1430   time modeling these warmer polar temperatures (Barron and Washington, 1982). Various attempts

1431   have been made to modify the input parameters to the climate models to produce simulations more

1432   consistent with the geological data. Initial attempts to fix this problem used extremely elevated

1433   levels of greenhouse gases to warm the poles (15x modern CO_2; Bice and Norris, 2002). However,

1434   there is no geological support for CO_2 concentrations in the Cenomanian/Turonian much above 5x

1435   the modern value (van der Meer et al., 2014). The extreme high levels of CO_2 needed to keep the

1436   polar regions ice-free would necessarily make terrestrial and shallow marine habitats at low

1437   latitudes uninhabitable (Jacobs et al., 2005).

1438   Another way to make the polar regions warmer is to modestly increase the concentration of

1439   greenhouse gases and also modify the land cover in polar regions to a darker, denser vegetation

1440   (Upchurch *et al.*, 1999). The darker vegetation has a lower albedo and consequently more solar

1441   energy is absorbed at the surface. In this model, positive feedbacks between high-latitude forests,

1442   the atmosphere, and the ocean all contribute to significantly warmer temperatures at high latitudes

1443   during the Late Cretaceous (Upchurch *et al.*, 1999).

1444   A third explanation invokes a Late Cretaceous "Super-Gulf Stream" that vigorously carried warmth

1445   from the Equator to the Poles (Brady *et al.*, 1998). Though intuitively appealing, an analysis of the

1446   dynamics indicates that it is not possible to carry enough heat poleward using ocean currents alone.

1447   The atmosphere must also play an important role. In addition, much like today, the paleogeography

1448   of the Late Cretaceous presents a nearly landlocked polar region that would have been isolated from

1449   Gulf Stream-like ocean currents.

1450   One of the more promising approaches has been to change the high-altitude cloud parameterization

1451   that is used in climate models like the Community Climate System Model version 3 (CCSM3, Kiehl

1452   and Shields, 2013). The high albedo of low-altitude cumulus clouds reflects incoming sunlight back

1453   to space, which cools the Earth. Wispy, high-altitude clouds, on the other hand, reflect thermal

1454   energy back to the surface of the Earth resulting in net global warming (Kump and Pollard, 2008).

1455   Fewer "warm clouds" form in the modern world because anthropogenic atmospheric pollution

1456   reduces the amount of warm cloud condensation nuclei. When cloud parameters characteristic of

1457   pristine regions are introduced into the climate model, significant additional warming occurs,

1458   especially in polar regions (Upchurch et al., 2015). Combined with a modest elevation in the

1459   concentration of atmospheric CO_2 (2x – 6x modern levels), the modelled temperature of polar

1460   regions remains above freezing throughout most of the year.

1461   The most radical hypothesis that has been proposed to explain the warm polar climates of the Late

1462   Cretaceous involves a fundamental rethinking of the way the atmosphere circulates. One of the

1463   basic features of the modern atmosphere is Hadley Cell circulation. In the Hadley Cell, warm air rises

1464   at the Equator, moves poleward, cools and descends over the subtropical desert belt (~35° N&S). In

1465   Hay's model (Hay,2008; Hay *et al.*, 2016), this simple, well-organized convective flow is replaced by a

1466   chaotic system of super-cyclonic eddies, which are like mega-hurricanes. Hundreds of these mega-

1467   hurricanes would have annually transferred vast amounts of heat from the Equator to the Poles

1468   during the Late Cretaceous. Though an intriguing and out-of-the-box proposition, no climate model

1469   can currently simulate this complex alternative to Hadley Cell circulation.

1470   After reaching peak Cretaceous temperatures during the Cenomanian-Turonian Thermal Maximum,

1471   temperatures gradually fell during the remainder of the Cretaceous. Maximum sea surface

1472   temperatures did not drop below 30°C until late in the Santonian (84 Ma) or early in the Campanian

1473   (O'Brien et al., 2017). This gradual cooling may have been punctuated by several, ephemeral cooling

1474   events at ~85Ma, ~76 Ma, and ~71 Ma (Miller et al., 1999, 2004, 2005a,b) as evidenced by $\partial^{18}O$

1475   temperature estimates from planktonic foraminifera. Also, an enigmatic dropstone deposit of

1476   Campanian – Maastrichtian age (75 – 70 Ma) has been reported from the region of the Anadyr River

1477   in Chukotka (Ahlberg et al., 2002).

1478   The modest, but steady, fall in temperatures during the Late Cretaceous was catastrophically

1479   interrupted by the arrival of the bolide that produced the 150 km diameter impact crater near the

1480   town of Chicxulub (Devil's Tail) in northern Yucatan (Alvarez and Alvarez, 1980; Schulte et al., 2010;

1481   Hildebrand et al., 1991). The Chicxulub impact is the largest known bolide impact of the Phanerozoic

1482   (Spray, 2020).

1483   The most likely scenario is that the impact event vaporized 3000 megatons of crustal material and

1484   injected this fine particulate matter high into the atmosphere. This material fell back to Earth

1485   forming a global "clay layer". The K/T boundary clay layer contains several unusual stratigraphic

1486   markers: 1) an iridium anomaly (Alvarez and Alvarez, 1980; Smit, 1999; Miller et al., 2010), 2)

1487   microtektites (Yancey and Guillemette,2008), 3) shocked quartz (Bohor et al., 1987; Smit, 1999), and

1488   4) soot (from forest fires) that connect it directly to the Chicxulub impact event. (It should noted that

1489   the authors prefer to use the term "K/T" rather than the more precise "K-Pg" to describe events

1490   occurring at the Cretaceous -Paleogene boundary. The term "K/T" has precedence, is still widely

1491   used, is more familiar to most readers, and is therefore a clearer descriptor than the technically

1492   correct, but more obscure and less euphonius, "K-Pg".)

1493   While suspended in the atmosphere, this delicate shroud of material blocked the sun and turned day

1494   into night - a night that lasted several months to a year. Without sunlight, plants on land and

1495   plankton in the oceans died. Small and large herbivores gradually starved. Without herbivores to

1496   prey on, predators then starved - all the while, snow continued to fall (probably for several

1497   decades). As a consequence of the collapse of the food chain, ~75% of all species were wiped out

1498   (Sepkoski, 1996). The effect of this extinction event on global ecosystems was second only to the

1499   great Permo-Triassic Extinction (McGhee et al., 2013).

1500   The ensuing "Impact Winter" scenario plunged the Earth into a frigid deep-freeze comparable to the

1501   coldest glacial stages of any Phanerozoic ice age. The drastic cooling, however, was short-lived

1502   (Vellekoop et al., 2014, 2016) and was followed by an equally short-lived period of global warming

1503   triggered by the final, massive eruption of the Deccan LIP (Ernst, 2014; Keller et al.,2017). The first

1504   eruptions of the Deccan LIP predate the Chicxulub impact by 1-2 million years (Chenet et al., 2008;

1505   Keller et al., 2011, 2014). It has been proposed that an earlier impact event (Shiva impact) triggered

1506   the Deccan eruptions (Chatterjee et al., 2006), however this hypothesis has not received much

1507   support. It seems likely, however, that the Chicxulub impact did influence or enhance Deccan

1508   volcanism. It has been noted by several authors (E. Shoemaker, pers. comm.) that the impact site in

1509   Yucatan is nearly antipodal to the eruption site of the Deccan LIP in India. Though the antipodal

1510   paleolatitudes are identical (26˚ N vs 26˚ S), the antipodal paleolongitudes are offset by several

1511   thousand kilometers. Nevertheless, it seems plausible that shockwaves from the impact passed

1512   through the earth and were reconcentrated beneath the Deccan hotspot stimulating more

1513   voluminous eruptions (Richards et al., 2015; Renne et al., 2015). In any event, the excess

1514   atmospheric CO_2 from the Deccan eruptions caused a 4-8˚ spike in global temperatures (Petersen et

1515   al., 2016; Bond and Grasby, 2017) that ushered in the Paleogene Warm interval.

1516   Following the KT impact Winter, global temperatures warmed during the Paleocene, reaching a

1517   maximum during the early-middle Eocene (Paleocene - Eocene Hothouse, W5, 62 - 39.4 Ma). This

1518   period of global warmth was probably triggered by CO_2 injected into the atmosphere by massive

1519   volcanic eruptions in the North Atlantic Igneous Province (NAIP; Ernst, 2014). It was in this global,

1520   tropical "Garden of Eden" that our mammalian ancestors diversified, crossed newly-erupted volcanic

1521   land bridges between northern Europe and Greenland, and expanded across the globe (Wallace,

1522   2004).

1523   The classic record of deep ocean temperatures based on benthic foraminifera assembled by James

1524   Zachos (Zachos et al., 2001, 2008; also Westerhold et al., 2020) provides a framework for describing

1525   the temperature fluctuations during the Paleocene-Eocene Hothouse and the Late Cenozoic

1526   Icehouse (Koeberl and Montanari, 2009). These deep ocean temperatures have been converted to

1527   global average temperatures using the technique described in section 3.3.

1528   The three most prominent features of this detailed temperature record are: 1) the Paleocene-

1529   Eocene Thermal Maximum (W5.8, 55.6 Ma; Rea et al., 1990; Kennett and Stott, 1991; Wing et al.,

1530   2003; McInerney and Wing, 2011), 2) the Early Eocene Thermal Maximum (W5.5, ~50 Ma), and the

1531   Middle Eocene Thermal Maximum (W5.1, ~41 Ma). These are certainly "event" driven changes in

1532   climate. The one explanation for these spikes in temperature is the rapid release of massive

1533   amounts of methane hydrates (clathrates) from the deep sea (Zeebe et al., 2009). Methane is a

1534   powerful greenhouse gas and the release of gigatons of methane into the atmosphere would have

1535   produced the observed rapid rise in global temperature. Other hypotheses, summarized by Wing

1536   and McInerney (2011, p 494), suggest that the excess amount of greenhouse gases may have come

1537   from wildfires, volcanic intrusions into organic-rich sediments, drying of epicontinental seas, or the

1538   thawing of Antarctic permafrost. Most recently, Gutjhar et al. (2017) and Jones et al. (2019) have

1539   proposed that massive eruptive episodes associated with the North Atlantic Igneous Province (NAIP)

1540   provided the excess CO_2 responsible for these thermal maxima.

1541   A prominent feature of the early Eocene Hothouse is the broad, dome-shaped rise and fall in

1542   temperature that defines the Middle Eocene Warm Interval (W5.4, 56-46 Ma). The shape of this

1543   curve indicates that systematic changes were taking place over millions of years (Huber and

1544   Caballero, 2011). These changes in global temperature were probably driven by gradually changing

1545   paleogeographic, plate tectonic, or paleoceanographic conditions. The final notable feature of the

1546   Zachos Curve is the rapid fall in temperature at the end of the Eocene (C4.3, Eocene Oligocene Rapid

1547   Cooling, 33-34 Ma). It has been proposed by many authors that this cooling event was driven by the

1548   development of a through-going Circum-Antarctic Current and the subsequent isolation and

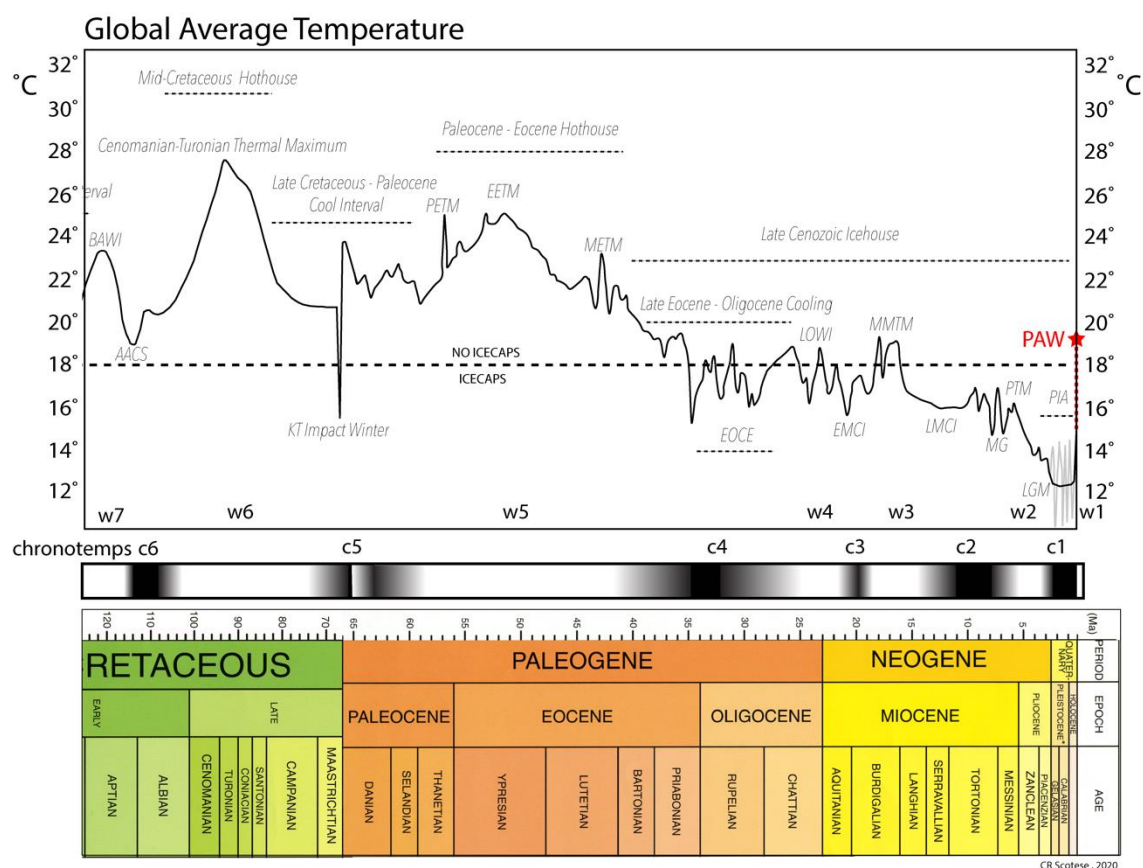1549   refrigeration of Antarctica.

Figure 21. A Cenozoic Paleotemperature Timescale. white = warm time intervals, black = cool time intervals; Light gray jagged lines = a schematic representation of >50 glacial/interglacial cycles during the Plio-Pleistocene. Solid black line = Global Average Temperatures (GAT),), < 18°C = large, permanent icecaps, > 18°C = no large, permanent icecaps. Timescale = International Chronostratigraphic Chart v2020/01. Refer to Table 3 for more information and sources for each chronotemp and abbreviations.

1550

1551   **5.9 Late Cenozoic Icehouse (C1 – C4, 1880 CE – 39.4 Ma), Table 7, Figure 21**

1552   *"And now there came both mist and snow*

1553   *And it grew wondrous cold*

1554   *And ice, mast-high, came floating by*

1555   *As green as emerald."*

1556   Samuel Taylor Coleridge, Rime of the Ancient Mariner (1798)

1557

1558   As illustrated in Figure 21, the cooling trend that began after the Early Eocene Thermal Maximum

1559   (W5.5, 52-50 Ma) continued during the middle and late Eocene, though it was interrupted briefly by

1560   the Middle Eocene Thermal Maximum (W5.1, 41 Ma). What Earth System event initiated the Late

1561   Cenozoic Icehouse? The generally accepted explanation is that the collision of India, which took

1562   place at the height of the Early Eocene Thermal Maximum (~50 Ma; Molnar and Tapponier, 1975;

1563   Rowley, 1996, 1998), triggered a cascade of events that lead to global cooling (Raymo and

1564   Ruddiman, 1992). The collision of India with south-central Asia resulted in the rapid uplift of the

1565   Himalaya Mountains. By ~35 Ma (late Eocene – early Oligocene), the Himalayas and Tibetan plateau

1566   had achieved 90% of their modern height (Rowley and Currie, 2006), though the Tibetan plateau was

1567   less than half its present area. These young mountains were in the path of the Asian monsoon,

1568   which brought warm temperatures and abundant moisture. This lead to rapid mechanical and

1569   chemical weathering. The flux of calcium to the world's oceans increased and these calcium cations

1570   combined with carbonate ions to form limestone which drew-down the amount of CO_2 in the

1571   atmosphere. The gradual decrease in atmospheric CO_2 cooled the Earth.

1572   As global temperatures began to cool, the high altitude glaciers on the Gamburtsev mountains and

1573   Trans-Antarctic Ranges (> 1000 m) coalesced into ice sheets. At the Eocene-Oligocene boundary

1574   (C4.3, 34-33 Ma), temperatures plunged precipitously signalling the first major accumulation of ice

1575   on Antarctica. Permanent sea ice also formed around the periphery of Antarctica generating

1576   increasing amounts of cold bottom water. Icebergs coursed through the southern oceans and the

1577   first record of ice-rafted debris appeared in the deep-sea record. The global cooling also forced

1578   plants to adapt to the harsher winter conditions (Wolfe, 1971, 1978, 1992, 1994). Paleoceanographic

1579   events in the Southern Hemisphere, in particular the formation of the Circum-Antarctic Current,

1580   played a key role in the chronology of these events (Kennett, 1995).

1581   The Drake Passage is the seaway that flows between the southern tip of South America (Patagonia)

1582   and the northern tip of the West Antarctic Peninsula (Palmer Peninsula). In the early Mesozoic,

1583   these two regions were part of a continuous Andean mountain range. The ligation between

1584   Patagonia and the Palmer Peninsula was tested when Gondwana began to rift apart in the late

1585   Jurassic. Despite being stretched and extended as the Weddell Sea opened during the Cretaceous,

1586   Patagonia and the Palmer Peninsula were not completely separate until the late Eocene (~40 Ma).

1587   The best estimate for the age of the opening of the Drake Passage is 45 Ma (shallow water

1588   connection, <1000m) to 35 Ma (deep water connection, >1000 m) (Livermore *et al*., 2005). An age

1589   of 41 Ma for the opening of the Drake Passage is based on the change in neodymium isotope ratios

1590   from sediments on the Agulhas Ridge that suggests an influx of shallow Pacific water (Scher and

1591   Martin, 2006).

1592   When the Southeast Indian Ocean between southern Australia and Antarctica (Wilkes Land) began

1593   to open in the Late Cretaceous, the eastern end of the rifted margin made a right-angle bend,

1594   hooking southward around Tasmania. This strike-slip boundary, the Tasman Fracture Zone,

1595   effectively closed off the eastern end of the Southeast Indian Ocean during the earliest phases of

1596   opening. When Australia began to move rapidly northward during the Late Eocene (40 Ma – 35 Ma),

1597   the overlapping bits of the Australian and Antarctic plates (South Tasman Rise and North Victoria

1598   Land, respectively) separated, allowing deep waters from the Indian Ocean and South Pacific Ocean

1599   to mix. The first deep water connection between the Indian Ocean and the South Pacific was

1600   through the Tasman Straits.

1601   Both the Drake Passage and the Tasman Gateway (Kennett et al., 1974; Exon et al., 2004; Kennett

1602   and Exon, 2004) were fully opened by the early Oligocene (34-30 Ma; Lawver and Gahagan, 2003).

1603   As a consequence, the Circum-Antarctic Current was able to isolate Antarctica from the world's

1604   oceans resulting in the "refrigeration" of Antarctica (C4.2, 34-28 Ma). The rapid growth of the

1605   Antarctic icecap during the Early Oligocene produced a major regression at the Rupelian/Chattian

1606   boundary (28.1 Ma). During the Oligocene, the massive Antarctic ice cap grew and shrank in fits and

1607   starts. These chaotic transitions are recorded in a dozen cooling and warming events (C4.1 and C4.2).

1608   Global temperatures remained cool until the end of the Oligocene when there was a slight warming

1609   (W4, 27-23 Ma). Though parts of West Antarctica were still forested during the Oligocene, mountain

1610   glaciers grew in the highlands of the Palmer Peninsula, reaching the ocean by the latest Oligocene. In

1611   the Northern Hemisphere there were local glaciers in Svalbard and central Greenland, but no

1612   permanent icecap.

1613   It is also worth noting that by the Early Oligocene, the collision between the Arabian peninsula and

1614   Iran was nearly complete. Though all the ocean floor had been subducted, a shallow seaway, the

1615   proto-Persian Gulf, filled the foredeep of the Zagros mountains of Iran and Iraq. During brief

1616   highstands of sea level during the late Oligocene and early Miocene, this shallow seaway connected

1617   with the deeper waters of the eastern Mediterranean. The closure of this westernmost extension of

1618   Tethys in the earliest Oligocene eliminated the westward flowing "Subtropical Eocene NeoTethys"

1619   (STENT) current. Some authors have speculated that this may have contributed to global cooling

1620   during the early Oligocene (Toggweiler et al. (2000), Hotinski and Toggweiler, 2003; Jovane et al.,

1621   2009).

1622   At the start of the Miocene, only Antarctica, straddling the South Pole, was covered by a permanent

1623   icecap. Cool conditions prevailed in the northern hemisphere as well, but there was no permanent

1624   ice. Global temperatures warmed in the middle Miocene (W3, 18 – 11 Ma), the Antarctic ice cap

1625   shrank and snow and ice disappeared from the northern hemisphere. By the end of the Miocene (~

1626   5 Ma), conditions had once again cooled (C2, 11 - 5.3Ma) and a permanent icecap had begun to form

1627   in the Arctic. The initiation of the Greenland ice sheet in the middle-late Miocene corresponds with

1628   the minimum sea level for the Miocene (~50 m; Miller et al., 2020).

1629   The growth of the Arctic icecap may have been triggered by two paleogeographic-

1630   paleoceanographic changes: 1) In the late Neogene (4-5 Ma), the Panama volcanic archipelago rose

1631   above sea level, creating the Panama land bridge. This land bridge connected North and South

1632   America, permitting the interchange of fauna and flora (Marshall *et al.*, 1982). More importantly,

1633   this land bridge served as a blockade, isolating the equatorial Atlantic and Pacific Oceans. Warm,

1634   equatorial Atlantic waters were diverted northward (the Gulf Stream). The warm waters of the Gulf

1635   Stream warmed the Arctic regions, but more importantly, provided a new source of moisture which

1636   fed winter snows. Increased snowfall lead to the growth of glaciers and the Arctic ice sheets grew

1637   large. 2) In the eastern hemisphere, the northward movement of Australia during the early Miocene

1638   and the collision of Australia with Southeast Asia during the middle-late Miocene (~10-15 Ma)

1639   blocked equatorial circulation between the western Pacific Ocean and the Indian Ocean. As a

1640   consequence, the distance that ocean waters circulated along the Equator was shortened resulting

1641   in a net cooling of tropical surfaces waters. This reduction in the Earth's thermal budget, in turn, may

1642   have led to increased cooling at the poles.

1643   Global temperatures continued to plummet during the Pliocene. During the late Pliocene (~3.3 Ma),

1644   global temperatures warmed sufficiently to melt enough of the North and South polar icecaps so

1645   that sea level rose (~60 m), flooding the continental margins (W2.1, Pliocene Thermal Maximum).

1646   The Pleistocene Ice Age (C1) began in the latest Pliocene (2.7 Ma) and ended 11,700 years ago

1647   (Younger C1.1 Dryas). Driven by the tilt of the Earth (obliquity) and the shape of the Earth's orbit

1648   (eccentricity), the polar ice sheets waxed and waned causing global sea level to rise and fall (Miller et

1649   al., 2020). When ice sheets were at their maximum, sea level was ~100 meters lower than today.

1650   During the interglacial part of the cycle, when much of the polar ice caps had melted away, sea level

1651   was ~70 meters higher than today.

1652   Sea level has risen and fallen more than 50 times during the last 2 million years. This cycle of sea

1653   level change has been recorded in the changing ratio of the $^{18}O/^{16}O$ preserved in benthic/planktonic

1654   foraminifera (Lisiecki and Raymo, 2005). This fluctuating record begins nearly 2.7 million years ago;

1655   for the first ~2 million years, the cycle of icecap growth and retreat was modulated by the changing

1656   tilt of the Earth's axis (40,000 year obliquity cycle). Starting nearly one million years ago, the

1657   frequency of ice cap formation slowed from every 40,000 years to every 100,000 years, as the

1658   changing, eccentric shape of the Earth's orbit became the major forcing function. It should be noted

1659   that most of these marine isotopic sequences (MIS) match a similar cycle of changing CO_2

1660   concentration recorded in mile-long ice cores from Greenland and Antarctica (Barnola et al., 1987;

1661   Petit et al, 1999; Alley, 2000; EPICA Community Members, 2004; Jouzel et al, 2007).

1662   We are currently about halfway through a typical glacial/interglacial cycle. If humans did not inhabit

1663   the Earth, about 20,000 years from now, global temperatures would have once again begun to fall

1664   and ice sheets would have expanded into the oceans surrounding Antarctica and would have

1665   descended from the Arctic to begin a slow and steady march across the northern continents.

1666   However, this will not happen. The Earth has entered a "super-interglacial". The injection of CO_2

1667   into the atmosphere as a consequence of the burning of fossil fuels has warmed the Earth more than

1668   1˚C and will continue to warm the Earth for another 300 years (~2300 CE). In the next section, we

1669   discuss how long anthropogenic global warming will continue and how warm the Earth will become.

1670

1671   5.10 Post-Anthropogenic Warming (W1) (2300 CE – 10,000 years in the future), Table 7, Figure 21

1672   It is well-established fact that burning fossil fuels releases CO_2, a greenhouse gas, into the

1673   atmosphere, causing the Earth to warm faster than it would naturally (Archer, 2005; Archer et al.,

1674   2009a,b; Kidder and Worsley, 2012; Steffen et al., 2019). How warm will it get? How quickly will it

1675   warm to those new levels? In order to answer these questions, we need to know future trends in 1)

1676   global population (United Nations, 2019), 2) the average "energy footprint" per global resident

1677   (British Petroleum, 2019), 3) the future mix of energy sources (oil, gas, coal, hydroelectric, nuclear,

1678   and renewables; British Petroleum, 2019; Rogner, 2012; Shell,2018), 4) the rate at which the natural

1679   environment will absorb excess CO_2 emissions (Tans, 2009), and 5) the warming effect of

1680   greenhouse gases (climate sensitivity; Royer, 2016; Farnsworth et al., 2019). Though these

1681   parameters are not known with any certainty, we can nevertheless make an informed estimate of

1682   future trends and produce a reasoned prediction of the potential amount of global warming during

1683   the next 300 years (Scotese, 2020).

1684   We have estimated the amount of future global warming using a straightforward carbon budget

1685   model that predicts the changing amount of atmospheric CO_2. This CO_2 budget model is described in

1686   Table 8. Using these carbon budget equations, a dynamic model was constructed that predicts the

1687   amount of global warming during the next 300 years.

1688   Assuming that the Global Average Temperature (GAT) in 2000 was roughly 14.5°C (58° F), and the

1689   concentration of atmospheric CO_2 was 369 ppm. This model predicts that in 2200 the concentration

1690   of atmospheric CO_2 will be ~777 ppm, which is a little more than double the concentration of CO_2 in

1691   the year 2000 and the global temperature will rise about 5° C from 14.5°C (58°F) to 19.5°C (67° F).

1692   This change in temperature is indicated by the red star in Figure 21.

1693   As has been widely reported (Collins et al., 2013), most future warming takes place during the mid-

1694   to-late twenty-first century. Rapid global warming is nearly unavoidable because two key

1695   parameters - global population and energy use per capita - will rapidly rise during the next several
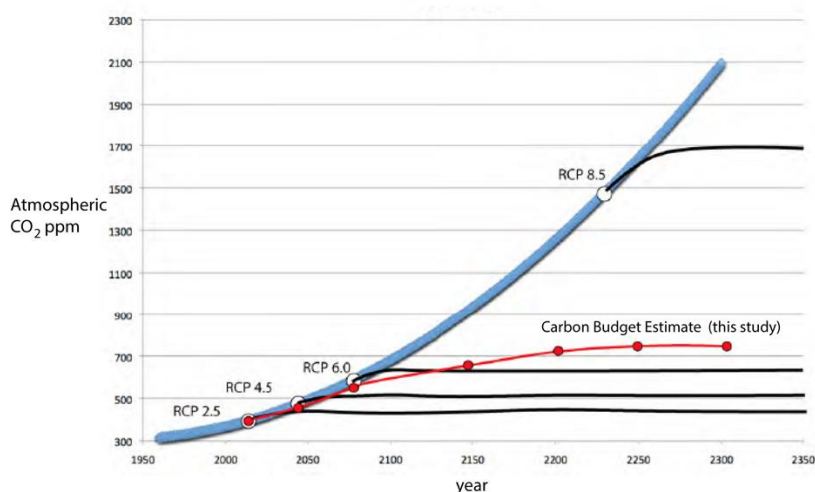
1696   decades.

Figure 22. IPCC Estimates of Global Warming compared to the Results Predicted by the Carbon Budget Model (this study). The blue curve represents the projected increase in atmopheric CO2 based on the continued burning of fossil fuels at the "modern rate" (1970 – 2020). The black curves are the CO2 levels used in the IPCC models RCP 2.5, RCP 4.5, RCP 6.0, and RCP 8.5. The red curve is the projected CO2 levels obtained in our model (between 750 ppm and 800 ppm at 2200 CE). Estimates from RCP 2.5 and RCP 4.5 are too low. The estimate of CO2 used in RCP 8.5 is much too high. Estimates of CO2 used in RCP 6.0 are about right.

1697

1698   According to the model, in the year 2100, global climate will have warmed beyond the 2˚C limit

1699   recommended by the Paris Accords (Figure 22). In 2200, after reaching a maximum temperature of

1700   19.5˚C, the global climate will begin to cool. This is due in part to natural processes, but most of the

1701   modelled decrease in global temperature is the result of proposed human intervention (i.e. carbon

1702   sequestration; Shell, 2018). If 10,000 carbon sequestration plants are built in the next 300 years, then

1703   by 2300 the combined action of these carbon sequestration plants will have removed 1.8 trillion

1704   gigatons of CO_2 from the atmosphere and the temperature will stabilize at 19.5˚C (Shell, 2018). If no

1705   carbon sequestration plants are built, then the projected future temperature will be closer to 20.5 C˚.

1706   Both of these predictions are in line with IPCC estimates.

1707   What will the world be like after the Warming? This is the question that is probably the most on

1708   people's minds. One can answer this question two ways. The first approach, taken by the

1709   Intergovernmental Council on Climate Change (IPCC) and Burke et al. (2018), has been to run

1710   hundreds of climate simulations that predict global climatic conditions using various global warming

1711   scenarios (Figure 22). These results are very detailed and make explicit predictions (IPCC, 2007,

1712   2018, 2019; Collins et al., 2013).

1713   Another way to understand our warmer future world is to compare the various possible warming

1714   outcomes to the climates of the past. The area shaded in red on Figure 23 represents the

1715   temperatures that lie within the range of the global warming predicted by the model presented here

1716   (16.5˚C – 19.5˚C). You can see that this shaded region is much cooler than some of the hothouse

1717   climates of the past. It is very good news that future global warming will likely not reach these

1718   extreme hot house temperatures. Along the time-axis in Figure 23, several boxes highlight time

1719   intervals in the deep past that had similar global climates. Of these, the Late Eocene – Miocene

1720   Icehouse is probably the best analog to the climate we might experience after this period of Post-

1721   Anthropogenic Warming (PAW).

1722
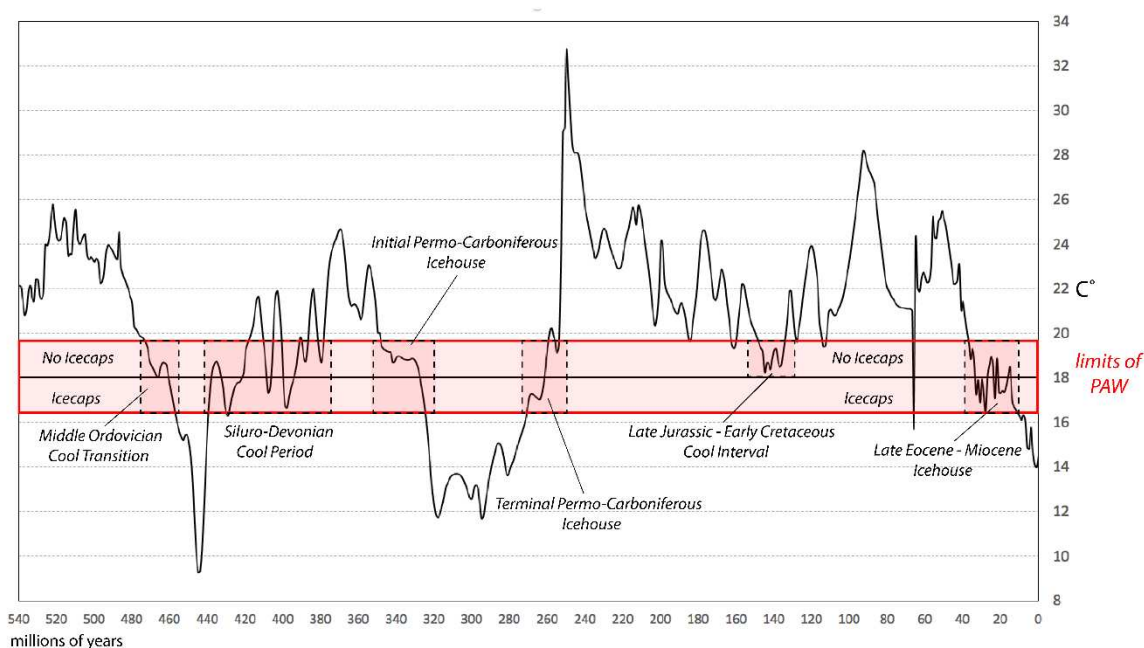
1723   Figure 23. Projection of Future Global Warming onto Phanerozoic Temperature Time Scale. The likely amount of Post-Anthropogenic Warming (PAW) (red line). The boxes indicate times in the geological past when global temperatures were within the range of predicted PAW. When the Global Average Temperature is below 18˚C large polar icecaps can form. When the Global Average Temperature is above 18˚C large polar icecaps are unlikely to form.

1724

1725   The geography of the early Oligocene world (30 million years ago) and the early Miocene world (15

1726   Ma) resembled the modern world (Figure 24). The continents were essentially in the same places

1727   and the oceans were about as wide as they are today. A large ice cap covered Antarctica, which was

1728 isolated from the other continents by the Circum-Antarctic Ocean. The northern hemisphere lacked

1729 any permanent ice cover, though snow covered the northernmost reaches of the continents during

1730 the winter.

1731 Unlike today's climate, the climate during the Oligocene and early Miocene was a little warmer near

1732 the Equator, and a diverse fauna thrived in tropical rain forests and in the oceans. Modern-sized

1733 desert belts separated the tropics from an expanded warm temperate belt that stretched across the

1734 northern hemisphere. The northern sub-polar regions, as well as Australia, were both wetter and

1735 warmer.

1736 These were worlds where land mammals thrived, diversified, and spread across the continents.

1737 Whales and enormous sharks ruled the seas. Plants also diversified. Grasslands covered the steppes

1738 and savannas and tropical and temperate forests provided a diverse set of habitats. All in all, the

1739 world was a reasonably nice place to live. Given enough time (5,000 -10,000 years; Archer, 2005;

1740 2009a,b), we might expect the same equable conditions to prevail after the Warming.

1741 The other five climatic "matches", though they had similar ranges of global temperature, had very

1742 different geographies. The climatic zones on a global Pangea would have been very different than

1743 the modern climatic belts.

1744 In conclusion, we are leaving our Ice Age heritage behind. A new, warmer world awaits us. The

1745 problem we face is not so much where we are headed, but rather how we will get there. The time

1746 for decisive action is quickly slipping away. Our stern challenge is to adapt to the rapid period of

1747 global warming that will take place during the next 100 years. To do this we must immediately take

1748 action to reduce our CO_2 emissions and take the steps needed to mitigate the undeniable damage

1749 that will be done to our environment, civilization, and society in the near future.

1750 **6. Summary and Conclusions**

1751   It has been long recognized that the Earth's climate, in particular the average global temperature,

1752   has alternated between "icehouse" and "hothouse" states. More than 70 years ago, Umbgrove

1753   (1947), and later Fischer (1981, 1982, 1984) recognized that these climatic "modes" varied on short-

1754   term, medium-term, and long-term timescales. During the past 20 years, beginning with the

1755   comprehensive pioneering work of Veizer et al. (1999) and followed by the insightful syntheses of

1756   Royer et al, (2004), Zachos et al. (2001, 2008), Grossman (2012 a,b), Boucot et al. (2013), Veizer and

1757   Prokoph (2015), O'Brien et al. (2017), Henkes et al. (2018), Valdes et al. (2018), and most recently

1758   Song et al. (2019), we now stand at the threshold to a deeper, more complete understanding of both

1759   the tempo and mode of global temperature change during the Phanerozoic.

1760   The goal of this essay has been to synthesize all of the available evidence for temperature change

1761   during the last 540 million years into a single, coherent, well-constrained global temperature curve

1762   (Figure 19-21, Table 3-7). Though the details may vary, there is good agreement between the

1763   temperature curve we present and earlier work (see Figure 1).
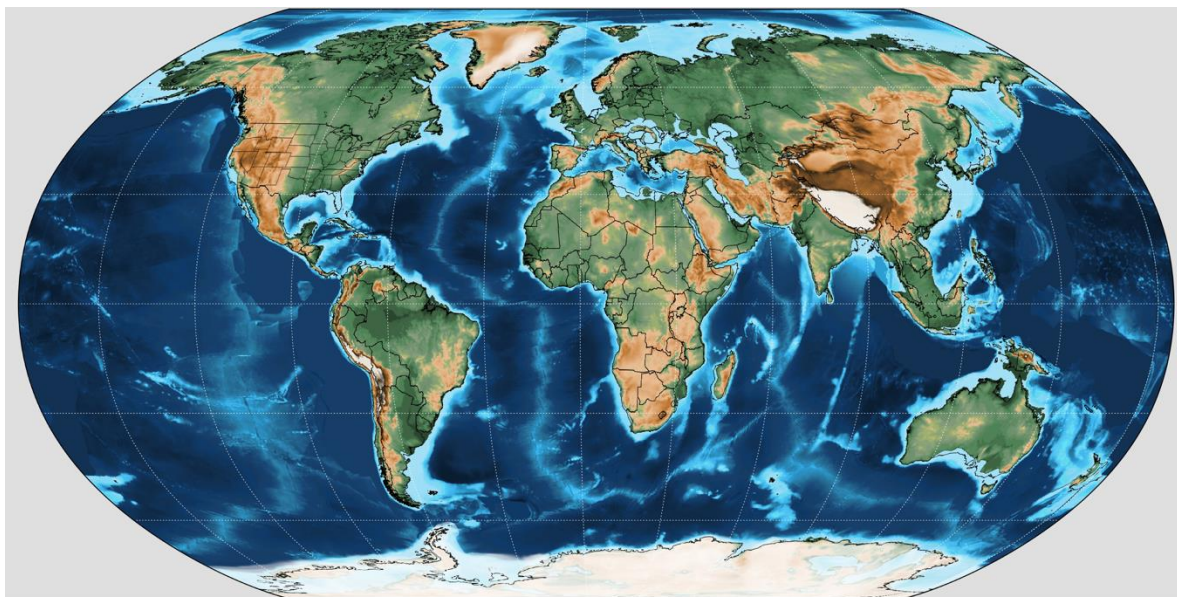
Middle Miocene Thermal Maximum (Langhian, 14.9 Ma)
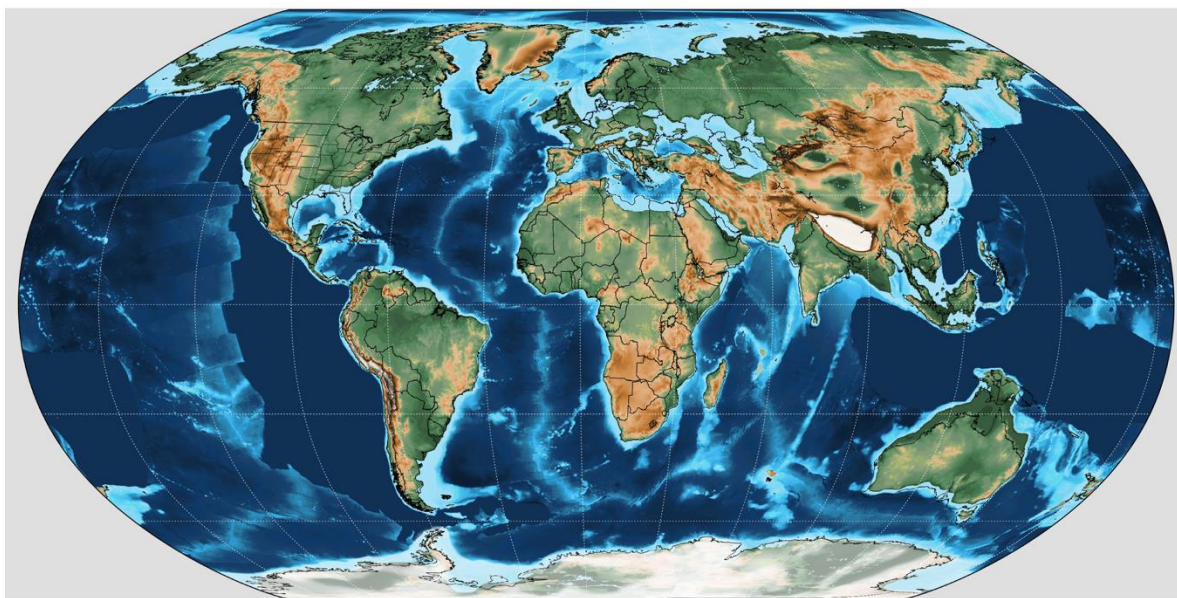
Early Oligocene Cool Interval (Rupelian, 31 Ma)

Figure 24. Paleogeographic maps for the early Oligocene (30 Ma) and early Miocene (15 Ma). These past time periods are a good climatic match for world after Anthropogenic Warming.

1764

1765   We have produced this model of Phanerozoic temperatures by deconstructing temperature change

1766   into three components: 1) long-term (>50 million years) temperature changes, 2) medium-term (10

1767   – 20 million years), and 3) short-term temperature changes (a few million years or less).

1768   The Earth's long-term temperature change is controlled by multiple tectonic and environmental

1769   processes that drive the Earth's climate from icehouse to hothouse conditions, and vice versa. These

1770 changes can be described by mapping the changing Pole-to-Equator gradient revealed by

1771 paleogeographic distribution of lithologic indicators of climate such as: tillites, dropstones,

1772 glendonites, high latitude mangroves, palms, and crocodiles; temperate coal, evaporites, calcretes,

1773 tropical coals, bauxites, and laterites, (see Figures 4 and 5; Boucot et al., 2013). Long-term

1774 temperature changes occur due to changes in the Earth's "climatic equilibrium" which is controlled

1775 by the level of greenhouse gases in the atmosphere (principally CO_2), the geographic configuration of

1776 the continents and ocean basins (paleogeography and paleoceanography), the effectiveness of

1777 erosion and chemical weathering, and the reflectivity of the Earth's surface (albedo). Many of these

1778 factors are interconnected by a complex network of positive and negative feedback loops that can

1779 accelerate or decelerate changes in long-term global temperature (Hay, 2016; Ruddiman, 2001).

1780 Figure 13 illustrates our best estimate of the long-term temperature of the Earth during the past 540

1781 million years.

1782 Medium-term (10 – 20 million years) changes in the Earth's temperature are revealed by the record

1783 of isotopic temperatures measured in carbonate and phosphatic fossils. Recent global compilations

1784 of isotopic measurements of temperature (Grossman, 2012a&b, Veizer and Prokoph, 2015; Song et

1785 al., 2019; Grossman and Joachimski, 2020) have allowed us to generate a first-order model that

1786 describes the variation in tropical and polar temperatures for the last 540 million years (Figure 17).

1787 There are still numerous uncertainties regarding the interpretation of isotopic temperatures. For

1788 example, the isotopic composition of seawater can vary due to excess evaporation or the local influx

1789 of freshwater, as well as the removal of ^{16}O from the oceans due to the growth of vast continental

1790 ice sheets. Also, the role that geographic and oceanographic variations play in $\delta^{18}O$ variability has yet

1791 to be rigorously examined. Despite these caveats, we believe that the temperature record obtained

1792 from oxygen isotope data is robust and that a testable, first-order signal is generally recognizable

1793 (Figure 9).

1794   The causes of medium-term fluctuations in temperature are many and complex. We have not yet

1795   unravelled these forcing functions, but they are likely to include tectonic and geologic events such

1796   as: continental collisions and subsequent mountain building and unroofing, periods of ophiolite

1797   obduction and subsequent chemical weathering, the opening of oceanic gateways, and some mega-

1798   evolutionary events such as the evolution of land plants. One of the predictions made by our analysis

1799   of medium-term temperature changes is that there may have been several "mini-ice ages",

1800   interspersed between the major glacial episodes (e.g. Hirnantian Ice Age, Late Paleozoic Icehouse,

1801   and Late Cenozoic Icehouse; Figure 16).

1802   Short-term changes in the Earth's temperature are probably the most demonstrable because they

1803   are related to well-documented geologic events, namely the eruption of enormous volcanic

1804   provinces (LIPs) and the impact of large bolides. In this essay, we have documented that the

1805   eruption of ~20 large LIPs are strongly correlated with times of warmer global temperatures (Figure

1806   15 Tables 3-7). Conversely, it appears that large bolide impacts are well-correlated with cooler

1807   periods in Earth history (Figure 15, Tables 3-7), though a cause and effect relationship is less certain.

1808   It remains possible that a few of the most dramatic cooling events in Earth history may have been

1809   caused by as yet unrecognized large impact events (e.g. "Khione" event, Hirnantian Ice Age).

1810   In this essay, we combined the long-term, medium-term, and short-term changes in global

1811   temperature to produce the Phanerozoic Temperature Timescale (Figure 19-21, Tables 3-7). The

1812   Phanerozoic Temperature Timescale is divided into 24 "chronotemps", or distinct warm and cool

1813   intervals. The youngest chronotemp (W1) is the current period of anthropogenic warming. The

1814   oldest postdates the Cryogenian "Snowball Earth". Tables 3-7 list the names, timing, and

1815   temperatures associated with each chronotemp.

1816   It can certainly be argued that constructing a Phanerozoic Temperature Timescale is premature and

1817   an effort filled with error and unproven assumptions. Though this is probably true, we believe that

1818   the effort is worthwhile because we now have a structure that can be built upon, refined, corrected,

1819 expanded, and compared to other temperature models that use data sets that we did not use (i.e.,

1820 clumped isotopes, TEX_{86}). Moreover, having a paleotemperature timescale is essential if we are to

1821 understand the tempo and mode of climate change during the past 720+ million years. By

1822 characterizing, in a quantitative way, the pattern of paleotemperature change through time, we may

1823 be able to gain important insights into the history of the Earth System and the fundamental causes

1824 of climate change. These insights may be helpful guide as we traverse an uncertain path into the

1825 future.

1826

1827 7. Acknowledgements

1842

1843

1844   References Cited

1845   Ahlberg, A., Herman, A.B., Raikevich, M., Rees, A., and Spicer, R., 2002. Enigmatic Late Cretacoeous
1846   high paleo-latitude lonestones in Chukotka, northeasternmost Asia, GFF, v. 124, p. 197-199.

1847   Ahlberg, A., Olsson, I., Simkevicius, P., 2003. Triassic–Jurassic weathering and clay mineral dispersal
1848   in basement areas and sedimentary basins of southern Sweden. Sedimentary Geology, v. 161, p. 15–
1849   29.

1850   Alley, R.B., 2000. The Two-Mile Time Machine, Princeton University Press, Princeton, 229 pp.

1851   Alley, N.F., and Frakes, L.A., 2003. First known Cretaceous glaciation: Livingstone Tillite Member of
1852   the Cadna-owie formation, Australian Journal of Earth Sciences, v. 50, p. 139-144.

1853   Alsenz, H., Regnery, J., Ashckenazi-Polivoda, S., Meilijson, A., Ron-Yankovich, L., Abramovich, S.,
1854   Illner, P., Almogi-Labin, A., Feinstein, S., Berner, Z., Püttmann, W., 2013. Sea surface temperature
1855   record of a Late Cretaceous tropical southern Tethys upwelling system. Palaeogeogr. Palaeoclimatol.
1856   Palaeoecol. 392, 350–358.

1857   Alvarez, L.W., and Alvarez, W., Asaro, F., and Michel, H.V., 1980. Extraterrestrial cause for the
1858   Cretaceous-Tertiary extinction, Science, 208:1095-1107, doi: 10.1126/science.208.4448.1095

1859   Archer, D., 2005. Fate of fossil-fuel CO_2 in geologic time, Journal of Geophysical Research, Oceans,
1860   doi: 10.1029/2004JC002625.

1861   Archer, D., 2009. The Long Thaw, How Humans Are Changing the Next 100,000 years of Earth's
1862   Climate, Princeton University Press, Princeton, 180 pp.

1863   Archer, D., Eby, M., Brovkin, V., Ridgwell, A., Cao, I., Mikolajewicz, U., Caldiera, K., Matsumoto, K.,
1864   Munhoven, G., Montenegro, A., and Tokos, K., 2009. Atmospheric lifetime of fossil fuel carbon
1865   dioxide, Annual Review of Earth and Planetary Sciences, v. 37, pp. 117-134.

1866   Arthur, M.A., and Sageman, B.B., 1994. Marine black shales: Depositional mechanisms and
1867   environments of Ancient Deposits, Annual Review of Earth and Planetary Sciences, 22: 499-552.

1868   Azmy, K., Veizer, J., Bassett, M.G., Copper, P., 1998. Oxygen and carbon isotopic composition of
1869   Silurian brachiopods: Implications for coeval seawater and glaciations, Geological Society of America,
1870   v. 110, no. 11, p. 1499–1512.

1871   Balini, M., Lucas, S.G., Jenks, J.F, and Spielmann, J.A., 2010. Triassic ammonoid biostratigraphy: an
1872   overview, Geological Society of London, Special Publications, v.334:221–262.

1873   Bambach, R.K., Knoll, A.H., Wang, S.C., 2004. Origination, extinction, and mass depletions of marine
1874   diversity. Paleobiology, v. 30, p. 522–542.

1875   Barnola, J.M., Raynaud, D., Korotkevich, Y.S., and Lorius, C., 1987. Vostok ice core provides 160,000-
1876   year record of atmospheric CO2, Nature, v. 329, p. 408-414

1877   Barral, A, Gomez, B., Legendre, S., Lécuyer, C., 2017. Evolution of the carbon isotope composition of
1878   atmospheric CO_2 throughout the Cretaceous. Palaeogeography, Palaeoclimatology, Palaeoecology,
1879   http://dx.doi.org/10.1016/j.palaeo.2017.01.034

Barron, E.J. and Washington,W.M., 1982. Cretaceous climate: A comparison of atmospheric simulations with the geologic record, Palaeogeography, Palaeoclimatology, and Palaeoecology, v. 40, p. 103-133, doi: 10.1016/0031-0182(82)90086-4.

Beerling, D.J., Berner, R.A., 2002. Biogeochemical constraints on the Triassic-Jurassic boundary carbon cycle event, Global Biogeochemical Cycles, v. 16, no. 3, p.1036, doi:10. 1029/2001GB001637

Benedetto, J.L., and Sanchez, T.M., 1996. The "Afro-South American Realm" and Silurian "Clarkeia Fauna", in P. Copper and J. Jin (editors), Brachiopods, Balkema, p. 29-33.

Benton M.J., 1993. Late Triassic extinctions and the origin of the dinosaurs, Science, v. 260, p. 769–770.

Benton M.J., Zhang, Q., Hu, S., Chen, Z.Q., Wen. W,, et al., 2013. Exceptional vertebrate biotas from the Triassic of China, and the expansion of marine ecosystems after the Permo-Triassic mass extinction. Earth-Science Reviews, v. 125, p. 199–243.

Bergmann, K.D., Al Balushi, S.A.K., Macley, T., Grotzinger, J.P., and Eiler, J.M., 2018a. A 600-million year carbonate clumped-isotope record from the Sultanate of Oman, Journal of Sedimentary Research, v. 88, p. 960–979, doi:org/10.2110/jsr.2018.51.

Bergmann, K.D., Finnegan, S., Creel, R., Eiler, J.M., Hughes, N.C., Popov, L.E., and Fischer, W.W., , 2018b. A paired apatite and calcite clumped isotope thermometry approach to estimating Cambro-Ordovician seawater temperatures and isotopic composition, Geochimica et Cosmochimica Acta, v. 224, p.18-41, doi: 10.1016/j.gca.201 7.11.015.

Bernardi, M., Gianolla, P., Petti, F.M., Mietto, P., and Benton, M.J., 2018. Dinosaur diversification linked with the Carnian Pluvial Episode, Nature Communications, v. 9 :1499, doi: 10.1038/s41467-018-03996-1.

Berner R. A., 1994. GEOCARB II: A revised model of atmospheric CO_2 over Phanerozoic time. American Journal Science 294(1):56–91.

Berner, R.A., 2004. The Phanerozoic Carbon Cycle: CO2 and O2. Oxford University Press, New York.

Berner, R.A., Lasaga, A.C., & Garrels, R.M. (1983). The carbonate silicate geochemical cycle and its effect on atmospheric carbon dioxide over the past 100 million years. *American Journal Science,* 283, 641-683.

Beuf, S., Biju-Duval, B., deCharpal, O., Rognon, P., Gariel, O., and Bennacef, A., 1971. Les Gres du Paleozoique inferieur au Sahara, Editions Technip, Paris, 464 pp

Bice, K.L., and Norris, 2002, Possible atmospheric CO_2 extremes of the middle Cretaceous (late Albian to Turonian), Paleoceanography, 17:1-17.

Black, B.A., and Gibson, S.A., 2019. Deep Carbon and the life cycle of Large Igneous Provinces, Elements, v. 15, p. 319-324.

Bluth, G.J.D., & Kump, L.R., 1991. Phanerozoic paleogeology. American Journal Science, 291, 284-308

Bohor, B.F., Triplehorn, D.M., Nichols, D.J., and Millard, H.T.,Jr., 1987. Dinosaurs, spherules, and the "majic" layer: A new K-T boundary clay site in Wyoming, Geology,15:896-899.

Bond, D.P.G., and Grasby, S.E., 2017. On the causes of mass extinctions, Palaeogeography, Palaeoclimatology, Palaeoecology, v. 478, p. 3–29, doi.org/10.1016/j.palaeo.2016.11.005

Bonis, N.R., Ruhl, M., Kurschner, W.M., 2010. Climate change driven black shale deposition during the end-Triassic in the western Tethys. Palaeogeography, Palaeoclimatology, Palaeoecology, v. 290, p. 151–159.

Boucot, A.J., Chen Xu, and Scotese, C.R, 2013. Phanerozoic Paleoclimate: An Atlas of Lithologic Indicators of Climate, SEPM Concepts in Sedimentology and Paleontology, (Print-on-Demand Version), No. 11, 478 pp., ISBN 978-1-56576-289-3, October 2013, Society for Sedimentary Geology, Tulsa, OK.

Boucot, A.J., 1990. Silurian biogeography, in W.S. McKerrow and C.R. Scotese (editors), Palaeozoic Palaeogeography and Biogeography, Geological Society of London Memoir No. 12, p. 191-196.

Brady, E.C., DeConto, R., Thompson, S.L., 1998, Deepwater formation and poleward ocean heat transport in the warm climate extreme of the Cretaceous (80 Ma), Geophysical Research Letters, 25: 4205-4208.

Brand, U., Azmy, K., and Veizer, J., 2006. Evaluation of the Salinic I tectonic, Cancañiri glacial and Ireviken biotic events: Biochemostratigraphy of the Lower Silurian succession in the Niagara Gorge area, Canada and U.S.A., Palaeogeography, Palaeoclimatology, Palaeoecology, v. 241, p. 192–213, doi:10.1016/j.palaeo.2006.03.004

Brass, G.W., Southam, J.R., Peterson, W.H., 1982. Warm Saline Bottom Water in the Ancient Ocean. Nature 296, 620-623.

Brassell, S.C., 2009. Steryl ethers in a Valanginian claystone: molecular evidence for cooler waters in the central Pacific during the Early Cretaceous? Palaeogeogr. Palaeoclimatol. Palaeoecol. 282, 45–57.

Brandley, R.T., and Krause, F.F., 1994. Thinolite-type pseudomorphs after ikait: indicators of cold water on the subequatorial western margin of Lower Carboniferous North America, Canadian Society of Petroleum Geologists Memoir 17, p. 333-334.

Brenchley, P.J., Marshall., J.D., Carden, G.A.F., Robertson, D.B.R., Long, D.G., Meidla, T., Hints, L., and Anderson, T.F., 1994. Bathymetric and isotopic evidence for a short-lived Late Ordovician glaciation in a greenhouse period, Geology, v. 22, p. 295-298.

Brett, C.E., Ivany, L.C., Bartholomew, A.J., Desantis, M.K., and Baird, G.C., 2009. Devonian ecological-evolutionary subunits in the Appalachian Basin: a revision and test of persistence and discreteness, in Devonian Change: Case Studies in Palaeogeography and Palaeoecology, P. Konigshof (editor), Geological Society of London, Special Publication v. 314, p. 7-36.

British Petroleum (BP), 2019, "BP Energy Outlook, 2019". https://www.bp.com/content/dam/bp/business-sites/en/global/corporate/pdfs/energy-economics/energy-outlook/bp-energy-outlook-2019.pdf

Bruckschen, P., Oesmann, S., and Veizer, J., 1999. Isotope stratigraphy of the European Carboniferous: proxy signals for ocean chemistry, climate and tectonics, Chemical Geology, v. 161, p. 127–163.

1955   Brune, S., Williams, S.E., Müller, R.D., 2017. Potential links between continental rifting, CO_2
1956   degassing and climate change through time,

1957   Buggisch, W., Joachimski, W.M., Sevastopulo, G., and Morrow, J.R., 2008. Mississippian $\delta^{13}C_{carb}$
1958   and conodont apatite $\delta^{18}O$ records - Their relation to the Late Palaeozoic Glaciation,
1959   Palaeogeography, Palaeoclimatology, Palaeoecology, v. 268, p. 273–292,
1960   doi:10.1016/j.palaeo.2008.03.043

1961   Burke, K.D., Williams, J.W. Chandler, M.A., Haywood, A.M., Lunt, D.J., and Otto-Bliesner, B.L., 2018.
1962   Pliocene and Eocene provide best analogs for near-future climates, Proceedings of the National
1963   Academy of Sciences, v. 115, no. 52, 13288-13293.

1964   Cantrill, D.J., and Poole, I., 2012. The Vegetation of Antarctica Through Geological Time, Cambridge
1965   University Press, Cambridge, England, 480 pp.

1966   Cao, W., Williams, S., Flament, N., Zahirovic, S., Scotese, C.R., and Müller, R.D., 2019. Paleolatitudinal
1967   distribution of lithologic indicators of climate in a paleogeographic framework, Geological Magazine,
1968   v. 156, no. 2, p. 331-354.

1969   Caputo, M.V., de Melo, J.H.G., Streel, M., and Isbell, J.L., 2008. Late Devonian and Early
1970   Carboniferous glacial records of South America, in C.R. Fielding, T.D. Frank. and J.L. Isbell (editors),
1971   Resolving the Late Paleozoic Ice Age in Time and Space, Geological Society of America Special Paper
1972   v. 441, p. 161-174.

1973   Chamberlin, T.C., 1906. On a possible reversal of deep sea circulation and its influence on geologic
1974   climates, Proceedings of the American Philosophical Society, v. 45, n. 182, p. 33-43.

1975   Chatterjee, S., Guven, N., Yoshinobu, A., and Donofrio, R., 2006. Shiva structure: A possible KT
1976   boundary impact cater on the western shelf of India, Museum of Texas Tech University, Special
1977   Publication, 40 pp.

1978   Chen, B., Joachimski, M. M., Shen, S.-Z., Lambert, L. L., Lai, X.-L., Wang, X.-D., Chen, J., and Yuan, D.-
1979   X., 2013, Permian ice volume and palaeoclimate history: Oxygen isotope proxies revisited,
1980   Gondwana Research, v. 24, no. 1, p. 77-89.

1981   Chen, B., Joachimski, M. M., Wang, X.-D., Shen, S.-Z., Qi, Y.-P., and Qie, W.-K., 2016, Ice volume and
1982   paleoclimate history of the Late Paleozoic Ice Age from conodont apatite oxygen isotopes from
1983   Naqing (Guizhou, China), Palaeogeography, Palaeoclimatology, Palaeoecology, v. 448, p. 151-161.

1984   Chenet, A. L., Fluteau, F., Courtillot, V., Gerard, M., & Subbarao, K. V., 2008. Determination of rapid
1985   Deccan eruptions across the Cretaceous- Tertiary boundary using paleomagnetic secular variation:
1986   Results from a 1200-m-thick section in the Mahabaleshwar escarpment. Journal of Geophysical
1987   Research, 113, B04101. https://doi.org/10.1029/2006JB004635

1988   Clapham, M.E., and Renne, P.R., 2019. Flood Basalts and Mass Extinctions. Annual Review of Earth
1989   Planetary Sciences, v. 47, p. 275–303, doi: 10.1146/annurev-earth-053018-060136

1990   Clarkson, M.O., Kasemann, S.A., Wood, R.A., Lenton, T.M., Daines, S.J., et al., 2015. Ocean
1991   acidification and the Permo-Triassic mass extinction, Science, v. 348, p. 229–232,

Cocks, L.R.M., 1972. The origin of the Silurian Clarkeia shelly fauna of South America, and its extension to West Africa, Palaeontology, v. 15, p.623-630.

Cocks, L.R.M., and Fortey, R.A., 1990. Biogeography of Ordovician and Silurian faunas, in Palaeozoic Palaeogeography and Biogeography, W.S. McKerrow and C.R. Scotese (editors), Geological Society of London Memoir No. 12, p. 97-104.

Colbath, G.K., 1986. Abrupt terminal Ordovician extinction in phytoplankton associations, southern Appalachians, Geology, v. 14, p. 943-946.

Collins, M.R., R. Knutti, J. Arblaster, J.-L. Dufresne, T. Fichefet, P. Friedlingstein, X. Gao, W.J. Gutowski, T. Johns, G. Krinner, M. Shongwe, C. Tebaldi, A.J. Weaver, and M. Wehner, 2013: Long-term Climate Change: Projections, Commitments and Irreversibility. In Climate Change 2013: The Physical Science Basis. Contribution of Working Group I to the Fifth Assessment Report of the Intergovernmental Panel on Climate Change [Stocker, T.F., D. Qin, G.-K. Plattner, M. Tignor, S.K. Allen, J. Boschung, A. Nauels, Y. Xia, V. Bex, and P.M. Midgley (eds.)]. Cambridge University Press, Cambridge, United Kingdom and New York NY, USA.

Courtillot, V., and Renne, X., 2003. On the ages of flood basalt events, Comptes Rendus Geosciences, v. 335, p. 113-140.

Cramer,B.S., Toggweiler, J.R., Wright, J.D., Katz, M.E., and Miller, K.G., 2009. Ocean overturning since the Late Cretaceous: Inferences from a new benthic isotope compilation, Paleoceanography 6, v. 24, PA4216, p. 1-14, doi: 10.1029/2008PA001683.

Crowley, T.J., 1994. Pangean Climates, in Pangea: Paleoclimate, Tectonics, and Sedimentation during Accretion, Zenith, and Breakup of a Supercontinent, (editor), G. D. Klein, Geological Society of America Special Paper 288, p. 25-39.

Crowley,T.J., and Baum, S.K., 1991. Toward reconciliation of Late Ordovician (~440 Ma) glaciation with very high CO_2 Levels, Journal of Geophysical Research, v. 96, no. D12, p. 22,597-22,610.

Crowley,T.J., and Baum, S.K., 1995. Reconciling Late Ordovician (440 Ma) glaciation with very high (14X) CO_2 Levels, Journal of Geophysical Research, v. 100, no. D1, p. 1093-1101.

Dal Corso, J., Benton, M. J., Bernardi, M., Franz, M., Gianolla, P., Hohn, S., and Zhang, Y., 2018a. First Workshop on the Carnian Pluvial Episode (Late Triassic): a report, Albertiana, v. 44, p. 49-57.

Dal Corso, J., Gianolla, P., Rigo, M., Franceschi, M., Roghi, G., Mietto, P., Manfrin, S., Raucsik, B., Budai, T., Jenkyns, H.C., Reymond, C.E., Caggiati, M., Gattolini, G., Breda, A., Merico, A., Preto, N., 2018b. Multiple negative carbon-isotope excursions during the Carnian Pluvial Episode (Late Triassic), Earth-Science Reviews, v. 185, p. 732–750, doi:org/10.1016/j.earscirev.2018.07.004

Davydov, V.I., and Cozar, P., 2017. The formation of the Alleghenian Isthmus triggered the Bashkirian glaciation: Constraints from warm-water benthic foraminifera, Palaeogeography, Palaeoclimatology, Palaeoecology, http://dx.doi.org/10.1016/j.palaeo.2017.08.012

Davydov, V.I., 2014. Warm water benthic foraminifera document the Pennsylvanian–Permian warming and cooling events — The record from the Western Pangea tropical shelves, Palaeogeography, Palaeoclimatology, Palaeoecology, v. 414, p. 284-295, doi.org/10.1016/j.palaeo.2014.09.013

2031 Davydov, V.I., Korn, D., Schmitz, M.D., 2010. The Carboniferous Period, Chapter 23, in The Geologic
2032 Time Scale 2012, volume 2, F.M. Gradstein, J.G. Ogg, M.D. Schmitz, and G.M. Ogg (editors), Elsevier,
2033 Amsterdam, p. 603-651.

2034 De Lurio, J.L. and Frakes, L.A., 1999. Glendonites as a paleoenvironmental tool: Implications for early
2035 Cretaceous high latitude climates in Australia, Geochimica et Cosmochimica Acta, Vol. 63, No. 7/8,
2036 pp.

2037 Demaison, G.J., and Moore, G.T., 1980. Anoxic environments and oil source bed genesis, American
2038 Association of Petroleum Geologists Bulletin, 64:1179-1209.

2039 Dera, G., Brigaud, B., Monna, F., Laffont, R., Pucéat, E., Deconinck, J.-F., Pellenard, P., Joachimski,
2040 M.M., and Durlet, C., 2011. Climatic ups and downs in a disturbed Jurassic world, Geology, v. 39, no.
2041 3., p. 215-218, doi: 10.1130/G31579.1

2042 Dettmann, M.E., 1989. Antarctica: Cretaceous cradle of austral temperate rainforests?, in Origins
2043 and Evolution of the Antarctic Biota, Geological Society of London Special Publication, J.A. Crame
2044 (editor), v. 47, p. 89-105.

2045 Díaz-Martínez, E., and Grahn, I., 2007. Early Silurian glaciation along the western margin of
2046 Gondwana (Peru, Bolivia and northern Argentina): Palaeogeographic and geodynamic setting.
2047 Palaeogeography, Palaeoclimatology, Palaeoecology, v. 245, p. 62–81,
2048 doi:10.1016/j.palaeo.2006.02.018

2049 Duncan, R.A., and Huard, J., 1997. Trace metal anomalies and global anoxia: the OJP-Selli
2050 hydrothermal plume connection, EOS Transactions American Geophysical Union, 78, F774.

2051 Elliot, D.H., Fleming, T.H., Kyle, P.R., and Foland, K.A., 1999. Long-distance transport of magmas in the
2052 Jurassic Ferrar large igneous province, Antarctica, Earth and Planetary Science Letters, v. 167, p. 89-
2053 104.

2054 Elrick, M., and Scott, L. A., 2010, Carbon and oxygen isotope evidence for high-frequency (10^4–10^5yr)
2055 and My-scale glacio-eustasy in Middle Pennsylvanian cyclic carbonates (Gray Mesa Formation),
2056 central New Mexico, Palaeogeography, Palaeoclimatology, Palaeoecology, v. 285, no. 3, p. 307-320.

2057 Emiliani, C. 1954. Temperatures of Pacific bottom waters and polar superficial waters during the
2058 Tertiary, Science, v. 119, issue 3103, p. 853-855, doi: 10.1126/science.119.3103.853

2059 Emiliani, C., 1955. Pleistocene temperatures, Journal of Geology, v. 63, no. 6, p. 538-578.

2060 EPICA Community Members, 2004. Eight glacial cycles from an Antarctic ice core, Nature 429: 623-
2061 628.

2062 Epstein, S. and Mayeda, T., 1953. Variation of O18 content of waters from natural sources,
2063 Geochemica et Cosmochemica Acta. 4 (5), 213-224.

2064 Erba, E., Bartolini, A., and Larson, R.L., 2004. Valanginian Weissert oceanic anoxic event, Geology
2065 32(2):149-152, doi 10.1130/G20008.1

2066 Erba, E., Duncan, R.A., Bottini, C., Tiraboschi, D., Weissert, H., Jenkyns, H.C., and Malinverno, A.,
2067 2015, Environmental consequences of Ontong Java Plateau and Kerguelen Plateau volcanism, in
2068 Neal, C.R., Sager, W.W, Sano, T., and Erba, E., eds., The Origin, Evolution, and Environmental Impact
2069 of Oceanic Large Igne- ous Provinces: Geological Society of America Special Paper 511, p. 271–303,
2070 doi:10.1130/2015.2511(15).

2071   Ernst, R.E., 2014. Large Igneous Provinces, Cambridge University Press, Cambridge, UK, 653 pp.

2072   Ernst, R.E., and Youbi, N., 2017. How Large Igneous Provinces affect global climate, sometimes cause
2073   mass extinctions, and represent natural markers in the geological record, Palaeogeography,
2074   Palaeoclimatology, Palaeoecology, v. 478, p. 30–52., doi:10.1016/j.palaeo.2017.03.014

2075   Erwin, D.H., 1993. The Great Paleozoic Crisis: Life and Death in the Permian, Columbia University
2076   Press, New York, 327 pp.

2077   Erwin, D.H., 1995. The End-Permian Mass Extinction, in *The Permian of the Northern Hemisphere*,
2078   volume 1: Paleogeography, Paleoclimates, Stratigraphy, P.A. Scholle, T.M. Peryt, D.S Ulmer-Scholle
2079   (editors), Springer-Verlag, Berlin, p. 3-19.

2080   Erwin, D.H., 2006. Extinction: How Life on Earth Nearly Ended 250 Million Years Ago, Princeton
2081   University Press, Princeton, 296 pp.

2082   Exon, N.F., Kennett, J.P., and Malone, M., 2004.The Cenozoic Southern Ocean: Tectonics,
2083   Sedimentation, and Climate Change between Australia and Antarctica, American Geophysical Union,
2084   Geophys. Monograph 151.

2085   Farnsworth, A., Lunt, D.J., O'Brien, C., Foster, G.L., Inglis, G.N., Markwick, P., Pancost, R.D., and
2086   Robinson, S.A., 2019. Climate sensitivity on geological timescales controlled by non-linear feedbacks
2087   and ocean circulation, Geophysical Research Letters.

2088   Fielding, C.R., Frank, T.D., Isbell, J.L., Henry, L.C., and Domack, E.W., 2010. Stratigraphic signature of
2089   the late Palaeozoic Ice Age in the Parmeener Supergroup of Tasmania, SE Australia, and inter-
2090   regional comparisons , Palaeogeography, Palaeoclimatology, Palaeoecology, v. 298, p. 70–90,
2091   doi:10.1016/j.palaeo.2010.05.023

2092   Fielding, C.R., Frank, T.D., Birgenheier, L.P., Rygel, M.C., Jones, A.T., and Roberts, J., 2008.
2093   Stratigraphic imprint of the Late Palaeozoic Ice Age in eastern Australia: a record of alternating
2094   glacial and nonglacial climate regime, Journal of the Geological Society, London, v. 165, p. 129–140.

2095   Fielding, C.R., Frank, T.D., Birgenheier, L.P., Rygel, M.C., Jones, A.T., and Roberts, J., 2008.
2096   Stratigraphic record and facies associations of the Late Paleozoic ice age in eastern Australia (New
2097   South Wales and Queensland), in C.R. Fielding, T.D. Frank. and J.L. Isbell (editors), Resolving the Late
2098   Paleozoic Ice Age in Time and Space, Geological Society of America Special Paper v. 441, p. 41-58.

2099   Finnegan, S., Bergmann, K., Eiler, J.M., Jones, D. S., Fike, D. A., Eisenman, I., Hughes, N. C., Tripati, A.
2100   K., and Fischer, W. W., 2011. The magnitude and duration of Late Ordovician – Early Silurian
2101   Glaciation, Science, v. 331, no. 6019, p. 903-906, doi: 10.1126/science.12000803.

2102   Finnegan, S., Heim, N.A., Peters, S.E., Fischer, and Fischer, W.W., 2012. Climate change and selective
2103   signature of the Late Ordovician mass extinction, Proceedings of the National Academy of Sciences,
2104   v.109, no. 18, p. 6829-6834.

2105   Fischer, A. G., 1981. Climatic oscillations in the biosphere, in M.H. Nitecki (editor), Biotic Crises in
2106   Ecological and Evolutionary Time, Academic Press, pp. 103-131.

2107   Fischer, A. G., 1982. Long-term Climatic Oscillations Recorded in Stratigraphy, in Studies in
2108   Geophysics: Climate in Earth History, W.H. Berger and J.C. Crowell (editors), Chapter 9., National
2109   Academy Press, Washington, D.C., pp. 97-104.

2110   Fischer, A. G., 1984. The Two Phanerozoic Supercycles, in Catastrophes and Earth History: The New
2111   Uniformitarianism, W.A. Berggren and J.A. Van Couvering, (editors), Chapter 7, Princeton University
2112   Press, Princeton, N.J., pp. 129 – 150.

2113   Flügel, E., 1994. Pangean shelf carbonates: Controls and paleoclimatic significance of Permian and
2114   Triassic reefs, in Pangea: Paleoclimate, Tectonics, and Sedimentation during the Accretion, Zenith,
2115   and Breakup of a Supercontinent, George D. Klein (ed.), Geol. Soc. America Special Paper, 288: 247-
2116   266.

2117   Flügel, E., 2002. Triassic reef patterns, In Kiessling, W., Flügel,, E. & Golonka, J. (eds): Phanerozoic
2118   Reef Patterns. SEPM (Society for Sedimentary Geology) Special Publications 72, 391-464.

2119   Flügel,, E. & Kiessling, W., 2002. Patterns of Phanerozoic reef crises. In Kiessling, W., Flügel,, E. &
2120   Golonka, J. (eds): Phanerozoic Reef Patterns. SEPM (Society for Sedimentary Geology) Special
2121   Publications 72, 691-733.

2122   Foster, G.L., Royer, D.L., and Lunt, D.J., 2017. Future Climate Forcing Potentially without precedent in
2123   the last 420 million years, Nature Communications, v. 8, 14845, doi:10.1038/ncomms14845.

2124   Fraenkel, G., 1960. Lethal High Temperatures for Three Marine Invertebrates: Limulus Polyphemus,
2125   Littorina littorea and Pagurus longicarpus, Oikos, v. 11 fasc. 2, p. 171-182.

2126   Frakes, L.A., 1989. Climates Through Geologic Time, Elsevier, Amsterdam, 310 pp.

2127   Frakes, L., and Francis, J.E., 1988. A guide to Phanerozoic cold polar climates from high latitude ice-
2128   rafting in the Cretaceous. Nature 333, 547–549.

2129   Frakes L. A. and Francis J. E., 1990. Cretaceous palaeoclimates. In Cretaceous Resources, Events, and
2130   Rhythms (ed. R. N. Ginsburg and B. Beaudoin), pp. 373–287. Kluwer Academic Publishers.

2131   Frakes, L.A., Francis, J.E., and Syktus, J.I., 1992. Climate Modes of the Phanerozoic, Cambridge
2132   University Press, Cambridge, 274 pp. Freeman and Hayes

2133   Francis J. E. and Frakes L. A., 1993. Cretaceous climates. Sediment. Rev. **1,** 17–30.

2134   Frakes, L.A., Alley, N.F., and Deynoux, M., 1995. Early Cretaceous ice rafting and climate zonation in
2135   Australia, International Geology Review, v. 37, p. 567-583.

2136   Frank, T.D., Schultis, A.I., Fielding, C.R., 2015. Acme and demise of the late Palaeozoic ice age: A
2137   view from the southeastern margin of Gondwana, Palaeogeography, Palaeoclimatology,
2138   Palaeoecology, v. 418, p. 176–192, doi.org/10.1016/j.palaeo.2014.11.016

2139   Friedman, M., Sallan, L.C., 2012. Five hundred million years of extinction and recovery: a
2140   Phanerozoic survey of large-scale diversity patterns in fishes, Palaeontology, v. 55, p. 707–742.

2141   Galili, N., Shemesh, A., Yam, R., Brailovsky, I., Sela-Adler, M., Schuster, E.M., Collom, C., Bekker, A.,
2142   Planavsky, N., Macdonald, F.A., Préat, A., Rudmin, M., Trela, W., Sturesson, U., Heikoop, J.M., Aurell,
2143   M., Ramajo, J., and Halevy, I., 2019. The geologic history of seawater oxygen isotopes from marine
2144   iron oxides, Science, v. 365, p. 469–473.

2145 Gasson, E.G.W., and Kiessling, B.A., 2020. The Antarctic Ice Sheet, A Paleoclimate Modeling
2146 Perspective, Oceanography, June 2020 Online Release, pp. 11, doi.org/10.5670/oceanog.2020.208

2147 Gersonde, R. Kyte, F.T., Bleil, U., Diekmann, J.A., Flores, J.A., Gohl, K, Grahl, G., Hagen, R., Kuhn, G.,
2148 Sierro, F.J., Volker, D., and Bostwick, J.A., 1997. Geological record and reconstruction of the late
2149 Pliocene impact of the Eltanin asteroid in the Southern Ocean, Nature, 390: 357-363.

2150 Gibbs, M.T., Bluth, G.J.S., Fawcett, P.J., & Kump, L.R., 1999. Global chemical erosion over the last 250
2151 My: variations due to changes in paleogeography, paleoclimate, and paleogeology. American Journal
2152 Science, 299, 611–651.

2153 Girard, C., Klapper, G., and Feist, R., 2005. Subdivision of the terminal Frasnian linguiformis conodont
2154 Zone, revision of the correlative interval of Montagne Noire Zone 13, and discussion of
2155 stratigraphically significant Associated trilobites, in Understanding Late Devonian and Permian-
2156 Triassic Biotic and Climatic Events; Towards an Integrated Approach, D.J. Over, J.R. Morrow, and P.B.
2157 Wignall (editors), Developments in Palaeontology & Stratigraphy, v. 20, p. 181-198, Elsevier,
2158 Amsterdam.

2159 Goddéris, Y., Donnadieu, Y., Lefebvre, V., Le Hir, G., & Nardin, E., 2012. Tectonic control of
2160 continental weathering, atmospheric CO_2, and climate over Phanerozoic times: Comptes Rendus
2161 Geoscience, 344, 652–662.

2162 Goddéris, Y., Donnadieu, Y., Le Hir, G., Lefebvre, V., & Nardin, E., 2014. The role of palaeogeography
2163 in the Phanerozoic history of atmospheric CO_2 and climate. Earth-Science Reviews, 128, 122–138.

2164 Gough, D.O., 1981. Solar interior structure and luminosity variation, Solar Physics, v. 74, p. 21-34.

2165 Gradstein, F.M., Ogg, J.G., Schmitz, M.D., and Ogg., G.M., 2012. The Geologic Time Scale 2012, v. 1,
2166 Elsevier, 435 pp.

2167 Grahn, Y., Caputo, M.V., 1992. Early Silurian glaciations in Brazil Palaeogeography,
2168 Palaeoclimatology, Palaeoecology, v. 99, p. 9–15.

2169 Grahn, Y., Gutiérrez, P., 2001. Silurian and Middle Devonian chitinozoa from the Zapla and Santa
2170 Bárbara Ranges, Tarija Basin, northwestern Argentina. Ameghiniana, v. 38, p. 35–50.

2171 Grasby, S.E., McCune, G.E., Beauchamp, B., Galloway, J.M., 2017. Lower Cretaceous cold snaps led to
2172 widespread glendonite occurrences in the Sverdrup Basin, Canadian High Arctic. Geol. Soc. Am. Bull.
2173 129, 771–787. http://dx.doi.org/10.1130/B31600.1.

2174 Grice, K., Cao, C., Love, G.D., Böttcher, M.E., Twitchett, R.J., et al., 2005. Photic zone euxinia during
2175 the Permian- Triassic superanoxic event, Science v. 307, p. 706–709.

2176 Greene, A.R., Scoates, J.S., and Weis, D., 2008. Wrangellia flood basalts in Alaska: A record of plume-
2177 lithosphere interaction in a Late Triassic accreted oceanic plateau. Geochemistry Geophysics
2178 Geosystems, v. 9, Q12004, doi: 10.1029/2008GC002092.

2179 Greene, A.R., Scoates, J.S., Weis, D., and Israel, S., 2009a. Geochemistry of flood basalts from the
2180 Yukon (Canada) segment of the accreted Wrangellia oce- anic plateau. Lithos, v. 110, p. 1–19, doi:
2181 10.1016/j .lithos.2008.11.010.

2182 Greene, A.R., Scoates, J.S., Weis, D., Nixon, G.T., and Kieffer, B., 2009b. Melting history and
2183 magmatic evolution of basalts and picrites from the accreted Wrangellia oceanic plateau, Vancouver
2184 Island, Canada: Journal of Petrology, v. 50, p. 467–505, doi: 10.1093/petrology/ egp008.

2185 Greene, A.R., Scoates, J.S., Weis, D., Katvala, E.C., Israel, S., and Nixon, G.T. 2010. The architecture of
2186 oceanic plateaus revealed by the volcanic stratigraphy of the accreted Wrangellia oceanic plateau,
2187 Geosphere, v. 6, p. 47–73.

2188 Grossman, E. L., I994. The carbon and oxygen isotope record during the evolution of Pangea
2189 Carboniferous to Triassic, in Klein. G. D., ed., Pangea: Paleoclimate, Tectonics, and Sedimentation
2190 During Accretion, Zenith, and Breakup of a Supercontinent: Boulder, Colorado, Geological Society of
2191 America Special Paper 288, p. 207-228.

2192 Grossman, E.L., 2012a. Oxygen Isotope Stratigraphy, in The Geologic Time Scale 2012, F. M.
2193 Gradstein, J.G. Ogg, M.D. Schmitz, and G.M. Ogg (editors), Elsevier, Amsterdam, volume 1, p. 181-
2194 206.

2195 Grossman, E.L., 2012b. Applying Oxygen Isotope Paleothermometry in Deep Time, in Reconstructing
2196 Earth's Deep-Time Climate: State of the Art in 2012, L. Ivany and B. Huber (editors), Paleontological
2197 Society Short Course, November 3, 2012, The Paleontological Society Papers, v. 18, pp. 39-67.

2198 Grossman, E.L., and Joachimski, M.M., 2020. Oxygen Isotope Stratigraphy, Chapter 10, in The
2199 Geologic Time Scale 2020, F. M. Gradstein, J.G. Ogg, M.D. Schmitz, and G.M. Ogg (editors), Elsevier,
2200 Amsterdam, volume 1, (in press).

2201 Grossman, E.L., Joachimski, M.M., Barney, B., Henkes, G.A., Ivany, L.C., Lunt, D.L., MacLeod,K.G.,
2202 Montañez, I.P., Scotese, C., and Wing, S.L., 2018. Toward a Phanerozoic History of Earth's Surface
2203 Temperature: The Oxygen Isotope Record of the Paleozoic to Early Cretaceous Time Slice (PalECTS),
2204 (abstract), American Geophysical Union, Monday, December 10, 2018, Convention Center, Hall A-C
2205 (Poster Hall), Fall Meeting 2018, #PP11F-11319, Washington, D.C.

2206 Grossman, E.L., Yancey, T.E., Jones, T.E., Bruckschen, P., Chuvashov, B., Mazullo, S.J., and Mii,
2207 Horng-sheng, 2008. Glaciation, aridification, and carbon sequestration in the Permo-Carboniferous:
2208 The isotopic record from low latitudes, Palaeogeography, Palaeoclimatology, Palaeoecology, v. 268,
2209 p. 222–233, doi:10.1016/j.palaeo.2008.03.053

2210 Gruszczynski, M., Halas S., Hoffman, A., and Malkowski, K., 1989. A brachiopod calcite record of the
2211 oceanic carbon and oxygen isotope shifts at the Permian/Triassic transition. Nature, v. 337, p. 64-68.

2212 Gutjahr, M., Ridgwell, A., Sexton, P.F., anagnoustou, E., Pearson, P.N., Pälike, H., Norris, R.D.,
2213 Thomas, E., and Foster, G.L., 2017. Very large release of mostly volcanic carbon during the
2214 Paleocene-Eocene Thermal Maximum, Nature, v. 548, p. 573-577.

2215 Haig, D.W., McCartain, E., Mory, A.J., Borges, G., Davydov,V.I., Dixon, M., Ernst, A., Groflin, S.,
2216 Håkansson, E., Keep, M., Dos Santos, Z., Shi, G.R., and Soares, J., 2014. Postglacial Early Permian (late
2217 Sakmarian–early Artinskian) shallow-marine carbonate deposition along a 2000 km transect from
2218 Timor to west Australia, Palaeogeography, Palaeoclimatology, Palaeoecology, v. 409, p. 180–204,
2219 doi.org/10.1016/j.palaeo.2014.05.009

2220 Hallam, A., 2002. How catastrophic was the end-Triassic mass extinction? Lethaia, v.35, p.147-157,
2221 doi: org/10.1111/j.1502-3931.2002.tb00075.x

Hames, W., McHone, J.G., Renne, P., and Ruppel, C., 2003. The Central Atlantic Magmatic Province: Insights from Fragments of Pangea, American Geophysical Union, Geophys. Monogr. Ser., vol. 136, 267 pp.

Hammer, W.R., and Hickerson, W.J., 1996. Implications of an early Jurassic vertebrate fauna from Antarctica, in M. Morales (editor), The Continental Jurassic, Transactions of the Continental Jurassic Symposium, October 21-23, 1996, Museum of Northern Arizona, Flagstaff, Arizona, Museum of Northern Arizona Bulletin, v. 60, p. 215-218.

Haq, B. U., & Schutter, S. R., 2009. A chronology of Paleozoic sea-level changes. Science, 322, 64-68.

Haq, B. U., Hardenbol, J., & Vail, P. R., 1987. Chronology of fluctuating sea levels since the Triassic. Science, 235, 1156-1167.

Hautmann, M., 2004. Effect of end-Triassic CO_2 maximum on carbonate sedimentation and marine mass extinction. Facies 50: 257–261.

Hautmann, M., Benton, M.J., and Tomašových, A., 2008. Catastrophic ocean acidification at the Triassic-Jurassic boundary. Neues Jahrb. Geologie Paläontologie, v. 249, p.119–127.

Hay, W.W., 2008. Evolving ideas about the Cretaceous climate and ocean circulation, Cretaceous Research, 29: 725-753.

Hay, W.W., 2016. Experimenting on a Small Planet: A History of Scientific Discoveries, a Future of Climate Change and Global Warming, Springer, Switzerland, 819 pp.

Hayes, P.A., Francis, J.E., Cantrill, D.J., and Crame, J.A., 2006. Palaeoclimate analysis of Late Cretaceous angiosperm leaf floras, James Ross Island, Antarctica, in *Cretaceous-Tertiary High-Latitude Palaeoenvironments, James Ross Basin, Antarctica*, J.E., Francis, D. Pirrie, and J.A. Crame, (editors), Geol. Soc. London Special Publications 258:49-62.

Hays, P. D., and Grossman, E. L., 1991, Oxygen isotopes in meteoric calcite cements as indicators of continental paleoclimate, Geology, v. 19, no. 5, p. 441-444.

Hearing, T.W., Harvey, T,H.P., Williams, M., Leng, M.J., Lamb, A.L., Wilby, P.R., Gabbott, S.E., Pohl, A., and Donnadieu, Y., 2018. An early Cambrian greenhouse climate, Science Advances, 4:eaar5690 9.

Heckel, P.H., 1994. Evaluation of evidence for glacio-eustatic control over marine Pennsylvanian cyclothems in North America and consideration of possible tectonic effects in J.M. Dennisonand F.R. Ettensohn (editors), Tectonic and Eustatic Controls on Sedimentary Cycles, SEPM Concepts in Sedimentology and Paleontology, v4, p. 65-87.

Heckel, P.H., 2008. Pennsylvanian cyclothems, in Midcontinent North Ameri- ca as far-field effects of waxing and waning of Gondwana ice sheets, in C.R. Fielding, T.D. Frank, and J.L. Isbell (editors), Resolving the Late Paleozoic Ice Age in Time and Space, Geological Society of America, Special Paper 441, p. 275-289.

Heckel, P.H., 2013. Pennsylvanian stratigraphy of Northern Midcontinent Shelf and biostratigraphic correlation of cyclothems, Stratigraphy, v. 10, no. 1–2, pp. 3–39.

2258 Henderson, C.M., Davydov, V.I., Wardlaw, B.R., 2012. The Permian Period, Chapter 24, in The
2259 Geologic Time Scale 2012, volume 2, F.M. Gradstein, J.G. Ogg, M.D. Schmitz, and G.M. Ogg (editors),
2260 Elsevier, Amsterdam, p.653-679.

2261 Henkes, G.A., Passey, B.H., Grossman, E.L., Shenton, B. J., Yancey, T. E., and Pérez-Huerta, A., 2018.
2262 Temperature evolution and oxygen isotope composition of Phanerozoic oceans from carbonate
2263 clumped isotope thermometry, Earth and Planetary Science Letters, v. 490, pp. 40-50,
2264 doi:10.1016/j.epsl.2018.02.001.

2265 Herrle, J.O., Schröder-Adams, C.J., Davis, W., Pugh, A.T., Galloway, J.M., and Fath, J., 2015. Mid-
2266 Cretaceous High Arctic stratigraphy, climate, and Oceanic Anoxic Events. Geology, 43(5): 403-406.

2267 Heydari, E., Arzani, N., and Hassanzadeh, J., 2008. Mantle plume: The invisible serial killer -
2268 Application to Permian-Triassic boundary mass extinction, Palaeogeography, Palaeoclimatology,
2269 Palaeoecology, v. 264, p. 147-162.

2270 Hildebrand, A.R., Penfield, G.T., Kring, D.A., Pilkington, M., Camargo, Z.A., Jacobsen, S.B., and Boynton,
2271 W.V., 1991. Chicxulub crater: A possible Cretaceous-Tertiary boundary impact crater on the Yucutan
2272 Peninsula, Mexico, Geology, 19:867-871.

2273 Hilgen, F.J., Lourens, L.J., and Van Dam, J.A., 2012. The Neogene Period, Chapter 29, in The Geologic
2274 Time Scale 2012, volume 2, F.M. Gradstein, J.G. Ogg, M.D. Schmitiz, and G.M. Ogg, (editors), p. 923-
2275 978, Elsevier, Amsterdam.

2276 Hochuli, P.A., Hermann, E., Vigran, J.O., Bucher, H., and Weissert, H., 2010. Rapid demise and recovery
2277 of plant ecosystems across the end-Permian extinction event, Global and Planetary Change, v. 74, p.
2278 144-155.

2279 Hodel, F., Macouin, M., Trindade, R.I.F., Triantafyllou, A., Ganne, J., Chavagnac, V., Berger, J.,
2280 Rospabé, M., Destrigneville, C., Carlut, J., Ennih, N., and Agrinier, P., 2018. Fossil black smoker yields
2281 oxygen isotopic composition of Neoproterozoic seawater, Nature Communications, 9:1453, doi:
2282 10.1038/s41467-018-03890

2283 Hoffman, P.F., Kaufman, A.J., Halverson, G.P., and Schrag, D.P., 1998. A Neoproterozoic snowball
2284 Earth, Science, 281: 1342-1346.

2285 Hoffman,P.F., and Schrag, D.P., 2000. Snowball Earth, Scientific American, v. 282, p. 68-75.

2286 Hoffman, P.F., and Schrag, D.P., 2002. The snowball Earth hypothesis: testing the limits of global
2287 change, Terra Nova, v. 14, p. 129-155.

2288 Hoffman, P.F., and Li, Z.-X., 2009. A palaeogeographic context for Neoproterozoic glaciation,
2289 Palaeogeogrphy, Palaeoclimatology, Palaeoecology, v. 277 (3-4), p 158-172.

2290 Hotinski, R., Bice, K.L., Kump, L.R., Najiar, R.G., and Arthur, M.A., 2001. Ocean stagnation and end-
2291 Permian anoxia. Geology, v. 29, p. 7-10.

2292 Hotinski, R.M., and Toggweiler, J.R., 2003. Impact of a Tethyan circumglobal passage on ocean heat
2293 transport and "equable" climates, Paleoceanography, 18:1007-1015.

2294 Hsu, K.J., Oberhansli, H., Gao, J.Y., Shu, S., Haihong, C., and Krahenbuhl, U., 1985. 'Strangelove ocean'
2295 before the Cambrian. Nature, v. 316, p. 809-811.

2296   Huber, B.T., 1998. Tropical paradise at the Cretaceous poles?, Science, v. 282, p. 2199-2200.

2297   Huber, B.T., MacLeod, K.G., and Wing, S.L., 2000. Warm Climates in Earth History, Cambridge
2298   University Press, 462 pp.

2299   Huber, M., and Caballero, R., 2011. The early Eocene equable climate problem revisited: Climate of
2300   the Past Discussions, v.7., p. 241-304, doi: 10.5194/cpd-7-241-2011.

2301   Hughes, D.W., 2003. The approximate ratios between the diameters of terrestrial impact craters and
2302   the causative incident bolides, Mon. Not. R. Astron, Soc., v. 338, p. 999-1003.

2303   IPCC 2007: Summary for Policymakers. IN: Climate Change 2007: The Physical Science Basis.
2304   Contribution of Working Group I to the Fourth Assessment Report of the Intergovernmental Panel
2305   on Climate Change [Solomon, S., D. Qin, M. Manning, Z. Chen, M. Marquis, K.B. Averyt, M. Tignor,
2306   and H.L. Miller (eds.)]. Cambridge University Press, Cambridge, United Kingdom and New York, USA.

2307   IPCC 2018: Summary for Policymakers. In: Global Warming of 1.5˚C. An IPCC Special Report on the
2308   impacts of global warming of 1.5˚C above pre-industrial levels and related greenhouse gas emission
2309   pathways, in the context of strengthening the global response to the threat of climate change,
2310   sustainable development, and efforts to eradicate poverty [Masson-Delmotte, V., P. Zhai, H.-O.
2311   Portner, D. Roberts, J. Skea, P.R. Sukla, A. Pirani, W. Moufouma-Okia, C. Pean, R. Pidcock, S. Connors,
2312   J.B.R. Matthews, Y. Chen, X. Zhou, M.I. Gomis, E. Lonnoy, T. Maycock, M. Tignor, and T. Waterfield
2313   (eds.)] Cambridge University Press, Cambridge, United Kingdom and New York, USA.

2314   IPCC 2019: Summary for Policymakers. In: IPCC Special Report on the Ocean and Cryosphere in a
2315   Changing Climate [H.-O. Portner, D.C. Roberts, V. Masson-Delmotte, P. Zhai, M. Tignor, E.
2316   Poloczanska, K. Mintenbeck, M. Nicolai, A. Okem, J. Petzold, B. Rama, N. Weyer(eds.)] Cambridge
2317   University Press, Cambridge, United Kingdom and New York, USA.

2318   Isozaki, Y., 1997. Permo-Triassic boundary superanoxia and startified superocean: Records from Lost
2319   Deep Sea. Science, v. 276, p. 235-238.

2320   Jacobs, L.L., Polcyn, M.J., Taylor, L.H., and Ferguson, K., 2005, Sea-surface temperatures and
2321   paleoenvironments of dolichosaurs and early mosasaurs, Netherlands Journal of Geosciences,
2322   Geologie en Mijnbouw, 84-3:269-281.

2323   Jaffres, J.B.P., Shields, G.A., and Wallman, K., 2007. The oxygen isotope evolution of seawater: a critical
2324   review of a long-standing controversy and an improved geological water cycle model for the past 3.4
2325   billion years, Earth-Science Reviews, 83:83-122.

2326   Jenkyns, H.C., Jones, C.J., Groeke, D.R., Hesselbo, S.P., and Parkinson, D.N., 2002. Chemostratigraphy
2327   of the Jurassic System: applications, limitations and implications for palaeoceanography, Journal of
2328   the Geological Society, London, v. 159, p. 351–378.

2329   Jenkyns, H.C., 2010. Geochemistry of oceanic anoxic events. Geochemical Geophysical Geosystems,
2330   11:Q03004.

2331   Jenkyns, H.C., Schouten-Huibers, L., Schouten, S., and Sinninghe Damste, J.S., 2012. Warm Middle
2332   Jurassic–Early Cretaceous high-latitude sea-surface temperatures from the Southern Ocean, Climate
2333   of the Past, 8:215-226, doi:10.5194/cp-8-215-2012

Joachimski, M. M., von Bitter, P. H., and Buggisch, W., 2006, Constraints on Pennsylvanian glacioeustatic sea-level changes using oxygen isotopes of conodont apatite, Geology, v. 34, no. 4, p. 277-280.

Joachimski, W.W., van Gelderin, R., Breisig, S., Buggisch, W., and Day, J., 2004. Oxygen isotope evolution of biogenic calcite and apatite during the Middle and Late Devonian, International Journal of Earth Sciences (Geol Rundsch), v. 93, p. 542–553, doi: 10.1007/s00531-004-0405-8

Joachimski, M.M., Breisig, S., Buggisch, W., Talent, J.A., Mawson, R., Gereke, M., Morrow, J.R., Day, J., and Weddige, K., 2009. Devonian climate and reef evolution: Insights from oxygen isotopes in apatite, Earth and Planetary Science Letters, v. 284, p. 599–609, doi:10.1016/j.epsl.2009.05.028

Johnson, J.G., Klapper, G., Sandberg, C.A., 1985. Devonian eustatic fluctuations in Euramerica. Geological Society of America Bulletin, v. 96, p. 567–587.

Johnson, J.G., 1988. Volcanism, eustacy, and extinctions. Geology, v. 16, p. 573–574.

Jones, C.E., and Jenkyns, H.C., 2001. Seawater strontium isotopes, oceanic anoxic events, and seafloor hydrothermal activity in the Jurassic and Cretaceous, American Journal of Science, 301:112-149.

Jones, S.M., Hoggett, M., Greene, S.E., and Jones, T.D., 2019. Lareg Igneous Province thermogenic greenhouse gas flux could have intiated Paleocene-Eocene Thermal Maximum climate change, Nature Communications, v.10, article number 5547.

Jourdan, F., Féraud, G., Bertrand, H., Kampunzu, A.B., Tshoso, G., Watkeys, M.K., and Le Gall, B. 2005. Karoo large igneous province: brevity, origin, and relation to mass extinction questioned by new $^{40}Ar/^{39}Ar$ age data. Geology, v. 33, p.745–748.

Jouzel, J., Masson-Delmotte, V., Cattani, O., Dreyfus, G., Falourd, S., Hoffmann, G., Minster, B., Nouet, J., Barnola, J.M., Chappellaz, J., Fischer, H., Gallet, J.C., Johnsen, S., Leuenberger, M., Loulergue, L., Luethi, D., Oerter, H., Parrenin, F., Raisbeck, G., Raynaud, D., Schilt, A., Schwander, J., Selmo, E., Souchez, R., Spahni, R., Stauffer, B., Steffensen, J.P., Stenni, B., Stocker, T.F., Tison, J.L., Werner, M., and Wolff. E.W., 2007. Orbital and Millennial Antarctic Climate Variability over the Past 800,000 Years, Science, v. 317, p.793-796.

Jovane, L., Coccioni, R., Marsili, A., Acton, G., 2009. The late Eocene greenhouse-icehouse transition: Observations from the Massignano global stratotype and point (GSSP), in C. Koeberl and A. Montanari, (eds.), The Late Eocene Earth: Hot House, Ice House, and Impacts, Geol. Soc. America, Special Paper 452149-168.

Judd, E., Bhattacharya, T., Ivany, L.C., 2020. A dynamical framework for interpreting ancient sea surface temperatures, Geophysical Research Letters, 47 (15):1-10, doi.org/10.1029/2020GL089044

Kamber, B.S., and Petrus, J.A., 2019. The influence of large bolide impacts on the Earth's Carbon Cycle, Elements, v.15, p.313-318.

Kamo, S.L., Czamanske, G.K., Amelin, Y., Fedorenko, V.A., Davis, D.W., and Trofimov, V.R., 2003. Rapid eruption of Siberian flood-volcanic rocks and evidence for coincidence with the Permian-Triassic boundary and mass extinction at 251 Ma. Earth and Planetary Science Letters, v. 214, p. 75-91.

2379 Kasting, J.F., Howard, M.T., Wellman, K.T., Veizer, J., Shields, G., and Jaffres, J., 2006. Paleoclimates,
2380 ocean depth, and the oxygen isotopic composition of seawater, Earth and Planetary Science Letters,
2381 v. 252, p. 82-93.

2382 Keller, G., 2011. Defining the Cretaceous-Tertiary boundary: a practical guide and return to first
2383 principles. In: Keller, G., Adatte, T. (Eds.), The KT Mass Extinction and the Chicxulub impact in Texas.
2384 SEPM Special Publication, 100, 23-42.

2385 Keller, G., 2014. Deccan volcanism, the Chicxulub impact, and the end-Cretaceous mass extinction:
2386 Coincidence? Cause and effect? In: Keller, G., Kerr, A. (Eds.), Volcanism, Impacts and Mass
2387 Extinctions: Causes and Effects. Geological Society of America Special Papers, 505, 57-89,
2388 doi:10.1130/2014.2505(03).

2389 Keller, G., Mateo, P., Punekar, J., Khozyem, H., Gertsch, B., Spangenberg, J., Bitchong, A., and Adatte,
2390 T., 2017. Environmental Changes during the Cretaceous-Paleogene Mass Extinction and Paleocene-
2391 Eocene Thermal Maximum: Implications for the Anthropocene, Gondwana Research, v. 56, p. 69-89,
2392 doi.org/10.1016/j.gr.2017.12.002

2393 Kennett,J.P., and Stott, L.D., 1991. Abrupt deep-water warming, palaeoceanographic changes and
2394 benthic extinctions at the end of the Paleocene, Nature, v. 353, p.225-229.

2395 Kennett, J.P., Houtz, R.E., Andrews, P.B., Edwards. A. R., Gostin, V.A., Hajos, M., Hempton, M.A.,
2396 Jenkins, D.G., Margolis, S.V., Ovenshine, A.T., and Perch-Nielsen, K., 1974. Development of the Circum-
2397 Antarctic current, Science, 186:144-147.

2398 Kennett, J.P., 1995. A review of polar climate evolution during the Neogene based on the marine
2399 sediment record, in Paleoclimate and Evolution with Emphasis on Human Origins, E.S. Vrba, G.H.
2400 Denton, T.C. Patridge, and L.H. Burckle (eds.), Yale University Press, New Haven, p.49-64.

2401 Kennett, J.P., and Exon, N.F., 2004. Paleoceanographic evolution of the Tasmanian Seaway and its
2402 climatic implications, in N.F. Exon, J.P. Kennett and M. Malone, (eds.), The Cenozoic Southern Ocean:
2403 Tectonics, Sedimentation, and Climate Change between Australia and Antarctica, American
2404 Geophysical Union, Geophys. Monograph 151:345-367.

2405 Kidder, D.L. and Worsley, T.R., 2010. Phanerozoic Large Igneous Provinces (LIPs), HEATT (Haline
2406 Euxinic Acidic Thermal Transgression) episodes, and mass extinctions, Palaeogeography,
2407 Palaoeclimatology, Palaeoecology, v. 295, pp. 162-191.

2408 Kidder, D.L. and Worsley, T.R., 2012. A human-induced hothouse climate?, GSA Today, v. 22, no. 2,
2409 pp. 4 – 11, doi: 10.1130/G131A.1.

2410 Kiehl, J.T., and Shields, C., 2013. Sensitivity of the Palaeocene-Eocene Thermal Maximum climate to
2411 cloud properties: Royal Society of London Philosophical Transactions, ser. A, v. 371, 20130093,
2412 doi:10.1098/rsta.2013.0093.

2413 Kiessling, W., Flügel, and Golonka, J., 2002. Phanerozoic Reef Patterns, SEPM (Society for
2414 Sedimentary Geology) Special Publication Number 72, 775 pp.

2415 King, C., A., 2016. A Revised Correlation of Tertiary Rocks in the British Isles and adjacent areas of NW
2416 Europe, A.S. Gale & T.L. Barry (editors), Geological Society Special Report no. 27, 719 pp.

2417 Koeberl, C., and Montanari, A., 2009. The Late Eocene Earth: Hot House, Ice House, and Impacts, Geol.
2418 Soc. America, Special Paper 452, Boulder, Colorado, 322 pp.

2419   Köppen, W., 1918. Klassification der Klimate nach Temperatur, Niederschlag and Jahreslauf,
2420   Petermanns Geographische Mitteilungen, v. 64, pp.193-248.

2421   Korte, C., Hesselbo, S.P., Jenkyns, H.C., Rickaby, R.E.M., Spotl, C., 2009. Palaeoenvironmental
2422   significance of carbon- and oxygen-isotope stratigraphy of marine Triassic–Jurassic boundary
2423   sections in SW Britain, Journal of the Geological Society of London, v. 166, p. 431–445.

2424   Korte, C., Jones, P.J., Brand, U., Mertmann, D., and Veizer, J., 2008. Oxygen isotope values from high-
2425   latitudes: Clues for Permian sea-surface temperature gradients and Late Palaeozoic deglaciation,
2426   Palaeogeography, Palaeoclimatology, Palaeoecology, v. 269, p. 1–16,
2427   doi:10.1016/j.palaeo.2008.06.012

2428   Korte, C., Jasper, T., Kozur, H.W., and Veizer, J., 2005. $d^{18}O$ and $d^{13}C$ of Permian brachiopods: A
2429   record of seawater evolution and continental glaciation, Palaeogeography, Palaeoclimatology,
2430   Palaeoecology, v. 224, p. 333–351, doi:10.1016/j.palaeo.2005.03.01

2431   Kustatscher, E., Ash, S.R., Karasev, E., Pott, C., Vajda, V., Yu, J. & McLoughlin, S. 2018. Flora of the
2432   Late Triassic. In: Tanner, L. (ed.) The Late Triassic World: Earth in a Time of Transition, Topics in
2433   Geobiology, v. 46, p. 545-622, Springer, ISBN 978-3-319-68008-8.

2434   Kump, L.R., Arthur, M.A., Patkowsky, M.E., Gibbs, M.T., Pinkus, D.S., and Sheehan, P.M., 1999a. A
2435   weathering hypothesis for glaciation at high atmospheric CO_2 during the Late Ordovician,
2436   Palaeogeography, Palaeoclimatology, and Palaeoecology, v. 152, p. 173-187.

2437   Kump, L.R., Kasting, J.F., and Crane, R.G., 1999b. The Earth System, Prentice Hall, Upper Saddle River,
2438   N.J., 351 p.

2439   Kump, L.R., Arthur, M.A., 1999c. Interpreting carbon-isotope excursions: carbonates and organic
2440   matter. Chemical Geology, v. 161, p. 181–198.

2441   Kump. L.R., Gibbs, M.T., Arthur, M.A., Patzkowsky, M.E., and Sheehan, P.M., 1995.Hirnantian
2442   Glaciation and the Carbon Cycle, Ordovician Odyssey: Short Papers for the Seventh International
2443   Symposium on the Ordovician System, Las Vegas, Nevada, USA, June, 1995, (editors) J.D. Cooper,
2444   M.L. Droser, and S.C. Finney, p. 299-302, Society for Sedimentary Geology (SEPM), Pacific Section,
2445   Fullerton, CA.

2446   Kump, L.R., Pollard, D., 2008. Amplification of Cretaceous warmth by biological cloud feedbacks.
2447   Science 320, 195.

2448   Kump, L.R., 1991. Interpreting carbon-isotope excursions: Strangelove oceans. Geology, v. 19, p. 299-
2449   302.

2450   Ladant, J.-B., Donnadieu, Y., 2016. Palaeogeographic regulation of glacial events during the
2451   Cretaceous supergreenhouse. Nat. Commun. 7.

2452   Landing, E., 2012. Time-specific black mudstones and global hyperwarming on the Cambro-
2453   Ordovician slope and shelf od the Laurentia palaeocontinent, Palaeogeog., Paleaoclim., Palaeoecol.,
2454   v. 367-368, p.256-272. Doi.org/10.1016/j.palaeo.2011.09.05

2455   Landing, E. 2018. Tropical weathering of the Taconic orogeny (i.e. "orogen") as a driver for
2456   Ordovician cooling, Geology Forum, doi.org/10.1130/G3998.7c1

2457 Landing, E., Schmitz, M.D., Geyer, G., Trayler, R.B., and Bowring, S.A., 2020. Precise early Cambrian
2458 U–Pb zircon dates bracket the oldest trilobites and archaeocyathids in Moroccan West Gondwana,
2459 Geological Magazine https://doi.org/10.1017/ S0016756820000369

2460 Landing E and Westrop SR, 2004. Environmental patterns in the origin and evolution loci of Early
2461 Cambrian skeletalized Metazoa: evidence from the Avalon microcontinent. In Neoproterozoic–
2462 Cambrian Biological Revolutions (eds JH Lipps and B Waggoner), pp. 93–105. Paleontological Society,
2463 Special Paper no. 10.

2464 Larson, R.L., 1991. Geological consequences of superplumes, Geology, 19:963-966.

2465 Larson, R.L., and Erba, E., 1999. Onset of the mid-Cretaceous greenhouse in the Barremian-Aptian:
2466 Igneous events and biological sedimentary, and geochemical responses, Paleoceanography, 14:663-
2467 678.

2468 Lawver, L.A., and Gahagan, L.M., 2003. Evolution of Cenozoic seaways in the circum-Antarctic region,
2469 Palaeogeog., Paleaoclim., Palaeoecol., 198:11-37.

2470 Lécuyer, C., Amiot, R., Touzeau, A., 2013. Calibration of the phosphate $\delta^{18}O$ thermometer with
2471 carbonate-water oxygen isotope fractionation equations, Chemical Geology, v. 347, pp. 217-226,
2472 doi:10.13039/501100004794.

2473 Legates, D.R., and Wilmott, C.J., 1990. Mean seasonal and spatial variability in global surface air
2474 temperature, Theoretical and Applied Climatology, v. 41, pp. 11-21.

2475 Lenton, T.M., Crouch, M., Johnson, M., Pires, N., and Dolan, L., 2012. First plants cooled the
2476 Ordovician, Nature Geoscience, v.5, p. 86-89.

2477 Ling, M.-X., Zhan, R.-B., Wang, G.-X., Wang, Y., Amelin, Y., Tang, P., Liu, J.-B., Jin, J., Huang, B., Wu, R.-
2478 C., Xue, S., Fu, B., Bennett, V.C., Wei, X., Luan, X.-C., Finnegan, S., Harper, D.A.T., Rong, J.-Y., 2019. An
2479 extremely brief end Ordovician mass extinction linked to abrupt onset of glaciation. Solid Earth
2480 Sciences, 4(4): 190-198.

2481 Lisiecki, L.E., and Raymo, M.E., 2005. A Pliocene-Pleistocene stack of 57 globally distributed benthic
2482 $\delta^{18}O$ records. Paleoceanography 20 (1), PA1003. http://dx.doi.org/10.1029/ 2004PA001071.

2483 Livermore, R., Nankivell, A., Eagles, G., And Morris, P., 2005. Paleogene opening of the Drake
2484 Passage, Earth and Planetary Science Letters, 236:459-470.

2485 Looy, C.V., Brugman, W.A., Dilcher, D.L., and Visscher, H., 1999. The delayed resurgence of equatorial
2486 forests after the Permian-Triassic ecologic crisis, Proc. National Acad. Sci., 96:13857-13862.

2487 Luz, B., Kolodny, Y., and Kovach, J., 1984, Oxygen isotope variations in phosphate of biogenic
2488 apatites, III. Conodonts, Earth and Planetary Science Letters, v. 69, no. 2, p. 255-262.

2489 Malchus, N., and Steuber, T., 2002. Stable isotope records (O, C) of Jurassic aragonitic shells from
2490 England and NW Poland: palaeoecologic and environmental implications, Geobios, v. 35, p. 29–39.

2491 Marshall, H.G., Walker, J.C.G., & Kuhn, W.R., 1988. Long-term climate change and the geochemical
2492 cycle of carbon. Journal of Geophysical Research, 93, 791–801.

2493 Marshall, L.G., Webb, D.S., Sepkoski, J.J., Raup, D.M., 1982. Mammalian evolution and the Great
2494 American Interchange, Science, 215:1351-1357.

2495 Martinez-Peréz, C., Cascales-Minana, B., Plasencia, P., and Botella, H., 2014. Exploring the major
2496 depletions of conodont diversity during the Triassic, Historical Biology, v. 27, p. 503–507.

2497 Marzoli, A., Renne, P.R., Piccirillo, E.M., Ernesto, M., Bellieni, G., and DeMin, A., 1999. Extensive 200-
2498 million-year-old continental flood basalts of the Central Atlantic Magmatic Province (CAMP), Science,
2499 v 284, p. 616-618.

2500 McArthur, J.M., Janssen,N.M.M, Reboulet, S., Leng, M.J., Thirwall, M.F., van de Schootbrugge, B.,

2501 2007. Palaeotemperatures, polar ice-volume, and isotope stratigraphy (Mc/Ca, ∂18O, ∂13C,
2502 87Sr/86Sr): The Early Cretaceous (Berriasian, Valanginian, Hauterivian), Palaeogeography,
2503 Palaeoclimatology, Palaeoecology, v. 248, p. 391-430, doi:10.1016/j.palaeo.2006.12.015

2504

2505 McCune A.R., and Schaeffer, B., 1986. Triassic and Jurassic fishes: patterns of diversity in The
2506 Beginning of the Age of Dinosaurs, (editor), Kevin Pandian, p. 171–181, Cambridge University Press,
2507 Cambridge, UK.

2508 McElwain J.C., Beerling D.J., and Woodward F.I., 1999. Fossil plants and global warming at the
2509 Triassic-Jurassic boundary, Science, v. 285, p. 1386–1390.

2510 McElwain J.C., Punyasena S.W., 2007. Mass extinction events and the plant fossil record. Trends in
2511 Ecology and Evolution, v. 22, p. 548–557.

2512 McGhee, G.R., Clapham, M.E., Sheehan, P.M., Bottjer, D.J., and Droser, M.L., 2013. A new ecological-
2513 severity ranking of major Phanerozoic biodiversity crises, Palaeogeography, Palaeoclimatology,
2514 Palaeoecology 370: 260–270

2515 McGhee, G.R., Jr., 1996. The Late Devonian Mass Extinction: The Frasnian/Famennian Crisis, Critical
2516 Moments in Paleobiology and Earth History Series,D. J. Bottjer and R.K. Bambach (editors), Columbia
2517 University Press, New York, 303 pp.

2518 McGhee, G.R., Jr., 2005. Modelling Late Devonian extinction hypotheses, in Understanding Late
2519 Devonian and Permian-Triassic Biotic and Climatic Events; Towards an Integrated Approach, D.J.
2520 Over, J.R. Morrow, and P.B. Wignall (editors), Developments in Palaeontology & Stratigraphy, v. 20,
2521 p. 37 – 50. Elsevier, Amsterdam.

2522 McHone, J.G., and Puffer, J.H., 2003. Flood Basalt Provinces of the Pangean Atlantic Rift: Regional
2523 Extent and Environmental Significance, in P.M. LeTourneau & P.E. Olsen (eds.), The Great Rift
2524 Valleys of Pangea in Eastern North America: Tectonics, Structure, and Volcanism, Volume 1,
2525 Columbia University Press, New York, p.141-154.

2526 McInerney, F.A., Wing, S.L., 2011. The Paleocene-Eocene Thermal Maximum: a perturbation of
2527 carbon cycle, climate, and biosphere with implications for the future. Annual Review of Earth
2528 Planetary Sciences,v. 39, p. 489–516.

2529 McKenzie, N.R., and Jiang,H., 2019. Earth's outgassing and climatic transitions: The slow burn
2530 towards environmental "catastrophes"?, Elements, v.15, p.325-330.

2531 McKerrow, W.S., Scotese, C.R., and Brasier, M., 1992. Early Cambrian continental reconstructions,
2532 Journal of the Geological Society of London, v. 149, p. 599-606.

2533 McLaren, D.J., 1970. Presidential address: Time, Life and Boundaries, Journal of Paleontology, v. 48,
2534 p. 801-815.

2535 McLaren, D., 1983. Bolides and biostratigraphy. Geol. Soc. Am. Bull. 94, 313–324.

2536 Melosh, H.J., 1989. Impact Cratering, A Geologic Process, Oxford University Press, New York, 253 p.

2537 Meyer, K.M., and Kump, L.R., 2008. Oceanic Euxinia in Earth History: Causes and Consequences,
2538 Annual Review of Earth and Planetary Sciences, 36:251-288.
2539
2540 Mii, H.-S., Shi, G.R., Wang, C.-A., 2013. Late Paleozoic middle-latitude Gondwana environment-
2541 stable isotope records from Western Australia, Gondwana Research, v. 24, p. 125–138,
2542 doi.org/10.1016/j.gr.2012.10.013

2543 Mii, H.-S., Grossman, E.L., and Yancey, T.E., 1999. Carboniferous isotope stratigraphies of North
2544 America: Implications for Carboniferous paleoceanography and Mississippian glaciation, Geological
2545 Society of America Bulletin, v. 111, no. 7, p. 960–973.

2546 Mii, H.-S., Shi, G.R., Cheng, C.-J., and Chen, Y.-Y., 2012. Permian Gondwanaland paleoenvironment
2547 inferred from carbon and oxygen isotope records of brachiopod fossils from Sydney Basin, southeast
2548 Australia, Chemical Geology, v. 291, p. 87–103, doi:10.1016/j.chemgeo.2011.10.002

2549 Milankovitch, M., 1920. Theorie Mathematique des Phenomenes Thermiques produits par la
2550 Radiation Solaire, Gauthier-Villars, Paris, 340 p.

2551 Miller, C.S., Petersen, F., da Silva, A.-C., Baranyi, V., Reichart, G.J., and Kürschner, W.M., 2017.
2552 Astronomical age constraints and extinction mechanisms of the Late Triassic Carnian crisis. Nature,
2553 Scientific Reports 7: doi:10.1038/s41598-017-02817-7.

2554 Miller, K.G., Fairbanks, R.G., and Mountain, G.S., 1987. Tertiary oxygen isotope synthesis, sea level
2555 history, and continental margin erosion, Paleoceanography, v. 2, p. 1-19.

2556 Miller, K.G., Barrera, E., Olsson, R.K., Sugarman, P.J., Savin, S.M., 1999. Does ice drive early
2557 Maastrichtian eustasy? Geology 27, 783–786.

2558 Miller, K.G., Sugarman, P.J., Browning, J.V., Kominz, M.A., Olsson, R.K., Feigenson, M.D., Hernández,
2559 J.C., 2004. Upper Cretaceous sequences and sea-level history, New Jersey coastal plain. Geol. Soc.
2560 Am. Bull. 116, 368–393.

2561 Miller, K.G., Kominz, M.A., Browning, J.V., Wright, J.D., Mountain, G.S., Katz, M.E., Sugarman, P.J.,
2562 Cramer, B.S., Christie-Blick, N., Pekar, S.F., 2005a. The Phanerozoic record of global sea-level change.
2563 Science 310, 1293–1298.

2564 Miller, K.G., Wright, J.D., J. V. Browning, J.V., 2005b. Visions of ice sheets in a greenhouse world.
2565 *Mar. Geol.* **217**, 215–231.

2566 Miller, K.G., Sherrell, R.M., Browning, J.V., Field, M.P., Gallagher, W., Olsson, R.K., Sugarman, P.J.,
2567 Tuorto, S., and Wahyudi, H., 2010. Relationship between mass extinction and iridium across the
2568 Cretaceous-Paleogene boundary in New Jersey, Geology, 38:867-870.

2569 Miller, K.G., Browning, J.V., Scmetz, W.J., Kopp, R.E., Mountain, G.S., and Wright, J.D., 2020.
2570 Cenozoic sea-level and cryosphere evolution from deep-sea geochemical and continental margin
2571 records, Science Advances, 6, eaaz1346.

2572 Mills, B.J.W., Krause, A.J., Scotese, C.R., Hill, D.J., Shields, G.A., and Lenton, T.M., 2019. Modelling the
2573 long-term carbon cycle, atmospheric CO_2, and Earth surface temperature from late Neoproterozoic
2574 to present-day, Gondwana Research, v. 67, p. 172-186, doi: 10.1016/j.gr.2018.12.001 1342-937.

2575 Molnar, P., and Tapponnier, P., 1975. Cenozoic tectonics of Asia: Effects of a continental collision,
2576 Science, 189:419-426.

2577 Montañez, I.P., Tabor, N.J., Niemeier, D., DiMichele, W.A., Frank, T.D., Fielding, C.R. Isbell, J.L.,
2578 Birgenheier, L.P., and Rygel, M.C., 2007. CO_2 -Forced Climate and Vegetation Instability During Late
2579 Paleozoic Deglaciation, Science, v. 315, n. 5808, p. 87-91, doi: 10.1126/science.1134207

2580 Montañez I.P., McElwain, J.C., Poulsen, C.J., White, J.D., DiMichele, W.A., Wilson, J.P., Griggs, G., and
2581 Hren, M.T., 2016. Climate, p CO_2, and terrestrial carbon cycle linkages during late Palaeozoic glacial-
2582 interglacial cycles, Nature Geoscience, v.9, p. 824-828, doi :10.1038/NGEO2822

2583 Montañez, I.P., and J.C., Poulsen, 2013. The Late Paleozoic Ice Age: An Evolving Paradigm, Annual
2584 Reviews of Earth and Planetary Sciences, v41, p.629-656.

2585 Moore, G.T., Hayashida, D.N., Ross, C.A., and Jacoboson, S.R., 1992, Paleoclimate of the
2586 Kimmeridgian/Tithonian (Late Jurassic) world: I. Results using a general circulation model,
2587 Palaeogeography, Palaeoclimatology, and Palaeoecology, 93:113-150.

2588 Moore, G.T., Jacobson, S.R., Ross, C.A., and Hayashida, D.N., 1994. A paleoclimate simulation of the
2589 Wenlockian (late Early Silurian) world using a general circulation model with implications for early land
2590 plant paleoecology, Palaeogeog., Paleaoclim., Palaeoecol., 110:115-144.

2591 Morley, R.J., 2011. Cretaceous and Tertiary climate change and the past distribution of megathermal
2592 rainforests,in Tropical Rainforest Responses to Climatic Change, M.B. Bush, J.R. Flenley, W.D.
2593 Gosling, (editors), p. 1-34, Springer-Verlag, Berlin.

2594 Mory, A.J., Redfern, J., and Martin, J.R., 2008. A review of Permian-Carboniferous glacial deposits in
2595 Western Australia, in C.R. Fielding, T.D. Frank. and J.L. Isbell (editors), Resolving the Late Paleozoic
2596 Ice Age in Time and Space, Geological Society of America Special Paper v. 441, p. 29-40.

2597 Mueller, S., Krystyn, L., and Kürschner, W.M. 2016a. Climate variability during the Carnian Pluvial
2598 Phase – a quantitative palynological study of the Carnian sedimentary succession at Lunz am See,
2599 Northern Calcareous Alps, Austria, Palaeogeography, Palaeoclimatology, Palaeoecology, v. 441, p.
2600 198–211.

2601 Mueller, S., Hounslow, M.W., and Kürschner, W.M. 2016b. Integrated stratigraphy and
2602 palaeoclimate history of the Carnian Pluvial Event in the Boreal realm; new data from the Upper
2603 Triassic Kapp Toscana Group in central Spitsbergen (Norway), Journal of the Geological Society, v.
2604 173, p. 186–202.

2605 Munnecke, A., Calner, M., Harper, D.A.T., and Servais, T., 2010. Ordovician and Silurian sea–water
2606 chemistry, sea level, and climate: A synopsis, Palaeogeography, Palaeoclimatology, Palaeoecology, v.
2607 296, p. 389–413, doi:10.1016/j.palaeo.2010.08.001

2608 Mutterlose, J., Pauly, S., and Steuber, T., 2009. Temperature controlled deposition of early
2609 Cretaceous (Barremian–early Aptian) black shales in an epicontinental sea, Palaeogeography,
2610 Palaeoclimatology, Palaeoecology, 273:330-345, doi:10.1016/j.palaeo.2008.04.026

2611 Nance, R.D., Murphy, J.B., Santosh, M., 2014. The supercontinent cycle: A retrospective essay,
2612 Gondwana Research, v. 25, p. 4-29, doi: 10.1016/j.gr.2012.12.026.

2613 Nance, R.D., and Murphy, J.B., 2018. Supercontinents and the case for Pannotia, in Fifty Years of the
2614 Wilson Cycle Concept in Plate Tectonics, R.W. Wilson, G.A. Houseman, K.J.W. McCaffrey, A.G. Dore,
2615 and S.J.H. Butler, Geological Society, London, Special Publications, 470, p. 1-17,
2616 doi:/10.1144/SP470.5.

2617 Nardin, E., Goddéris, Y., Donnadieu, Y., Le Hir, G., & Blakey, R.C., 2011. Modeling the early Paleozoic
2618 long-term climatic trend. *Geological Society of America Bulletin.* doi: 10.1130/B30364.1

2619 Navarro-Ramirez, J.P., Bodin, S., Consorti, L., and Immenhauser, A., 2017. Response of western South
2620 American epeiric-neritic ecosystem to middle Cretaceous Oceanic Anoxic Events, Cretaceous
2621 Research, v. 75, p. 61–80

2622 O'Brien, C.L., Robinson, S.A., Pancost, R.D., Sinninghe Damsté, J. S., Schouten, S., Lunt, D. J., Alsenz,
2623 H., Bornemann, A., Bottini, C., Brassell, S. C., Farnsworth, A., Forster, A., Huber, B. T., Inglis, G. N.,
2624 Jenkyns, H. C., Linnert, C., Littler, K., Markwick, P., McAnena, A., Mutterlose, J., Naafs, B. D. A.,
2625 Püttmann, W., Sluijs, A., van Helmond, N. A. G. M., Vellekoop, J., Wagner, T., and Wrobel, N. E.,
2626 2017. Cretaceous sea-surface temperature evolution: Constraints for TEX 86 and planktonic
2627 foraminiferal Oxygen isotopes, Earth-Science Reviews, v. 172, p. 224-247, doi:
2628 10.1016/j.earscirev.2017.07.012. 2018

2629 Ogg, J.G. 2015. The mysterious Mid-Carnian "Wet Intermezzo" global event, Journal of Earth Science,
2630 v. 26, p. 181–191.

2631 Ogg, J.G., Ogg, G.M., and Gradstein, F.M., 2016. A Concise Geological Time Scale 2016, Elsevier,
2632 Amsterdam, 234 pp.

2633 Otto-Bliesner, B.L., 1995. Continental drift, runoff, and weathering feedbacks: Implications from
2634 climate model experiments. *Journal of Geophysical Research*, 100, 11,537-11,548

2635 Pankhurst, R.J., Leat, P.Y., Sruoga, P., et al., 1998. The Chon Aike province of Patagonia and related
2636 rocks in West Antarctica: a silicic large igneous province, Journal of Volcanology and Geothermal
2637 Research, 81: 113-136.

2638 Pankhurst, R.J., Riley, T.R., Fanning, C.M.,and Kelley, S.P., 2000. Episodic silicic volcanism in
2639 Patagonia and the Antarctic peninsula: chronology of magmatism associated with the break-up of
2640 Gondwana, Journal of Petrology, 41:605-625.

2641 Park, J., and Royer, D.L., 2011. Geological constraints on the glacial amplification of Phanerozoic
2642 climate sensitivity, American Journal of Science, v. 311, p. 1-26, doi: 10.2475/01.2011.01.

2643 Parrish, J.T., 1993, Climate of the supercontinent Pangea, J. Geology, v. 101, p. 217-235.

2644 Parrish, J.T., 1998. Interpreting Pre-Quaternary Climate from the Geologic Record, Columbia
2645 University Press, New York, 338 pp.

2646 Parrish, J.T., and Spicer, R.A., 1988, Late Cretaceous terrestrial vegetation: A near polar temperature

2647 curve, Geology, 16:22-25.

2648 Peng, S., Babcock, L.E., and Cooper, R.A., 2012. The Cambrian Period, Chapter 19, in The Geologic
2649 Time Scale 2012, volume 2, F.M. Gradstein, J.G. Ogg, M.D. Schmitz, and G.M. Ogg (editors), Elsevier,
2650 Amsterdam, p. 437-488.

2651 Petersen, S.V., Dutton, A., Lohmann, K.C., 2016. End-Cretaceous extinction in Antarctica linked to
2652 both Deccan volcanism and meteorite impact via climate change, Nature Communications, 7:12079
2653 doi: 10.1038/ncomms12079

2654 Petit J.R., Jouzel,J., Raynaud, D., Barkov, N.I., Barnola, J.-M., Basile, I., Bender, M., Chappellaz, J.,
2655 Davis, M., Delaygue, G., Delmotte, M., Kotlyakov, V.M., Legrand, M., Lipenkov, V.Y., Lorius, C., Pe´pin,
2656 L., Saltzman, E., and Stievenard,M., 1999. Climate and atmospheric history of the past 420,000 years
2657 from the Vostok ice core, Antarctica, Nature, V. 299, p. 429-436.

2658 Pillans, B., and Gibbard, P., 2012. The Quaternary Period, Chapter 30, in The Geologic Time Scale 2012,
2659 volume 2, F.M. Gradstein, J.G. Ogg, M.D. Schmitiz, and G.M. Ogg, (editors), p. 855-922, Elsevier,
2660 Amsterdam.

2661 Pirrie, D., Doyle, P., Marshall, J., Ellis, G., 1995. Cool Cretaceous climates: new data from the Albian
2662 of Western Australia. J. Geol. Soc. 152: 739–742.

2663 Pirrie, D., Marshall, J., Doyle, P., Riccardi, A., 2004. Cool early Albian climates; new data from
2664 Argentina. Cretaceous Research 25:, 27–33.

2665 Podlaha, O.G., Mutterlose, J., and Veizer, J., 1998. Preservation of d18O and d13C in belemnite
2666 rostra from Jurassic/early Cretaceous successions, American Journal of Science, v. 298, p. 324-347.

2667 Powell, C. McA., Li, Z.X., McElhinny,M.W., Meert, J.G., and Park, J.K., 1993. Paleomagnetic
2668 constraints on the timing of the Neoproterozoic breakup of Rodinia and the Cambrian formation of
2669 Gondwana, Geology, v. 21, pp. 889-892.

2670 Powell, C. McA., 1995. Are Neoproterozoic glacial deposits preserved on the margins of North
2671 America related to the fragmentation of two supercontinents (Comment), Geology, v. 23, pp. 1053-
2672 1054.

2673 Preto, N., Kustatscher, E., and Wignall, P.B. 2010. Triassic climates—state of the art and
2674 perspectives. Palaeogeography, Palaeoclimatology, Palaeoecology, 290:1–10.

2675 Price, G.D., 1999. The evidence and implications of polar ice during the Mesozoic. Earth Sci. Rev. 48,
2676 183–210.

2677 Price, G., Mutterlose, J., 2004. Isotopic signals from late Jurassic–early Cretaceous (Volgian–
2678 Valanginian) sub-Arctic belemnites, Yatria River, Western Siberia. J. Geol. Soc. 161, 959–968.

2679 Price, G.D., Nunn, E.V., 2010. Valanginian isotope variation in glendonites and belemnites from Arctic
2680 Svalbard: transient glacial temperatures during the Cretaceous greenhouse. Geology 38, 251–254.

2681 Price, G.D., Passey, B.H., 2013. Dynamic polar climates in a greenhouse world: evidence from
2682 clumped isotope thermometry of Early Cretaceous belemnites. Geology 41, 923–926.

2683 Prokoph, A., Shields, G. A., and Veizer, J., 2008, Compilation and time-series analysis of a marine
2684 carbonate $\delta^{18}O$, $\delta^{13}C$, $^{87}Sr/^{86}Sr$ and $\delta^{34}S$ database through Earth history, Earth-Science Reviews, v. 87,
2685 no. 3, p. 113-133.

2686 Pucéat, E., Lécuyer, C., Sheppard, S.M., Dromart, G., Reboulet, S., Grandjean, P., 2003. Thermal
2687 evolution of Cretaceous Tethyan marine waters inferred from oxygen isotope composition of fish
2688 tooth enamels. Paleoceanography 18, 1029. http://dx.doi. org/10.1029/2002PA000823.

2689 Punekar, J., Mateo, P., and Keller, G., 2014. Effects of Deccan volcanism on paleoenvironment and
2690 planktic foraminifera: A global survey, Geological Society of America Special Paper, v. 505, p. 91-116,
2691 doi:10.1130/2014.2505(04)

2692 Quiron, P.C., and MacLeod, K.G., 2014. Oxygen isotopes from conodont apatite of the midcontinent,
2693 US: Implications for Late Ordovician climate evolution, Palaeogeography, Palaeoclimatology,
2694 Palaeoecology, v. 404, p. 57–66, doi.org/10.1016/j.palaeo.2014.03.036

2695 Racki, G., 2020. A volcanic scenario for the Frasnian–Famennian major biotic crisis and other Late
2696 Devonian global changes: More answers than questions?, Global and Planetary Change, v. 189,
2697 doi.org/10.1016/j.gloplacha.2020.103174

2698 Racki, G., 2005. Toward understanding Late Devonian global events: few answers, many questions,
2699 in Understanding Late Devonian and Permian-Triassic Biotic and Climatic Events; Towards an
2700 Integrated Approach, D.J. Over, J.R. Morrow, and P.B. Wignall (editors), Developments in
2701 Palaeontology & Stratigraphy, v. 20, p. 5-36, Elsevier, Amsterdam.

2702 Rampino. M.R., 2020. Relationship between impact-crater size and severity of related mass
2703 extinction episodes (in press).

2704 Rampino. M.R., Caldiera, K., and Prokoph, A., 2019. What causes mass extinctions? Large
2705 asteroid/comet impacts, flood-basalt volcanism, and ocean anoxia— Correlations and cycles, *in*
2706 Koeberl, C., and Bice, D.M., eds., 250 Million Years of Earth History in Central Italy: Celebrating 25
2707 Years of the Geological Observatory of Coldigioco: Geological Society of America Special Paper 542,
2708 p. 1–32, https://doi.org/10.1130/2019.2542(14).

2709 Rampino, M.R., and Self, S., 2015. Large Igneous Provinces and Biotic Extinctions, in The
2710 Encyclopedia of Volcanoes, second edition, H. Sigurdsson, B. Houghton, H. Rymer, J. Stix, and S.
2711 McNutt (editors), p.1049-158, Elsevier, Amsterdam.

2712 Rampino. M.R., and Shen, S.-Z., 2019. The end-Guadalupian (259.8 Ma) biodiversity crisis: the sixth
2713 major mass extinction?, Historical Biology, doi: 10.1080/08912963.2019.1658096

2714 Raup, D.M., 1979. Size of the Permo-Triassic bottleneck and its evolutionary implications. Science, v.
2715 206, p. 217-218.

2716 Raymo, M.E., Kozdon, R. , Evans, D., Lisiecki, L., and Ford, H.L., 2018. The accuracy of mid-Pliocene
2717 $\delta^{18}O$-based ice volume and sea level reconstructions, Geochimica et Cosmochimica Acta, Vol. 63,
2718 No. 7/8, pp. 1039–1048.

2719 Raymo, M.E., and Ruddiman, W.F., 1992. Tectonic forcing of Late Cenozoic Climate, Nature 359:117-
2720 122.

2721 Raymo, M.E., Ruddiman, W.F., & Froelich, P.N. 1988. Influence of late Cenozoic mountain building on
2722 ocean geochemical cycles. *Geology*, 16, 649–653.

2723 Rea, D.K., Zachos, J.C., Owen, R.M., and Gingerich, P.D., 1990. Global change at the Paleocene-
2724 Eocene boundary: climatic and evolutionary consequences of tectonic events, Palaeogeography,
2725 Palaeoclimatology, Palaeoecology 79:117-128.

2726 Rees, P.McA., Ziegler, A.M., and Valdes, P.J., 2000, Jurassic phytogeography and climates: new data
2727 and model comparisons, in Warm Climates in Earth History, BT. Huber, K.G. MacLeod, and S. Wing
2728 (editors), Cambridge University Press, Cambridge, p. 297-318.

2729 Reichow, M.K., Saunders, A.D., White, R.V., Al'Mukhamedov, A.I., and Medvedev, A.Ya., 2005.
2730 Geochemistry and petrogenesis of basalts from the West Siberia Basin: an extension of the Permo-
2731 Triassic Siberian Traps, Russia. Lithos, v. 79, p. 425-452.

2732 Reichow, M. K., Pringle, M. S., Al'Mukhamedov, A. I., Allen, M. B., Andreichev, V. L., Buslov, M. M.,
2733 Davies, C. E., Fedoseev, G. S., Fitton, J. G., Inger, S., Medvedev, A. Y., Mitchell, C., Puchkov, V. N.,
2734 Safonova, I. Y., Scott, R. A., and Saunders, A. D., 2009, The timing and extent of the eruption of the
2735 Siberian Traps large igneous province: Implications for the end-Permian environmental crisis, Earth
2736 and Planetary Science Letters, v. 277, no. 1-2, p. 9-20.

2737 Renne, P.R., Sprain, C.J., Richards, M.A., Self, S., Vanderkluysen, L., and Pande, K., 2015. State shift in
2738 Deccan volcanism at the Cretaceous-Paleogene boundary, possibly induced by impact, Science 350
2739 (6256):76-78.

2740 Retallack, G., 2013. Permian and Triassic greenhouse crises, Gondwana Research, v. 24, p. 90–103,
2741 doi:10.1016/j.gr.2012.03.003.

2742 Retallack , G.J., Sheldon, N.D., Carr,P.F., Fanning, M., Thompson, C.A., Williams, M.L., Jones, B.J., and
2743 Hutton, A., 2011. Multiple Early Triassic greenhouse crises impeded recovery from Late Permian
2744 mass extinction, Palaeogeography, Palaeoclimatology, Palaeoecology, v. 308, 233–251, doi:
2745 10.1016/j.palaeo.2010.09.022

2746 Richards, M.A., Alvarez, W., Self, S., Karlstrom,L., Renne, P.R., Manga, M., Sprain, C.J., Smit, J.,
2747 Vanderkluysen, L., and Gibson, S.A., 2015. Triggering of the largest Deccan eruptions by the
2748 Chicxulub impact, Geological Society of America Bulletin, 127 (11-12):1507-
2749 1520,doi:10.1130/B31167.1

2750 Rigo, M., and Joachimski, M.M., 2010. Palaeoecology of Late Triassic conodonts: constraints from
2751 oxygen isotopes in biogenic apatite, Acta Palaeontologica Polonica, v. 55, p. 471–478.

2752 Rigo, M., Preto, N., Roghi, G., Tateo, F., and Mietto, P. 2007. A rise in the Carbonate Compensation
2753 Depth of western Tethys in the Carnian (Late Triassic): deep-water evidence for the Carnian Pluvial
2754 Event, Palaeogeography, Palaeoclimatology, Palaeoecology, v. 246, p. 188–205.

2755 Roghi, G., Gianolla, P., Minarelli, L., Pilati, C., and Preto, N., 2010. Palynological correlation of Carnian
2756 humid pulses throughout western Tethys, Palaeogeography, Palaeoclimatology, Palaeoecology, v.
2757 290, p. 89–106.

2758 Rogner, H.H., 2012. Energy Resources and Potential, Chapter 7, in Yeager, Kurt, Dayo, Felix, Fisher,
2759 Brian, Fouquet, Roger, Gilau, Asmerom, Rogner, Hans-Holger, Haug, Marianne, Hosier,
2760 Richard, Miller, Alan, Schnitteger, Sabine, Lustig, Nora, Johansson, Thomas B., Nakicenovic,

Nebojsa, Patwardhan, Anand and Gomez-Echeverri, Luis (2012) *Energy and economy.* In: Global Energy Assessment (Gea). Cambridge University Press, Cambridge, UK, pp. 385-422. ISBN 9780511793677

Rosenau, N. A., Tabor, N. J., and Herrmann, A. D., 2014, Assessing the paleoenvironmental significance of middle–late Pennsylvanian conodont apatite $\delta^{18}O$ values in the illinois basin conodont apatite $\delta^{18}O$ values, Palaios, v. 29, no. 6, p. 250-265.

Rowley, D.B., 1996. Age of inititation of collision between India and Asia: A review of stratigraphic data, Earth and Planetary Sciences, v. 145: 1-13.

Rowley, D.B., 1998. Minimum age of initiation of collision between India and Asia north of Everest based on the subsidence history of the Zhepure mountain section, Journal of Geology, v. 106: 229-235.

Rowley, D.B. and Currie, B.S., 2006. Palaeo-altimetry of the late Eocene to Miocene Lunpola basin, central Tibet, Nature, v. 439/9, p. 677-681, doi:10.1038/nature04506

Royer, D.L., Berner, R.A., Montañez, I.P., Tabor, N.J., and Beerling, D.J., 2004. CO_2 as a primary driver of Phanerozoic climate, GSA Today, v. 14, no. 3, p. 4-10, doi: 10.1130/1052-5173 (2004) 014<0004: CAAPDO>2.0.CO:2.

Royer, D., 2016. Climate Sensitivity in the Geological Past, Annual Review of Earth and Planetary Sciences, v. 44, pp. 277-293., https://doi.org/10.1146/annrev-earth-100815-024150.

Ruddiman, W.F., 2001. Earth's Climate: Past and Future, W.H. Freeman and Company, New York, NY, 465 pp.

Ruffell, A., Simms, M.J., and Wignall, P.B., 2015. The Carnian Humid Episode of the late Triassic: a review, Geological Magazine, v. 153, p. 271–284.

Sandberg, C.A., Morrow, J.R., Ziegler, W., 2000. Late Devonian events and mass extinc- tions. In: Catastrophic Events and Mass Extinctions: Impacts and Beyond. 1053. Lunar and Planetary Institute Contribution, Houston, Texas, pp. 188–189.

Sandberg, C.A., Morrow, J.R., Ziegler, W., 2002. Late Devonian sea-level changes, catastrophic events, and mass extinctions. In: Koeberl, C., MacLeod, K.G. (Eds.), Catastrophic Events and Mass Extinctions: Impacts and Beyond, Geological Society of America Special Paper 356, p. 473–487.

Sanei, H., Grasby, S., and Beauchamp, B., 2012. Latest Permian mercury anomalies. Geology, v. 40, p. 63-66.

Saunders, A.D., England, R.W., Reichow, M.K., and White, R.V., 2005. A mantle plume origin for the Siberian traps: uplift and extension in the West Siberian Basin, Russia, Lithos, 79:407-424.

Suarez, C.A., Edmonds, M., and Jones, A.P., 2019. Earth catastrosphes and their impact on the Carbon Cycle, Elements, v.15, p. 301-306.

Savin, S.M., Douglas, R.G., and Stehli, F.G., 1975. Tertiary marine paleotemperatures, Geological Sociaty of America Bulletin, v. 86, p. 1499-1510.

2797 Savin, S.M., 1977. The history of the Earth's surface temperature during the past 100 Ma, Annual
2798 Reviews of Earth and Planetary Sciences, v. 5, p. 319-355.

2799 Savitsky, A., and Golay, M.J.E., 1964. Smoothing and Differentiation of Data by Simplified Least
2800 Squares Procedures, Analytical Chemistry, v. 36, no. 8, pp. 1627-1639.

2801 Scher, H.D., and Martin, E.E., 2006. Timing and Climatic Consequences of the opening of Drake
2802 Passage, Science, 312:428-430.

2803 Schlanger, S.O., and Jenkyns, H.C., 1976. Cretaceous oceanic anoxic events: causes and
2804 consequences, Geol. Mijnbouw, 55:179-184.

2805 Schmitz, M.D., and Davydov, V.I., 2012. Quantitative radiometric and biostratigraphic calibration of
2806 the Pennsylvanian–Early Permian (Cisuralian) time scale and pan-Euramerican chronostratigraphic
2807 correlation, Geological Society of America Bulletin, v. 124, no. 3/4, p. 549–577, doi: 10.1130/B30385.

2808 Schobben, M., van de Schootbrugge, B., Wignall, P.B., 2019. Interpreting the carbon isotope record
2809 of mass extnctions, Elements, v. 15, p.331-337.

2810 Scholle, P.A., 1995. Carbon and sulfur isotope stratigraphy of the Permian and Adjacent Intervals, in
2811 *The Permian of the Northern Hemisphere*, volume 1: Paleogeography, Paleoclimates, Stratigraphy, P.A.
2812 Scholle, T.M. Peryt, D.S Ulmer-Scholle (editors), Springer-Verlag, Berlin, p. 133-149.

2813 Schouten, S., Hopmans, E.C., Schefuß, E., Sinninghe Damsté, J.S., 2002. Distributional variations in
2814 marine crenarchaeotal membrane lipids: a new tool for reconstructing ancient sea water
2815 temperatures? Earth Planet. Sci. Lett. 204, 265–274.

2816 Schuchert, C.,1910. Palaeogeography of North America, Geological Society of America Bulletin, 20,
2817 427-606.

2818 Schuchert, C.,1955. (published posthumously), Atlas of paleogeographic Maps of North America, C.
2819 O. Dunbar & C. M. Levene (Eds.), John Wiley & Sons, New York, and Chap Mann & Hall, Ltd., London,
2820 177 pp.

2821 Schulte, P., Alegret, L., Arenillas, I., et al., 2010. The Chicxulub asteroid impact and mass extinction at
2822 the Cretaceous-Paleogene boundary, Science,327:1214-1218.

2823 Scotese, C.R., Boucot, A.J., and McKerrow, W.S., 1999. Gondwanan paleogeography and
2824 paleoclimatology, in Gondwana 10: Event Stratigraphy, Journal of African Earth Sciences, v. 28, issue
2825 1, pp. 99-114.

2826 Scotese, C.R., 2009. Late Proterozoic plate tectonics and paleogeography: A tale of two
2827 supercontinents, Rodinia and Pannotia, in Global Neoproterozoic petroleum systems: The emerging
2828 potential in North Africa, J. Craig, J. Thurow, A. Whitman, and Y. Abutarruma (editors), Geological
2829 Society of London Special Publication 326, pp. 67-83.

2830 Scotese, C.R., 2014. Atlas of Permo-Carboniferous Paleogeographic Maps (Mollweide Projection),
2831 Maps 53-64, volume 4, The Late Paleozoic, PALEOMAP Project Atlas for ArcGIS, PALEOMAP Project,
2832 Evanston, IL.

2833 Scotese, C.R., 2016. A New Global Temperature Curve for the Phanerozoic, (abstract), Deological
2834 Society of America Annual Meeting, Sunday, September 25, 2016, Session no. 74, #287, Recent

2835 Advances in Paleoclimatology and Paleoceanography (Posters). Exhibit Hall E/F (Colorado
2836 Convention Center), Geological Society of America Annual Meeting, Denver, CO.

2837 Scotese, C.R., 2020. Global Warming during the next 300 years, A Global Warming Calculator
2838 (student exercise with Excel spreadsheet), PALEOMAP Project, Evanston, IL. 49 pp.

2839 Sellwood, B.W., and Valdes, P.J., 2006. Mesozoic climates: General circulation models and the rock
2840 record, Sedimentary Geology 190:269–287, doi:10.1016/j.sedgeo.2006.05.013

2841 Şengör, A.M.C., and Atayman, S., 2009. The Permian Extinction and the Tethys: An exercise in global
2842 geology, Geological Society of America Special Papers, v. 448, 96 pp.

2843 Sepkoski, J.J., Jr., 1989. Periodicity in extinction and the problem of catastrophism in the history of life.
2844 Journal of the Geological Society of London, v. 146, p. 7-19.

2845 Sepkoski Jr., J.J., 1996. Patterns of Phanerozoic extinction: a perspective from global data bases, in
2846 O.H. Walliser (editor), Global Events and Event Stratigraphy in the Phanerozoic, Springer-Verlag,
2847 Berlin, pp. 35–51.

2848 Sheehan, P.M., 2001. The Late Ordovician Mass Extinction, Annual Reviews of Earth and Planetary
2849 Sciences, v. 29, p. 331–364.

2850 Sheehan, P.M., and Coorough, P.J., 1990. Brachiopod zoogeography across the Ordovician – Silurian
2851 extinction event, in Palaeozoic Palaeogeography and Biogeography, W.S. McKerrow and C.R. Scotese
2852 (editors), Geological Society Memoir No. 12, p. 181-187.

2853 Shi, G.R., 2001. Possible influence of Gondwanan glaciation on low-latitude carbonate sedimentation
2854 and trans-equatorial faunal migration: the Lower Permian of South China, Papers from IGCP Project
2855 No. 411 on the Geodynamic Processes of Gondwanaland-derived Terranes in Eastern Asia,
2856 Geosciences Journal, v. 5, no. 1, p. 57-63.

2857 Simms, M.J., and Ruffell, A.H. 1989. Synchroneity of climatic change and extinctions in the Late
2858 Triassic, Geology, v. 17, p. 265–268.

2859 Shell (2018), Shell Scenarios: SKY, Meeting the Goals of the Paris Agreement,
2860 https://www.shell.com/promos/business-customers-promos/download-latest-scenario-
2861 sky/_jcr_content.stream/1530643931055/eca19f7fc0d20adbe830d3b0b27bcc9ef72198f5/shell-
2862 scenario-sky.pd

2863 Sloss, L.L., 1963. Sequences in the cratonic interior of North America, Geological Society of America
2864 Memoir 39, pp. 91-124.

2865 Smit, J., 1999. The global stratigraphy of the Cretaceous Tertiary boundary impact ejecta, Annual
2866 Review of Earth and Planetary Sciences, 27:75-91, doi:10.1146/annrev.earth.27.1.75.

2867 Song, H., Wignall, P.B., Chu, D., Tong, J., Sun, Y., He, W., and Tian, L., 2014. Anoxia/high temperature
2868 double whammy during the Permian-Triassic marine crisis and its aftermath, Scientific Reports,
2869 4:4132, doi: 10.1038/srep04132

2870 Song, H., Wignall, P.B., Song, H., Dai, X., and Chu, D., 2019. Seawater temperature and dissolved
2871 oxygen over the past 500 million years, Journal of Earth Sciences, v.30, no. 2, p. 236-243,
2872 doi:10.1007/s12583-028-1002-2.

2873   Song, H., Huang, S., Jia, E., Dai, X., Wignall, P.B., Dunhill, A.M., 2020. Flat latitudinal diversity gradient
2874   caused by the Permian–Triassic mass extinction. Proceedings of the National Academy of Sciences,
2875   117(30): 17578-17583.

2876   Spicer, R.A., Ahlberg, A., Herman, A.B., Hofmann, C.C., Raikevich, M., Valdes, P.J., and Markwick, P.J.,
2877   2008. The Late Cretaceous continental interior of Siberia: A challenge for climate models, Earth and
2878   Planetary Science Letters, v. 267, p. 228-235, doi:10.1016/j.espl.2007.11.049.

2879   Spray, J., 2020. Earth Impact Database (EID),
2880   http://passc.net/EarthImpactDatabase/New%20website_05-2018/Index.html

2881   Stanley, G. D., 2003. The evolution of modern corals and their early history, Earth Science Reviews, v.
2882   60, p. 195–225.

2883   Stanley, S.M., 2016. Estimates of the magnitudes of major marine mass extinctions in earth history,
2884   Proceedings of the National Academy of Sciences, USA., v. 113, E6325–E6334.
2885
2886   Steffen. W., Rockstrom, J., Richardson, K., Lenton, T.M., Folke, C., Liverman, D., Summerhayes, C.P.,
2887   Barnosk, A.D., Cornell, S.E., Crucifix, M., Donges, J.F., Fetzer, I., Lade, S.J., Scheffer, M., Winkelmann,
2888   R., and Schellnhuber, H.J., 2019. Trajectories of the Earth System in the Anthropocene, Proc.
2889   National Academy of Sciences, www.pnas.org/cgi/doi/10.1073/pnas.181014115, 8 p.
2890
2891   Stock, C.W., 2005. Devonian stromatoporoid originations, extinctions, and paleobiogeography: how
2892   they relate to the Frasnian-Famennian extinction, in Understanding Late Devonian and Permian-
2893   Triassic Biotic and Climatic Events; Towards an Integrated Approach, D.J. Over, J.R. Morrow, and P.B.
2894   Wignall (editors), Developments in Palaeontology & Stratigraphy, v. 20, p. 71 – 92, Elsevier,
2895   Amsterdam.
2896
2897   Sullivan,D.L., Brandon, A.D., Eldrett, J., Bergman, S.C., Wright, S., and Minisini, D., 2020. High
2898   resolution osmium data record three distinct pulses of magmatic activity during Cretaceous Oceanic
2899   Anoxic Event 2 (AOE-2), Geochimica et Cosmochimica Acta, v. 285, p. 257-273.

2900   Summerhayes, C.P.,2015. Earth's Climate Evolution, Wiley-Blackwell, Chichester, UK, 394 pp.

2901   Sun, Y., Joachimski, M.M., Wignall, P.B., Yan, C., Chen, Y., Jiang, H., Wang, L., and Lai, X., 2012.
2902   Lethally Hot Temperatures During the Early Triassic Greenhouse, Science, v. 338, p. 366-370.

2903   Sun, Y.D., Wignall, P.B., Joachimski, M.M., Bond, D.P.G., Grasby, S.E., Lai, X.L., Wang, L.N., Zhang,
2904   Z.T., Sun, S., 2016. Climate warming, euxinia and carbon isotope perturbations during the Carnian
2905   (Triassic) Crisis in South China, Earth and Planetary Science Letters, v. 444, p. 88-100,
2906   doi:org/10.1016/j.epsl.2016.03.037

2907   Swanson-Hysell, N.L., and Macdonald, F.A., 2017. Tropical weathering of the Taconic Orogeny as a
2908   driver for Ordovician cooling, Geology, v.45, p. 719-722., doi.org/10.1130/G38985.1

2909   Tans, P. 2009. An accounting of the observed increase in oceanic and atmospheric CO_2 and an
2910   outlook for the future, Oceanography, v. 22,No.4, pp. 26 -35.

2911   Taylor, B., 2006. The single largest oceanic plateau: Ontong Java–Manihiki–Hikurangi. Earth and
2912   Planetary Science Letters, v. 241, p. 372–380.

2913 Taylor, E.L., Taylor, T.N.,and Cuneo, R., 2000. Permian and Triassic high latitude paleoclimates:
2914 evidence from fossil biotas, in Huber, B.T., MacLeod, K.G., and Wing, S.L., (editors), Warm Climates in
2915 Earth History, Cambridge University Press, p. 321-350.

2916 Toggweiler, J.R., and Bjornsson, H., 2000. Drake Passage and palaeoclimate, Journal of Quaternary
2917 Science, 15:319-328.

2918 Tollefsen, E., Balic-Zunic, T., Mörth, C. et al., 2020.

2919 Torsvik, T.H., Svensen,H. H., Steinberger, B., Royer,D. L., Jerram, D.A., Jones, M.T, and Domeier,
2920 M., 2020. Connecting the Deep Earth and the Atmosphere, in Mantle Convection and Surface
2921 Expression S. Cottaar et al. (editors), AGU Monograph (in press).

2922 Trotter, J., Williams, I.S., Barnes, C.R., Männik, P., and Simpson, A., 2016. New conodont δ^{18}O
2923 records of Silurian climate change: Implications for environmental and biological events,
2924 Palaeogeography, Palaeoclimatology, Palaeoecology, v. 443, p.34–48,
2925 doi.org/10.1016/j.palaeo.2015.11.011

2926 Trotter, J.A., Williams, I.S., Barnes, C.R., Lécuyer , C., and Nicoll, R.S., 2008. Did Cooling Oceans
2927 Trigger Ordovician Biodiversification? Evidence from Conodont Thermometry, Science, v. 321, no.
2928 5888, p. 550-554, DOI: 10.1126/science.1155814

2929 Trotter, A.J., Williams, S.I., Nicora, A., Mazza, M., and Rigo, M., 2015, Long-term cycles of Triassic
2930 climate change: A new d^{18}O record from conodont apatite, Earth and Planetary Science Letters, v.
2931 415, p. 165–174.

2932 Umbgrove, J.H.F., 1947. The Pulse of the Earth, Martinus Niijhoff, The Hague, Netherlands, 358 pp.

2933 United Nations, 2019. United Nations Report on World Population,
2934 (https://www.un.org/development/desa/publications/world-population-prospects-2019-
2935 highlights.html).

2936 Upchurch, G.R., Otto-Bliesner, B.L., and Scotese, C.R., 1999, Terrestrial vegetation and its effects on
2937 climate during the latest Cretaceous, in *Evolution of the Cretaceous Ocean-Climate System*, E.
2938 Barrera and C. Johnson, (editors), Geological Society of America, Special Paper 332, pp.407-426.

2939 Upchurch, G.R., Kiehl, J., Shields, C., Scherer, J., and Scotese, C.R., 2015. Latitudinal temperature
2940 gradients and high latitude temperatures during the latest Cretaceous: Congruence of geologic data
2941 and climate models, Geology, v. 43, no. 9, p. 683-686.

2942 Urey, H.C., Lowenstam, H.A., Epstein, S., McKinney, C.R., 1951. Measurements of paleotemperatures
2943 and temperatures of the Upper Cretaceous of England, Denmark, and the southeastern United
2944 States, Geological Society of America Bulletin, v. 62, p. 399-416.

2945 Valdes, P.J., 1994, Atmospheric general circulation models of the Jurassic, in *Palaeoclimates and their*
2946 *modeling: with special reference to the Mesozoic Era*, J.R.L. Allen, B.J. Hoskins, B.W. Sellwood, R.A.
2947 Spicer, and P.J. Valdes (editors), Chapman and Hall, London, p. 109-118.

2948 Valdes, P.J., Lunt, D.L., and Scotese, C.R., 2018. Modelling the Climate History of the Phanerozoic,
2949 (abstract), American Geophysical Union, Monday, December 10, 2018, Convention Center, Hall A-C
2950 (Poster Hall), Fall Meeting 2018, #PP11F-1031, Washington, D.C.

2951 Valdes, P.J., Scotese, C.R., and Lunt, D.J., 2020. Deep ocean temperatures through time, Climates of
2952 the Past (in press).

2953 Valdes, P.J. and Sellwood, B.W., 1992, A palaeoclimate model for the Kimmeridgian, Palaeogeography,
2954 Palaeoclimatology, and Palaeoecology, 95:47-72.

2955 Vandenberghe, N., Hilgen, F.J., Speijer, R.P., 2012. The Paleogene Period, Chapter 28, in The Geologic
2956 Time Scale 2012, volume 2, F.M. Gradstein, J.G. Ogg, M.D. Schmitiz, and G.M. Ogg, (editors), p. 855-
2957 922, Elsevier, Amsterdam.

2958 van der Meer, D.G., Zeebe, R.E., van Hinsbergen, J.J., Sluijs, A., Spakman, W., and Torsvik, T., 2014.
2959 Plate tectonic controls on atmospheric CO_2 levels since the Triassic, Proceedings of the National
2960 Academy of Sciences, v. 111, no. 12, p. 4380-4385, doi/10.1073/pnas.1315657111

2961 van der Meer, D.G., van den Berg van Saparoea, A.P.H., van Hinsbergen, D.J.J., van de Weg, R.M.B.,
2962 Godderis, Y., Le Hir, G., and Donnadieu, Y., 2017. Reconstructing first-order changes in sea level
2963 during the Phanerozoic and Neoproterozoic using strontium isotopes, Gondwana Research, v. 44,
2964 22-34.

2965 van de Schootbrugge, B., Tremolada, F., Rosenthal, Y., Bailey, T.R., Feist-Burkhardt, S., Brinkhuis, H.,
2966 Pross, J., Kent, D.V., and Falkowski,P.G., 2007. End-Triassic calcification crisis and blooms of organic-
2967 walled 'disaster species', Palaeogeography, Palaeoclimatology, Palaeoecology 244:126–141,
2968 doi:10.1016/j.palaeo.2006.06.026

2969 van de Schootbrugge, B., Quan, T.M., Lindström, S., Püttmann, W., Heunisch, C., Pross, J., Fiebig, J.,
2970 Petschick, R., Röhling, H.-G., Richoz, S., Rosenthal,Y., Falkowski, P.G., 2009. Floral changes across the
2971 Triassic/Jurassic boundary linked to flood basalt volcanism, Nature Geoscience, v.2, p. 589-594.

2972 van de Schootbrugge, B., Bachan, A., Suan, G., Richoz, S., and Payne, J.L., 2013. Microbes, mud and
2973 methane: cause and consequence of recurrent Early Jurassic anoxia following the end-Triassic mass
2974 extinction, Palaeontology, v. 56, p. 685–709.

2975 van Gelderin, R., Joachimski, M.M., Day, J., Jansen, U., Alvarez, F., Yolkin, E.A., and Ma, X.-P., 2006.
2976 Carbon, oxygen and strontium isotope records of Devonian brachiopod shell calcite,
2977 Palaeogeography, Palaeoclimatology, Palaeoecology, v. 240, p. 47–67.
2978 doi:10.1016/j.palaeo.2006.03.045

2979 Vaughan, A.P.M., 2007. Climate and geology – A Phanerozoic perspective, in Deep-Time Perspectives
2980 on Climate Change: Marrying the Signal from Computer Models and Biological Proxies, Williams, M.,
2981 Haywood, A.M., Gregory, F.J., and Schmidt, D.N., (editors), p. 5-59, Micropalaeontological Society
2982 Special Publication, Geological Society of London, London.

2983 Veevers, J.J., Conaghan,P.J., and Shaw, S.E., 1994. Turning point in Pangean environmental history at
2984 the Permian/Triassic (P/Tr) boundary, in Pangea: Paleoclimate, Tectonics, and Sedimentation during
2985 the Accretion, Zenith, and Breakup of a Supercontinent, George D. Klein (ed.), Geol. Soc. America
2986 Special Paper, 288: 187-196.

2987 Veizer, J., Fritz, P., and Jones, B., 1986. Geochemistry of brachiopods – oxygen and crbon isotopic
2988 records of Paleozoic oceans, Geochemica et Cosmochemica Acta, v. 40, pp. 1387-1395.

2989 Veizer, J., Ala, D., Azmy, K., Bruckschen, P., Buhl, D., Bruhn, F., Carden, G.A.F.,Diener, A., Ebneth, S.,
2990 Godderis, Y., Jasper, T., Korte, C., Pawellek, F., Podlaha, O.G., and Strauss, H., 1999. $^{87}Sr/^{86}Sr$, $\delta^{13}C$
2991 and $\delta^{18}O$ evolution of Phanerozoic seawater, Chemical Geology, v. 161, no. 1-3, pp. 59-88.

2992 Veizer, J.T., Godderis, Y., Francois, L.M., 2000. Evidence for decoupling of atmospheric CO_2 and
2993 global climate during the Phanerozoic Eon, Nature, v. 408, no. 6813, p. 698-701, doi:
2994 10.1038/35047044. 2000

2995 Veizer, J., and Hoefs, J., 1976, The nature of O^{18}/O^{16} and C^{13}/C^{12} secular trends in sedimentary
2996 carbonate rocks, Geochimica et Cosmochimica Acta, v. 40, no. 11, p. 1387-1395.

2997 Veizer. J.T., and Prokoph. A., 2015. Temperatures and Oxygen isotopic composition of Phanerozoic
2998 oceans, Earth-Science Reviews, v. 146: p. 92-104, doi: 10.1016/j.earscirev.2015.03.008.

2999 Vellekoop, J., Sluijs, A., Smit., J., Schouten, S., Weijers, J.W.H., Sinninghe Damsté, and Brinkhuis, H.,
3000 2014. Rapid short-term cooling following the Chicxulub impact at the Cretaceous-Paleogene
3001 boundary, Proceedings of the National Academy of Science, v. 111, n. 21, pp. 7537-7541.

3002 Vellekoop, J., Esmeraysenlet, S., Miller, K.G., Browning, J.V., Sluijs, A., De Schootbrugge, B.V.,
3003 Damste, J.S.S., Brinkhuis, H., 2016. Evidence for Cretaceous-Paleogene boundary bolide "impact
3004 winter" conditions from New Jersey, USA. Geology, 44(8): 619-622.

3005 Verard, C. and Veizer, J., 2019. On plate tectonics and ocean temperatures, Geology, v. 47, p. 881-
3006 885.

3007 Vickers, M.L., Bajnai, D., Price, G.D., Linckens, J., and Fiebig, J., 2019. Southern high-latitude warmth
3008 during the Jurassic–Cretaceous: New evidence from clumped isotope thermometry, Geology,
3009 doi.org/10.1130/G46263.1

3010 Walker, J.C.G., Hays, P.B., and Kasting, J.F., 1981. A negative feedback mechanism for the long-term
3011 stabilization of Earth's surface temperature. Journal of Geophysical Research, 86, 9776–9782.

3012 Wallace, D.R., 2004. Beasts of Eden, Walking Whales, Dawn Horses, and Other Enigmas of Mammal
3013 Evolution, University of California Press, Berkeley, 340 pp.

3014 Wanless, H.R. and Shepherd, F.P., 1936. Sea level and climatic changes related to late Paleozoic
3015 cycles. Geological Society of America Bulletin, v. 47, p. 1177-1206.

3016 Wanless, H.R. and Weller, J.M., 1932. Correlation and extent of Pennsylvanian cyclothems.
3017 Geological Society of America Bulletin, v. 43, p. 1003-1016.

3018 Waterhouse, J.B., and Shi, G.R., 2013. Climatic implications from the sequential changes in diversity
3019 and biogeographic affinities for brachiopods and bivalves in the Permian of eastern Australia and
3020 New Zealand, Gondwana Research, v. 24, p. 139–147, doi:10.1016/j.gr.2012.06.008

3021 Webby, B.D., Paris, F., Droser, M.L., and Percival, I.G., 2004. The Great Ordovician Biodiversification
3022 Event, Columbia University Press, New York, 884 pp.

3023 Weirzbowski, H., and Joachimski, M., Reconstruction of late Bajocian–Bathonian marine
3024 palaeoenvironments using carbon and oxygen isotope ratios of calcareous fossils from the Polish
3025 Jura Chain (central Poland), Palaeogeography, Palaeoclimatology, Palaeoecology, v. 254, p. 523–540,
3026 doi:10.1016/j.palaeo.2007.07.010

3027   Wenzel, B., LeCuyer, C., and Joachimski, M.M., 2000. Comparing oxygen isotope records of Silurian

3028   calcite and phosphate - $\partial^{18}O$ compositions of brachiopods and conodonts, Geochimica et

3029   Cosmochimica Acta, v. 64, no. 11, p. 1859–1872.

3030   Wenzel, B., and Joachimski, M.M., 1996. Carbon and oxygen isotopic composition of Silurian

3031   brachiopods (Gotland/Sweden)" palaeoceanographic implications, Palaeogeography,

3032   Palaeoclimatology, Palaeoecology, v. 122, p. 143-166.

3033   Westerhold. T., Marwan, N., Drury, A.J., Liebrand, D., Agnini., C., Anagnostou, E., Barnet, J.S.K.,

3034   Bohaty, S.M., De Vleeschouwer, D., Florindo, F., Frederichs, T., Hodell, D.A., Holbourn, A.E.,

3035   Kroon, D., Lauretano, V., Littler, K., Lourens, L.L., Lyle, M., Pälike, H., Röhl, U., Tian, J., Wilkens,

3036   R.H., Wilson, P.A., Zachos, J.C., 2020. An astronomically dated record of Earth's climate and its

3037   predictability over the last 66 million years, Science 369: 1383-1387.

3038   Whiteside, J.H., and Grice, K., 2016. Biomarker Records Associated with Mass Extinction Events,

3039   Annual Review of Earth Planetary Sciences, v. 44, p. 581–612, doi: 10.1146/annurev-earth-060115-

3040   012501

3041   Whiteside, J.H., Olsen, P.E., Eglinton, T., Brookfield, M.E., and Sambrotto, R.N., 2010. Compound-

3042   specific carbon isotopes from Earth's largest flood basalt eruptions directly linked to the end-Triassic

3043   mass extinction, Proceedings of the National Academy of Sciences, v. 107, p. 6721–6725.

3044   Wierzbowski, H., and Joachimsky, M., 2007. Reconstruction of the late Bajocian-Bathonian marine

3045   paleoenvironments using carbon and oxygen isotope ratios of calcareous fossils from the Polish Jura

3046   Chain (central Poland), Palaeogeography, Palaeclimatology, Palaeoecology, v. 254, p. 523-540, doi:

3047   10.1016/j.palaeo.2007.07.010.

3048   Wignall, P.B., and Hallam, A., 1992. Anoxia as a cause of the Permian/Triassic mass extinction: facies

3049   evidence from northern Italy and the western United States. Palaeogeography, Palaeoclimatology,

3050   Palaeoecology, v. 93, p. 21-446.

3051   Wignall, P.B., 2001. Large igneous provinces and mass extinctions. Earth-Science Reviews, v. 53, p.1-

3052   33.

3053   Wignall, P.B., 2015. The Worst of Times, How life on Earth Survived Eighty Million Years of

3054   Extinctions, Princeton University Press, Princeton, NJ, 199 p.

3055   Wilf, P., Johnson. K., and Huber, B.T., 2003. Correlated terrestrial and marine evidence for global

3056   climate changes before mass extinction at the Cretaceous – Paleogene boundary, Proceedings of the

3057   National Academy of Sciences, v. 100, no. 2, p. 599-604, doi /10.1073/pnas.0234701100

3058   Willis, K.J., and McElwain, J.C., 2014. The Evolution of Plants, Oxford University Press, Oxford, UK,

3059   378 pp.

3060   Wing, S.L., Gingerich, P.D., Schmitz, B., and Thomas, E., 2003. Causes and Consequences of Globally

3061   Warm Climates in the Early Paleogene, Geol. Soc. America, Special Paper 369, Boulder, Colorado, 614

3062   pp.

3063   Wing, S., and Huber, B., 2019. Earth's Temperature History Workshop, Smithsonian National

3064   Museum of Natural History, March 30-31, 2018, Washington, D.C.

3065 Wolfe, J. A. and G. R. Upchurch, 1987. North American nonmarine climates and vegetation during
3066 the Late Cretaceous, Palaeogeography, Palaeoclimatology, Palaeoecology 61: 33-77.

3067 Wolfe, J.A., 1971. Tertiary climatic fluctuations and methods of analysis of Tertiary floras, Palaeogeog.,
3068 Palaeoclim., Palaeoecol., 9:27-57.

3069 Wolfe, J.A., 1978. A paleobotanical interpretation of Tertiary climates in the northern hemisphere,
3070 American Scientist, 66:694-703.

3071 Wolfe, J.A., 1992. Climatic, floristic, and vegetational changes near the Eocene/Oligocene boundary in
3072 North America, in Eocene-Oligocene Climatic and Biotic Evolution, D.R. Prothero and W.A. Berggren
3073 (eds.), Princeton University Press, Princeton, 421-436. pp.

3074 Wolfe, J.A., 1994. Tertiary climatic changes at middle latitudes of western North America, Palaeogeog.,
3075 Palaeoclim., Palaeoecol., 108:195-205.

3076 Worsley, T.R. & Kidder D.L., 1991. First-order coupling of paleogeography and CO2, with global
3077 surface temperature and its latitudinal contrast. Geology, 19, 1161-1164.

3078 Yancey, T.E., and Guillemette, R.N., 2008. Carbonate accretionary lapilli in distal deposits of the
3079 Chicxulub impact event: Geol. Soc. America Bulletin, 120:1105-1118.

3080 Young, S.A., Saltzman, M.R., Foland, K.A., Linder, J.S., and Kump, L.R., 2009. A major drop in seawater
3081 $^{87}Sr/^{86}Sr$ during the Middle Ordovician (Darriwilian): Links to volcanism and climate?, Geology v. 9,
3082 no. 10, p. 951–954, doi: 10.1130/G30152A.1

3083 Zachos, J., Pagani, M., Sloan, L., Thomas, E., and Billups, K. 2001. Trends, rhythms and abberations in
3084 global climate 65 Ma to present, Science, v. 292, p. 686-693.

3085 Zachos, J.C., Dickens, G.R., and Zeebe, R.E., 2008. An early Cenozoic perspective on greenhouse
3086 warming and carbon-cycle dynamics, Nature, v. 45117, p. 279-283.

3087 Zeebe RE, Zachos JC, Dickens GR. 2009. Carbon dioxide forcing alone insufficient to explain
3088 Palaeocene- Eocene Thermal Maximum warming. *Nat. Geosci.* 2:576–80

3089 Zeng, J., Cao, C.-Q., Davydov, V.I., and Shen, S.-Z., 2012. Carbon isotope chemostratigraphy and
3090 implications of palaeoclimatic changes during the Cisuralian (Early Permian) in the southern Urals,
3091 Russia, Gondwana Research, v. 21, p. 601–610, doi:10.1016/j.gr.2011.06.002

3092 Zhang, L., Chen, D., Huang, T., Yu, H., Zhou, X., Wang, J., 2020. An abrupt oceanic change and
3093 frequent climate fluctuations across the Frasnian–Famennian transition of Late Devonian:
3094 constraints from conodont Sr isotope. Geol. J. https://doi.org/10. 1002/gj.3657. (in press).

3095 Zhang, R.M.J., Follows, Grotzinger, J., and Marshall, J., 2001. Could the Late Permian deep ocean
3096 have been anoxic? Palaeocenography, v. 16, p. 317-329.

3097 Zhu, M.-Y., Babcock, L.E., and Peng, S.-C., 2006. Advances in Cambrian stratigraphy and
3098 paleontology: Integrating correlation techniques, paleobiology, taphonomy and paleoenvironmental
3099 reconstruction, Palaeoworld, v.15, p. 217–222, doi:10.1016/j.palwor.2006.10.016

3100 Ziegler, A.M., Eshel, G., Rees, P.Mc., Rothfus, T.A., Rowley, D.B., and Sunderlin, D., 2003. Tracing the
3101 tropics across land and sea: Permian to present, Lethaia, v. 36, p. 227-254.

3102 Ziegler, A.M., Hulver, M.L., Rowley, D.B., 1997, Permian World Topography and Climate, in *Late Glacial*
3103 *and Postglacial Environmental Changes: Quaternary, Carboniferous-Permian, and Proterozoic*, I. Peter
3104 Martini (editor), Oxford University Press, Oxford, p. 111-146.

3105 Ziegler, A.M., Parrish, J.M., Jiping, Y., Gyllenhaal, E.D., Rowley, D.B., Parrish, J.T., Sahngyou, N.,
3106 Behher, A., and Hulver, M.L., 1994. Early Mesozoic phytogeography and climate, in Allen, J., Hoskins,
3107 B.J., Sellwood, B.W., Spicer, R.S., Valdes, P.J. (editors), Paleoclimates and Their Modelling: with
3108 Sprecial Reference to the Mesozoic Era, Chapman and Hall, London, pp. 89-97.

3109 Ziegler, A.M., Rowley, D.B., Lottes, A.L., Sahagian, D.L., Hulver, and Gierlowski, T.C., 1985.
3110 Paleogeographic Interpretation: With an Example from the Mid-Cretaceous, Annual Reviews of Earth
3111 and Planetary Sciences, v. 13, p. 385-425

3112

3113

3114

3115

3116   Figure Captions

3117   Figure 1. Estimates of Phanerozoic Global Average Temperature (GAT). Sources: Wing and Huber
3118   (2019), Valdes et al. (2018), Mills et al. (2019), and This study.

3119   Figure 2. "Double Hump" pattern of Phanerozoic Climate (Fischer, 1981; 1982), I = icehouse, G =
3120   greenhouse.

3121   Figure 3. Modern Köppen belts and the average temperature of each belt.

3122   Figure 4. Early Permian (280 Ma) lithologic indicators of climate and continental paleo-Köppen Belts

3123   (Boucot et al., 2013).

3124   Figure 5. Mid-Cretaceous (100 Ma) lithologic indicators of climate and continental paleo-Köppen

3125   Belts (Boucot et al., 2013).

3126   Figure 6. Long-Term Phanerozoic temperature trend calculated by estimating the changing area of

3127   paleo-Köppen belts (see Supplementary Materials for data and details of calculations).

3128   Figure 7. Raw and mean values of oxygen isotopes from phosphatic and carbonate fossils for
3129   reconstructing sea surface temperatures over the past 500 million years (modified after Song et al.,
3130   2019). The scale of $\delta^{18}O_{Phos}$ is used for phosphatic fossils, i.e., phosphatic brachiopod, conodont, and
3131   fish. The scale of $\delta^{18}O_{Carb}$ is used for carbonate fossils, i.e., belemnite, bivalve, brachiopod, planktonic
3132   foraminifer, and others. Magenta curve represents the mean values of sea surface temperatures per
3133   million years. Shaded area represents 95% confidence intervals.

3134   Figure 8. Phanerozoic Isotopic Temperature (Song et al., 2019). A. = Each dot represents the
3135   average of all temperatures that fall within a given one million year interval. The best-fit curve was
3136   obtained using the Savitsky-Golay smoothing technique (window 11-15, degree 4). B. Change in
3137   Tropical Temperature (ΔT°_{trop}). The black dots along the x-axis are the times when no data are
3138   available.
3139
3140   Figure 9. Modifications to the Phanerozoic Isotopic Temperature Curve. The dashed line is the
3141   isotopic temperature curve (see Figure 8). The colored lines represent modifications and
3142   adjustments made to that curve based on geological and paleontological constraints.

3143   Figure 10. Comparison of isotopic temperature data from the late Pennsylvanian of South China

3144   (open dots) and the USA (black dots) (Song et al., 2019).

3145   Figure 11. Comparison of Cenozoic deep ocean isotopic temperatures and tropical temperatures A.

3146   gray line = low resolution Tropical Temperatures (this study), and the black line = high resolution Δ

3147   Tropical Temperatures for the Cenozoic. B. isotopic temperatures from deep ocean, benthic

3148   foraminifera (Zachos et al., 2001, 2008; Westerhold et al., 2020).

3149   Figure 12. Phanerozoic Global Average Temperature (GAT), blackline = Global Average Temperature,

3150   dashed line = Long-term temperature change derived from changes in the pole-to-Equator

3151   temperature gradient calculated from the changing area of Köppen Climatic Belts (see Figure 6).

3152   When the Global Average Temperature is below 18˚C large polar icecaps can form. When the Global

3153   Average Temperature is above 18˚C large polar icecaps are unlikely to form.

3154   Figure 13. Timing and magnitude of Large Igneous Provinces (rectangles) eruptions and bolide

3155   impacts (circles). The size of the rectangles indicates the relative eruptive intensity (10^6 km^2/my)

3156   (left-hand scale). See Table 1 and 2 for abbreviations. Sources: Ernst (2014), Spray (2020).

3157   Figure 14. Comparison of the timing of LIPS (black squares, Table 1), large bolide impacts (circles

3158   with dots, Table 2), and putative large impact events (light gray circles with x's) with the changes in

3159   Tropical Temperature (ΔT°_{trop}). The size of the lettering is roughly proportional to the size of the LIP

3160   or bolide imapact. See Table 1 and 2 for abbreviations. Sources: Ernst (2014), Spray (2020).

3161   Figure 15. Phanerozoic Ice Ages. gray = global area of snow and ice cover (10^6 km^2), dotted line =

3162   snow and ice predicted by Global Average Temperatures (GAT < 18˚C, Figure 12), numbers =

3163   number of glacial deposits (tillites, dropstones, and glendonites). Note inverted temperature scale

3164   (left side).

3165   Figure 16. Tropical, Global Average, Deep Ocean, and Polar Temperatures. (a) red line = tropical

3166   temperature (15 N - 15 S), (b) black line = global average temperature (GAT), (c) blue line = deep

3167   ocean temperatures (after Valdes et al., 2020) (d) light blue line = polar temperature (> 67 N&S). The

3168   chronological resolution of this diagram, ~ 5 million years, matches the chronological resolution of

3169   the paleo-Köppen maps (see Supplementary Materials).

3170   Figure 17. The polar temperature and the Pole to Equator temperature gradient for different Global

3171   Average Temperatures (GAT). Polar Temperature = average temperature above 67˚ latitude (N&S),

3172   Deep Sea = the average temperature at the bottom of the oceans (after Valdes et al., 2020). Pole to

3173   Equator Gradient = the average change in temperature for every one degree of latitude measured

3174   between 30˚ and 60˚ latitude. The Pole to Equator temperature gradient is shallow near the Equator

3175   and steepens rapidly near the Pole. The plus signs are the combined average temperatures for the

3176   present-day northern and southern hemispheres. Frequency = the percent of the time during the

3177   Phanerozoic characterized by this Pole-to-Equator temperature gradient. All of these calculations

3178   are based on an average tropical temperature of 26˚C (15 N – 15 S).

3179   Figure 18. Comparison of Phanerozoic global average temperatures (black line) with strontium flux

3180   ratio relative to the present-day flux (dashed line). Red line highlights when the trends are

3181   coincident.

3182   Figure 19. A Paleozoic Paleotemperature Timescale. white = warm time intervals, black = cool time
3183   intervals. Solid black line = Global Average Temperatures (GAT), < 18˚C = large permanent,
3184   icecaps, > 18˚C = no large, permanent icecaps. Light gray jagged lines = a schematic representation
3185   of >50 glacial/interglacial cycles during the Permo-Carboniferous. Timescale = International
3186   Chronostratigraphic Chart v2020/01. Refer to Table 3 for more information about each chronotemp
3187   and abbreviations.

3188   Figure 20. A Mesozoic Paleotemperature Timescale. white = warm time intervals, black = cool time
3189   intervals. Solid black line = Global Average Temperatures (GAT), < 18˚C = large, permanent
3190   icecaps, > 18˚C = no large, permanent icecaps. Timescale = International Chronostratigraphic Chart
3191   v2020/01.Refer to Table 3 for more information about each chronotemp and abbreviations.

3192   Figure 21. A Cenozoic Paleotemperature Timescale. white = warm time intervals, black = cool time
3193   intervals; Light gray jagged lines = a schematic representation of >50 glacial/interglacial cycles during
3194   the Plio-Pleistocene. Solid black line = Global Average Temperatures (GAT),), < 18˚C = large,
3195   permanent icecaps, > 18˚C = no large, permanent icecaps. Timescale = International
3196   Chronostratigraphic Chart v2020/01. Refer to Table 3 for more information about each chronotemp
3197   and abbreviations.

3198   Figure 22. IPCC Estimates of Global Warming compared to the Results Predicted by the Carbon
3199   Budget Model (this study). The blue curve represents the projected increase in atmospheric CO_2
3200   based on the continued burning of fossil fuels at the "modern rate" (1970 – 2020). The black curves
3201   are the CO_2 levels used in the IPCC models RCP 2.5, RCP 4.5, RCP 6.0, and RCP 8.5. The red curve is
3202   the projected CO_2 levels obtained in our model (between 750 ppm and 800 ppm at 2200 CE).
3203   Estimates from RCP 2.5 and RCP 4.5 are too low. The estimate of CO_2 used in RCP 8.5 is much too
3204   high. Estimates of CO_2 used in RCP 6.0 are about right.

3205   Figure 23. Projection of Future Global Warming onto Phanerozoic Temperature Time Scale. The likely
3206   amount of Post-Anthropogenic Warming (PAW) (red line). The boxes indicate times in the geological
3207   past when global temperatures were within the range of predicted PAW. When the Global Average
3208   Temperature is below 18˚C large polar icecaps can form. When the Global Average Temperature is
3209   above 18˚C large polar icecaps are unlikely to form.

3210   Figure 24. Paleogeographic maps for the early Oligocene (30 Ma) and early Miocene (15 Ma). These
3211   past time periods are a good climatic match for world after Anthropogenic Warming.

3212